NASA CONTRACTOR REPORT 145353

Evaluation of Composite Flattened Tubular Specimen

T. LIBER and I. M. DANIEL

IIT RESEARCH INSTITUTE
10 WEST 35TH STREET
CHICAGO, ILLINOIS 60616

IITRI PROJECT NO. D6131
NASA CONTRACT NAS1-14663
JUNE 1978

NASA
National Aeronautics and
Space Administration
Langley Research Center
Hampton, Virginia 23665

FOREWORD

This is the Final Report on IIT Research Institute Project No. D6131, "Evaluation of Composite Flattened Tubular Specimen," prepared by IITRI for NASA-Langley Research Center under Contract No. NAS1-14663. The work described herein was performed in the period of October 14, 1976 to December 31, 1977. It was financially supported by the Structures Laboratory, USARTL (AVRADCOM). Dr. G.L. Roderick was the Technical Representative of the Contracting Officer. IITRI personnel who made primary contributions to the program are Drs. I.M. Daniel and T. Liber, and Mr. T. Niiro. Additional contributions to the program were made by Messrs. L.C. Bennett and R. LaBedz.

Respectfully submitted,
IIT RESEARCH INSTITUTE

T. Liber
Senior Research Engineer

I.M. Daniel
Science Advisor
Mechanics of Materials Division

APPROVED:

S.A. Bortz
Director
Mechanics of Materials Division

EVALUATION OF COMPOSITE FLATTENED TUBULAR SPECIMEN*

ABSTRACT

The objective of the program was to systematically evaluate flattened tubular specimens of composite materails under static and cyclic uniaxial tensile loading and to compare them directly with flat coupon data of the same materials generated under corresponding loading conditions. The program required additional development for the refinement of the flattened specimen configuration and fabrication. The specimens investigated were made of graphite/epoxy, S-glass/epoxy, Kevlar-49/epoxy, and graphite/S-glass/epoxy hybrid materials. They were eight-ply laminates of $[\pm 45/0_2]_s$ construction except for the graphite/epoxy material which also included specimens of eight-ply $[0_2/\pm 45]_s$ construction. Fabrication techniques and fixturing were developed for quantity production of these specimens, including the special end tab and insert design devised to minimize gripping tab constraints. Flattened tube specimens and flat coupons of corresponding materials and layup were fabricated and tested under tensile static and fatigue loads and the results compared. Residual properties of fatigue specimens which survived 10 million cycles were also determined. Statically tested graphite/epoxy, S-glass/epoxy and Kevlar 49/epoxy flattened tube specimens exhibit somewhat higher average strengths than their corresponding flat coupons. They failed with acceptable test section failures. Flattened tube specimens of the graphite/S-glass/epoxy hybrid and the graphite/epoxy flattened tube specimens of $[0_2/\pm 45]_s$ construction failed in parasitic modes with consequential lower strength than the corresponding flat coupons. Fatigue tested flattened tube specimens failed in parasitic modes resulting in lower fatigue strengths than the corresponding flat coupons. Surviving fatigue specimens of both types showed in most cases a decrease in residual strength, in fewer cases a decrease in modulus and generally no significant changes of Poisson's ratio.

*The contract research effort which has led to the results in this report was financially supported by the Structures Laboratory, USARTL (AVRADCOM).

TABLE OF CONTENTS

LIST OF FIGURES

LIST OF FIGURES (Cont'd)

LIST OF FIGURES (Cont'd)

LIST OF FIGURES (Cont'd)

LIST OF FIGURES (Cont'd)

LIST OF FIGURES (Cont'd)

LIST OF FIGURES (Cont'd)

LIST OF TABLES

LIST OF TABLES (Cont'd)

EVALUATION OF COMPOSITE FLATTENED TUBULAR SPECIMEN

1.0 INTRODUCTION

Static and fatigue tensile properties of composite laminates are normally evaluated by testing flat coupons. It has been shown analytically[1,2] and verified experimentally[3,4] that significant interlaminar stress components exist near free edges in uniaxially loaded angle-ply laminates. These stresses are restricted to a region near the edge approximately equal to the laminate thickness. It has been hypothesized that damage due to loading of such specimens is initiated at the edges by these stresses and propagates toward the interior. This damage propagation mechanism may be more pronounced under cyclic than under static loading. It has also been observed that fatigue failures in composite materials are preceded by material degradation corresponding to a reduction in residual stiffness.[5] It is not certain that the indicated stiffness degradation is a true material response or attributable to specimen geometry.

The influence of the edge effects on the tensile properties of angle-ply laminate composites can be eliminated by utilizing an edgeless specimen. The most common edgeless specimen is the round tubular specimen. Laminated tubular specimens can be manufactured with properties identical to those of flat laminates. However, attempts to conduct valid uniaxial tests with round tubular specimens have been generally unsuccessful because of the differential Poisson effect between the test section and the grips. This problem has been particularly more difficult under cyclic loading which is more sensitive to stress discontinuities.

A new type of edgeless cylindrical specimen was developed at IITRI to circumvent these difficulties. It is a flattened hollow tube consisting of two flat sides connected by curved sections and it can be handled much like the standard flat coupon. Initial developments and testing was done and reported under a prior NASA-Langley Research Center contract.[6]

The objective of the present program under contract with NASA-Langley Research Center was to systematically evaluate angle-ply flattened tubular specimens of composite materials under static and cyclic uniaxial tensile loading and to compare them directly with flat coupon data of the same materials generated under corresponding loading conditions. The program included additional development for the refinement of the flattened specimen configuration and fabrication. The materials investigated were graphite/epoxy, S-glass/epoxy and Kevlar-49/epoxy. The angle-ply specimens were all eight-ply laminates of $[\pm 45/0_2]_s$ construction, except for the graphite/epoxy which also included eight-ply specimens of $[0_2/\pm 45]_s$ construction.

This report describes fabrication techniques and fixturing developed for quantity production of the flattened tubular specimens, the special end tab and insert design devised to minimize the detrimental Poisson's effect constraints, the test program performed to evaluate the flattened tubular specimen under tensile static and fatigue loading, comparison of the results with those obtained by testing corresponding flat coupon specimens, and the determination of tensile residual properties of specimens which survived 10 million fatigue cycles.

2.0 THE FLATTENED TUBULAR SPECIMEN

The development of a successful fabrication technique for flattened tubular specimens and specimen tabbing for valid tests required substantial effort. Many promising approaches were pursued but most failed to produce specimens of consistent and satisfactory quality or test section failures. The approach finally selected is described in the following sections.

2.1 Specimen Configuration

The geometric configuration and nominal dimensions of the flattened tubular specimen are shown in Fig. 2.1. The specimen is 22.9 cm (9 in.) long, 2.3 cm (0.90 in.) wide, with 3.80 cm (1.5 in.) long and 2.54 cm (1 in.) wide flat fiberglass loading tabs, tab extensions and inserts at each end. These dimensions are essentially the same as used for flat coupon specimens. The thickness across the flattened tube shown in Fig. 2.1, (0.58 cm; 0.23 in.) is only a typical one. It varies with the number of plies in the laminate and the ply thickness of the material used.

The cross sectional area A of the specimen is determined by the formula

$$A = (G-\pi t)t$$

where G = the specimen girth (outer circumference)

t = laminate thickness

The girth is readily measured with satisfactory accuracy by wrapping a single strip of paper around the specimen and marking the length of a single wrap. The thickness t used, is generally a nominal one determined from thickness measurements of cured flat coupons of the same material batch and layup.

2.2 Fabrication Technique for Flattened Composite Tubes

The flattened tube specimens are fabricated individually.

The techniques and fixturing specifically developed for this purpose are described below.

Specimen layup is done on a flat aluminum split mandrel with rounded edges consisting of three wedged segments and covered with a tightly fitting silicon rubber tube of 0.08 cm (0.030 in.) wall thickness, used for internal pressurization of the specimen during the curing process. The mandrel and tube are illustrated in Fig. 2.2. Fabrication starts by manually rolling the prepreg plies around the mandrel covered with the rubber tube. The first ply is rolled directly on the rubber tube which has been sprayed with mold release to permit extraction after specimen cure. Subsequent plies are each rolled on top of the preceeding one.

The prepreg tape is cut for this purpose into strips parallel to the fiber direction. Zero-degree plies are produced by rolling such strips with their long edges butting and parallel to the axis of the mandrel. Strips for 45-degree plies are rolled in a spiral fashion with the edges butting and at 45-degrees to the axis of the mandrel. The specimen is overwrapped with one layer of separator cloth (Emfab TX1040 Teflon treated 104 fiber-glass cloth). The separator cloth is spirally overwrapped with strips of paper bleeder (Mochburg CW1850 glass fiber paper). Then, the middle wedge of the mandrel is pushed against the two outer ones to expand the mandrel and tighten the layup. The fixture used for this purpose is shown in Fig. 2.3.

The specimen with its mandrel are subsequently transferred into the cavity of an aluminum molding tool, whose surfaces have been sprayed with mold release. The molding tool is shown in open view in Figs. 2.4 and 2.5. It consists of a lower and upper platen, two side restraining bars, an end cap with a pressure tap, two specimen edge mold bars whose edges come in contact

with the specimen and two silicon rubber strips. The thermal expansion of the rubber strips during specimen curing exerts a compacting pressure on the specimen edges. The edge bars are made in various thicknesses, to accomodate specimens of various numbers of plies. The end cap contains a central pipe used to pressurize the silicone rubber tube inside the specimen. All parts of the molding tool are assembled and fastened tightly by means of screws. The molding tool is then bagged for vacuum application during cure. The assembled tool is shown in Fig. 2.6.

Curing is done by raising the temperature gradually to the recommended cure temperature and applying internal pressurization and vacuum as required by the curing cycle. After curing the specimen is removed from the mold, the mandrel with its rubber tube is extracted from the specimen, and the specimen is post-cured as required after visual inspection indicates satisfactory quality. The specimen ends are subsequently trimmed and end tabs provided to make it into a tensile test specimen.

Figure 2.7 shows a photograph of a typical specimen section obtained by the process described. The specimen wall thickness is basically uniform with the exception of a small thickening toward the center of the flat sections and local thickness ridges at the transition from the rounded edges to the flat sides. These ridges become critical factors affecting the fatigue test results.

2.3 Specimen Loading Tabs

Figure 2.1 illustrates the geometry and dimensions of the specimen loading tabs. At each end the tab system consits of two flat outer tabs and outer tab extensions and a flat plug insert. The plug insert is necessary to prevent specimen crushing during tightening of the gripping jaws of the test machine. All tab sections were made from glass/epoxy laminates.

To minimize the constraining effect of transverse tab stiffness on the specimen transverse strains due to Poisson's ratio, the glass/epoxy tab sections were of $[\pm 45]_n$ construction, i.e., with their fiber at ± 45 degrees with the load (longitudinal) axis. The outer tabs were generally 7-ply laminates. The tab extensions and the plug insert were custom-made to the required thickness.

To minimize the occurrence of specimen failure near the tabs during static and fatigue testing the transition region between the outer tabs and specimen test section was reinforced by means of a specially configured extension of the plug insert. This is illustrated in Fig. 2.1, where it is seen that the plug insert extends into the specimen with a slotted section beyond the end of the outside tabs. The cantilevered configuration of this extension, bonded to the specimen, provides a flexible reinforcement of the tab to specimen transition region.

Figure 2.8 shows at one end the five tab sections comprising the tabbing system and also the specimen before the tab bonding operation. The outer tabs have a 20- to 30-degree taper at the transition from tab to test section. The plug insert extends the full width of the specimen inside, and has rounded edges to conform to the specimen. It is slightly undersized to accomodate an adhesive layer for bonding. The insert slat is filled with flexible structural foam to prevent adhesive clogging during bonding.

Tab, plug insert and outer tab extension bonding is done by spreading an adhesive layer on all mating surfaces, sliding the inserts in place into the tube ends, placing the flat tabs on the specimen ends, placing the tab extensions on the protruding plugs and clamping the whole tab assembly in place with a set of spring clamps until the adhesive cures. The adhesive used was Hysol Epoxy-Patch Kit 0151 Clear (Hysol Division of the Dexter

Corporation). After the tab bonds are cured the tab flats are machined to uniform thickness and the sides are sanded to the desired width of 2.54 cm (1 in.). Figure 2.9 shows such a finished specimen.

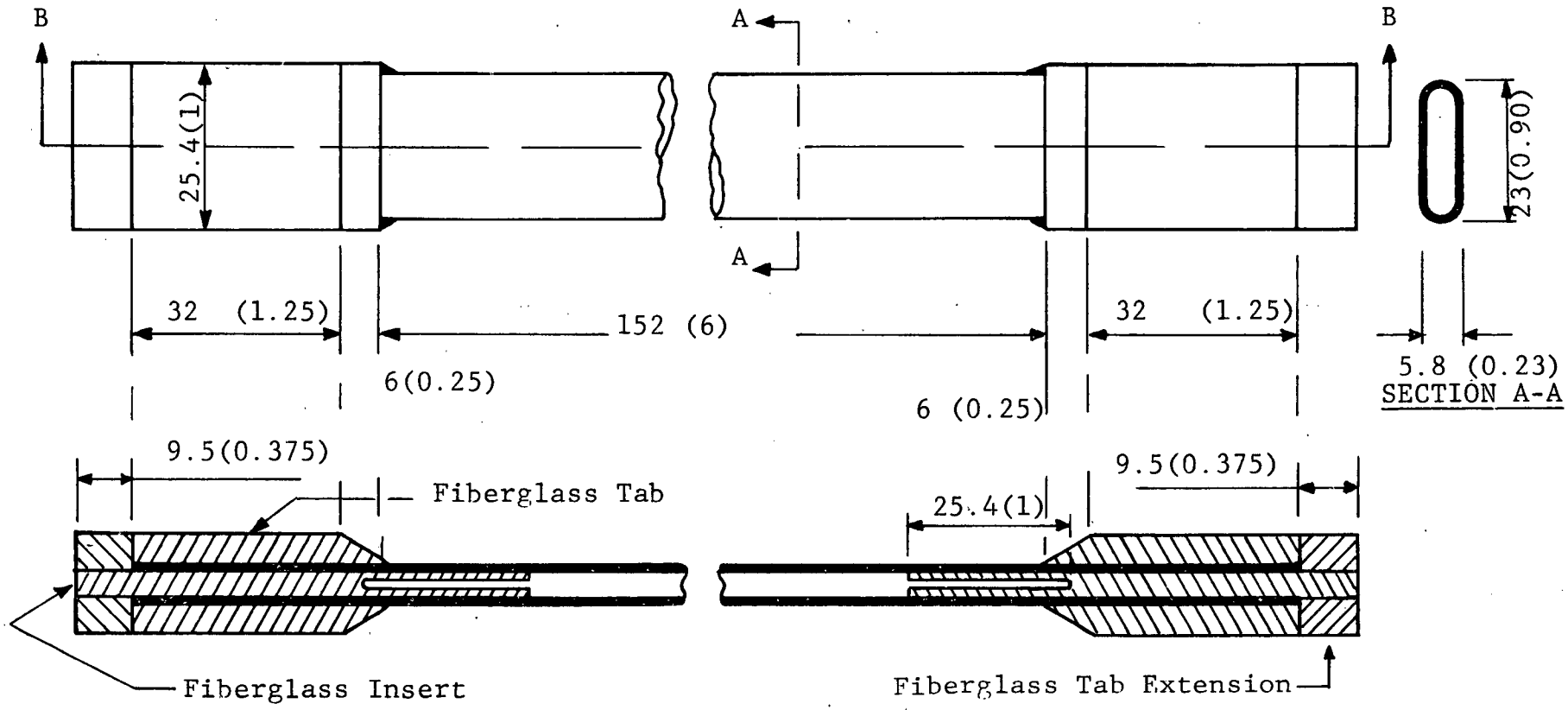

Figure 2-1 Dimensions of Flattened Composite Tubular Specimen (Dimensions are in mm and inches)

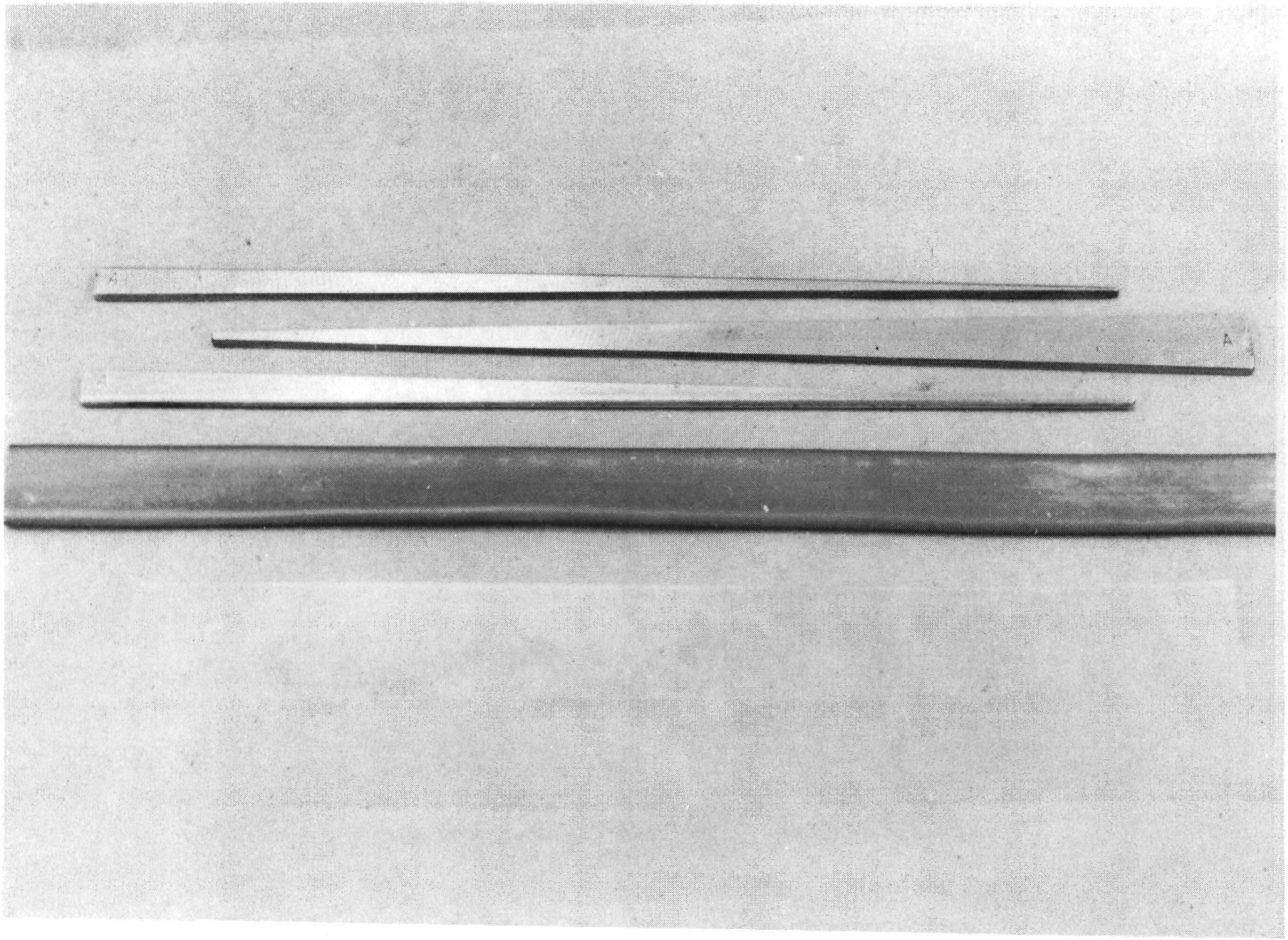

Figure 2.2 Three Piece Split Mandrel and Silicon Rubber Pressurization Tube

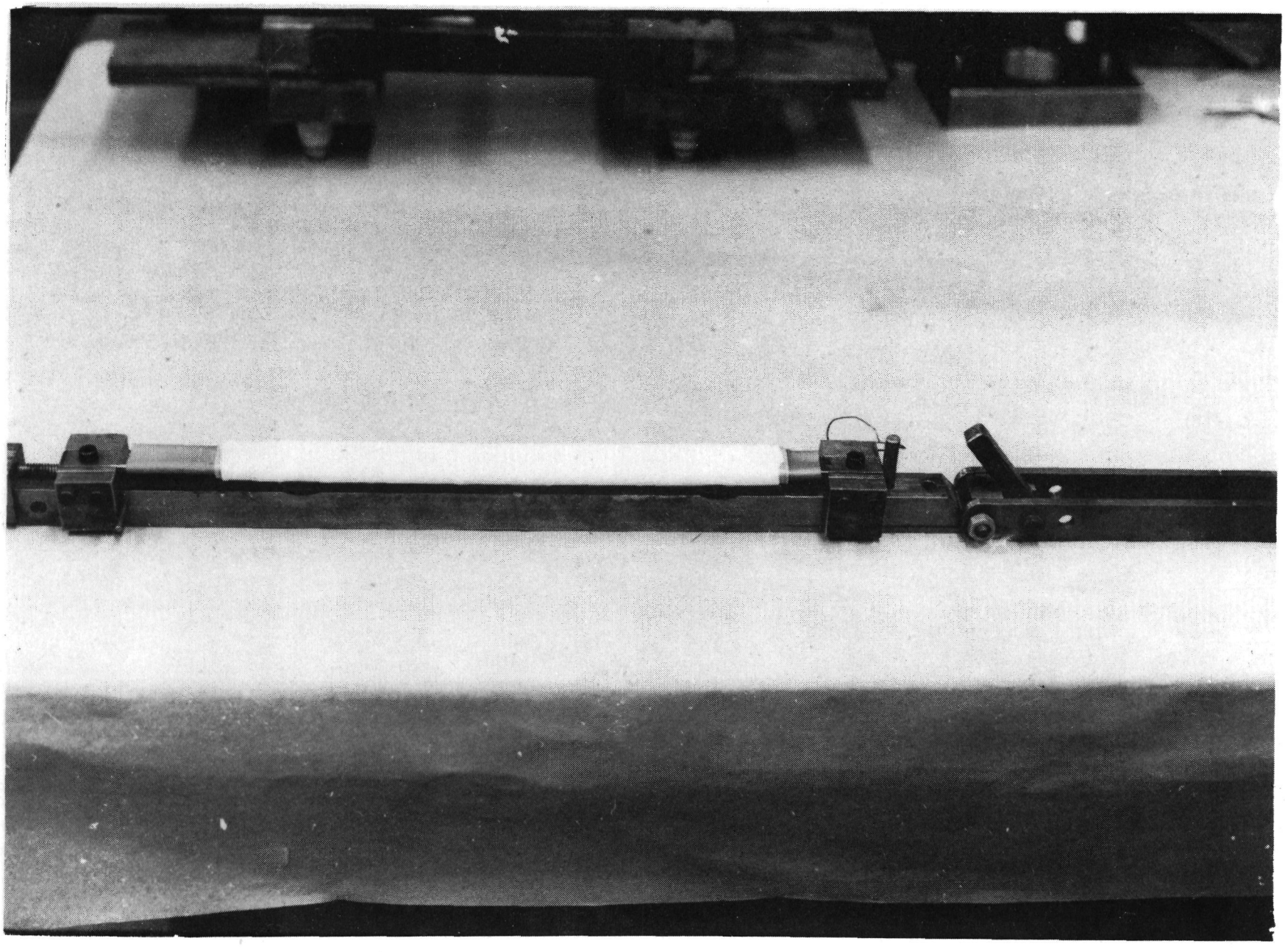

Figure 2.3 Fixture for Specimen Layup Tightening by Expanding Three Piece Mandrel Inside Specimen

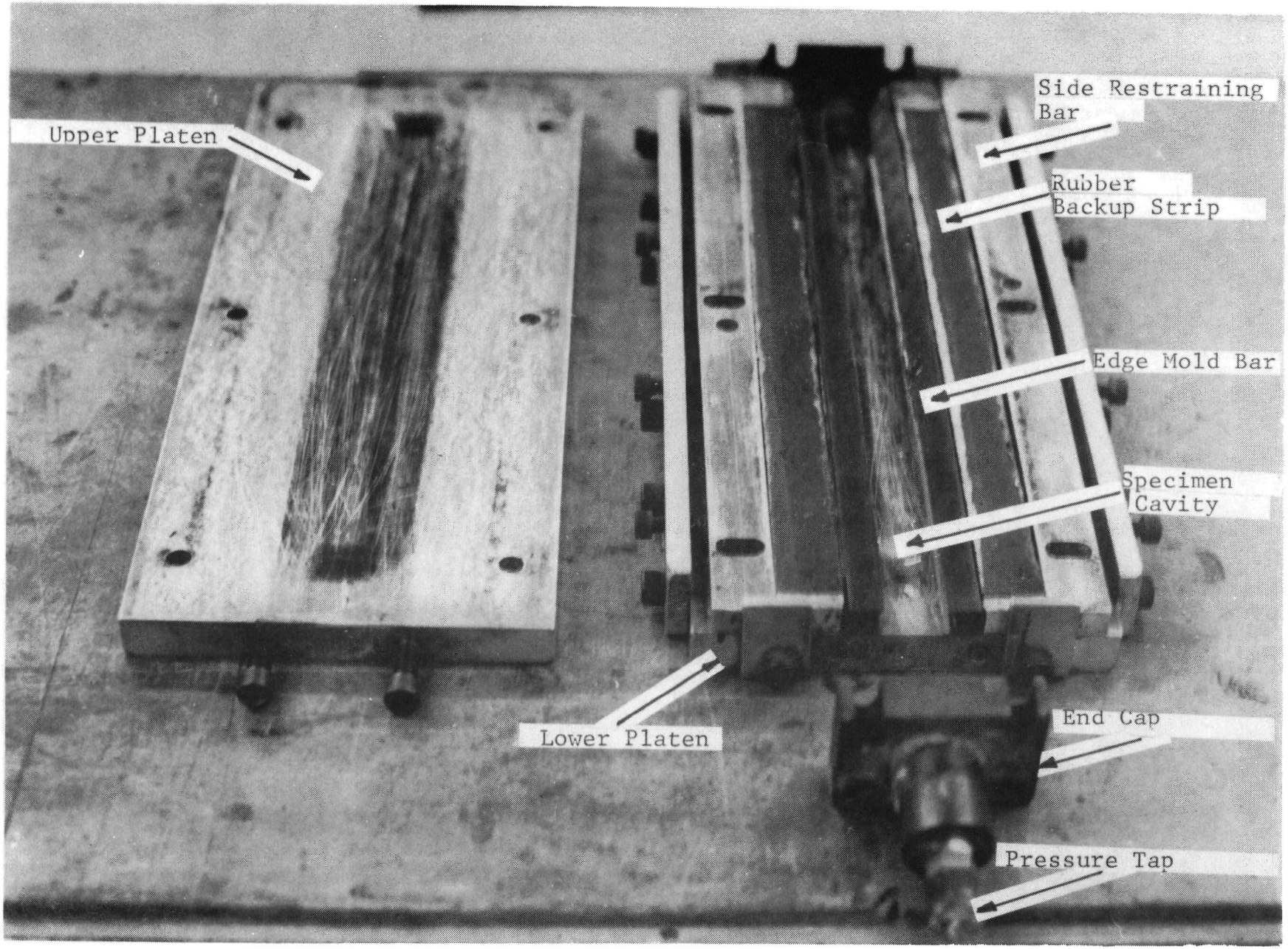

Figure 2.4 Open View of Flattened Tube Specimen Molding Tool

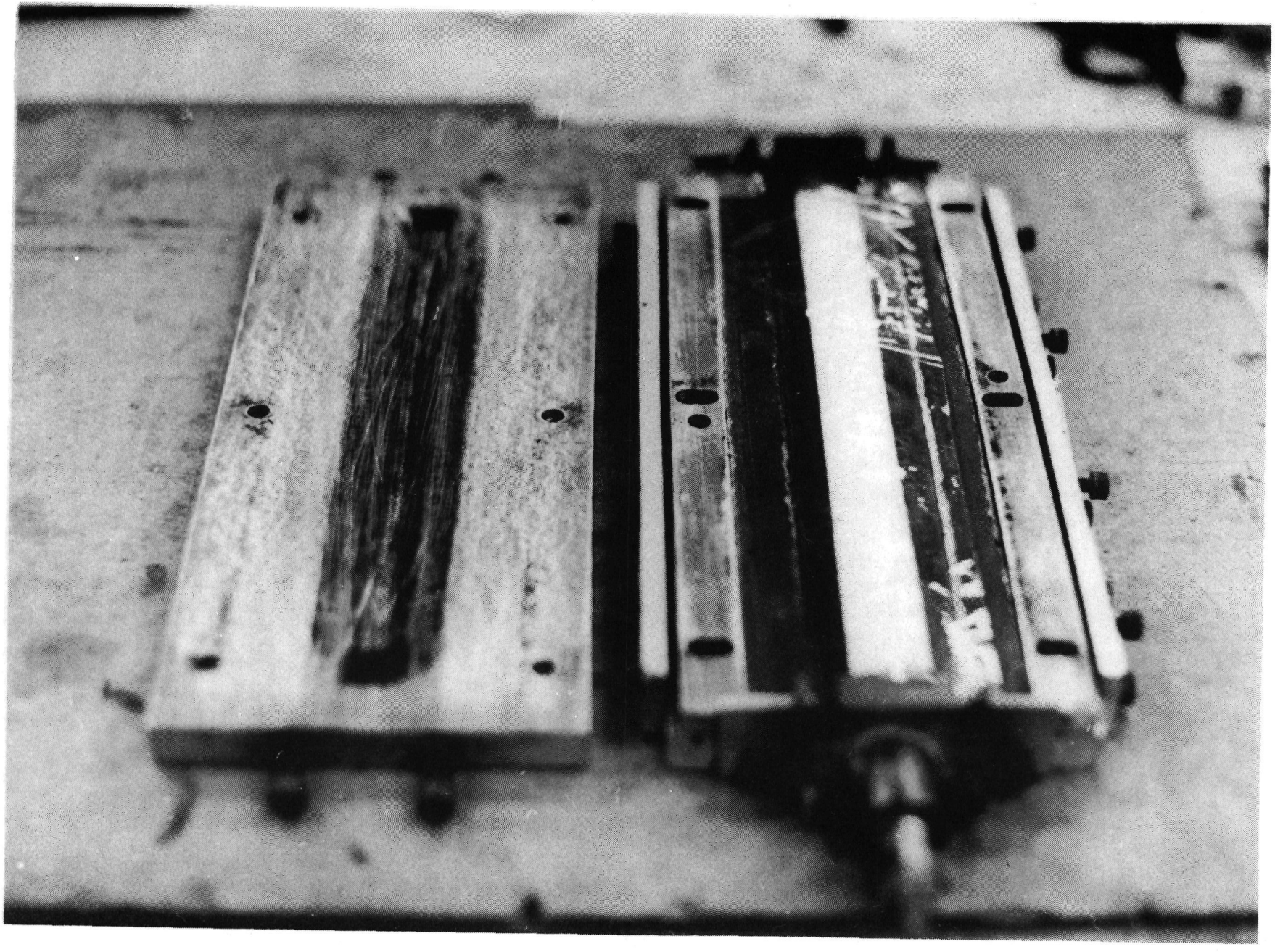

Figure 2.5 Open Molding Tool with Specimen

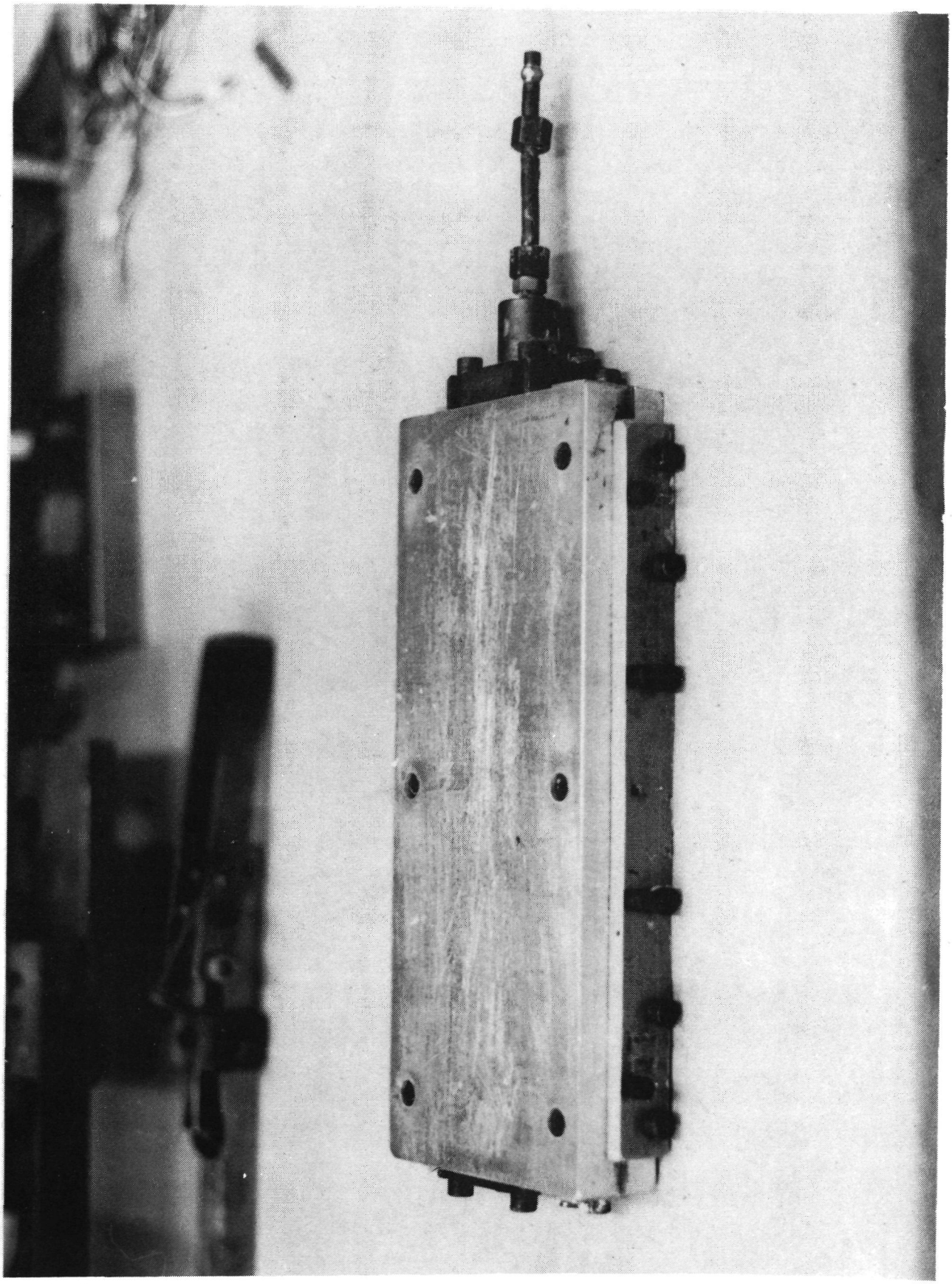

Figure 2.6 Assembled Molding Tool

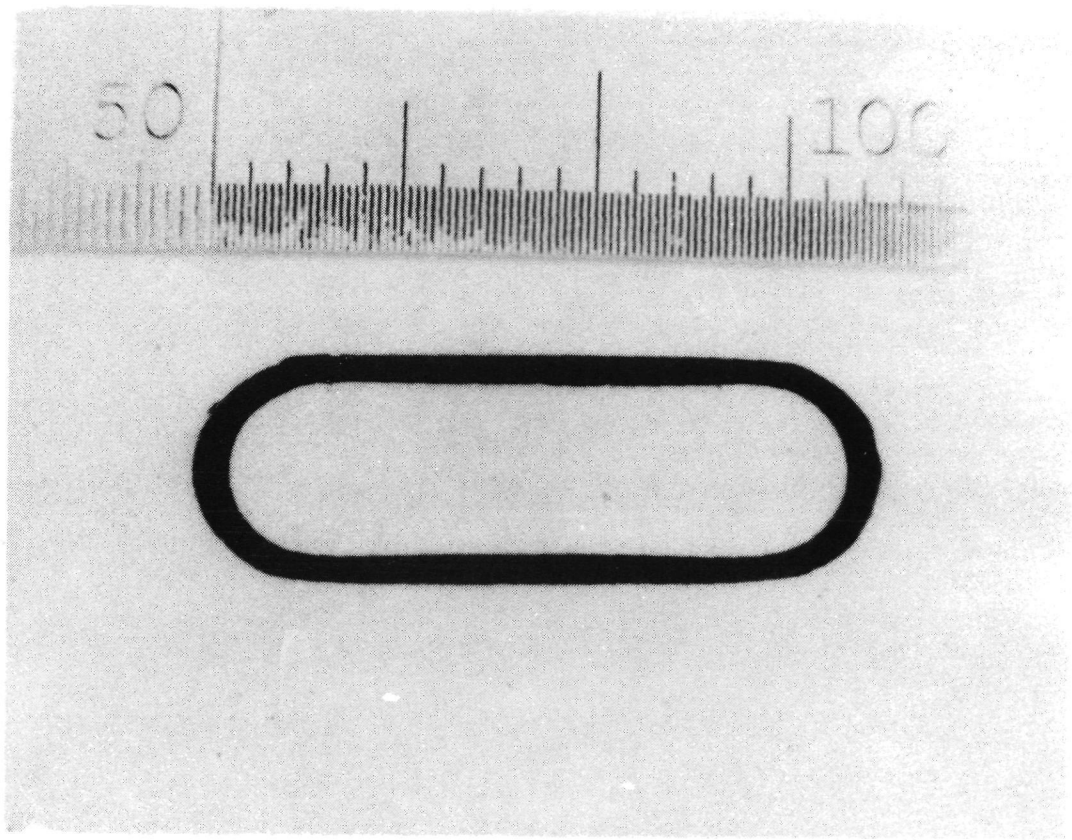

Figure 2.7 Photograph of Flattened Tubular Specimen Cross Section (Small divisions are 0.01 in.)

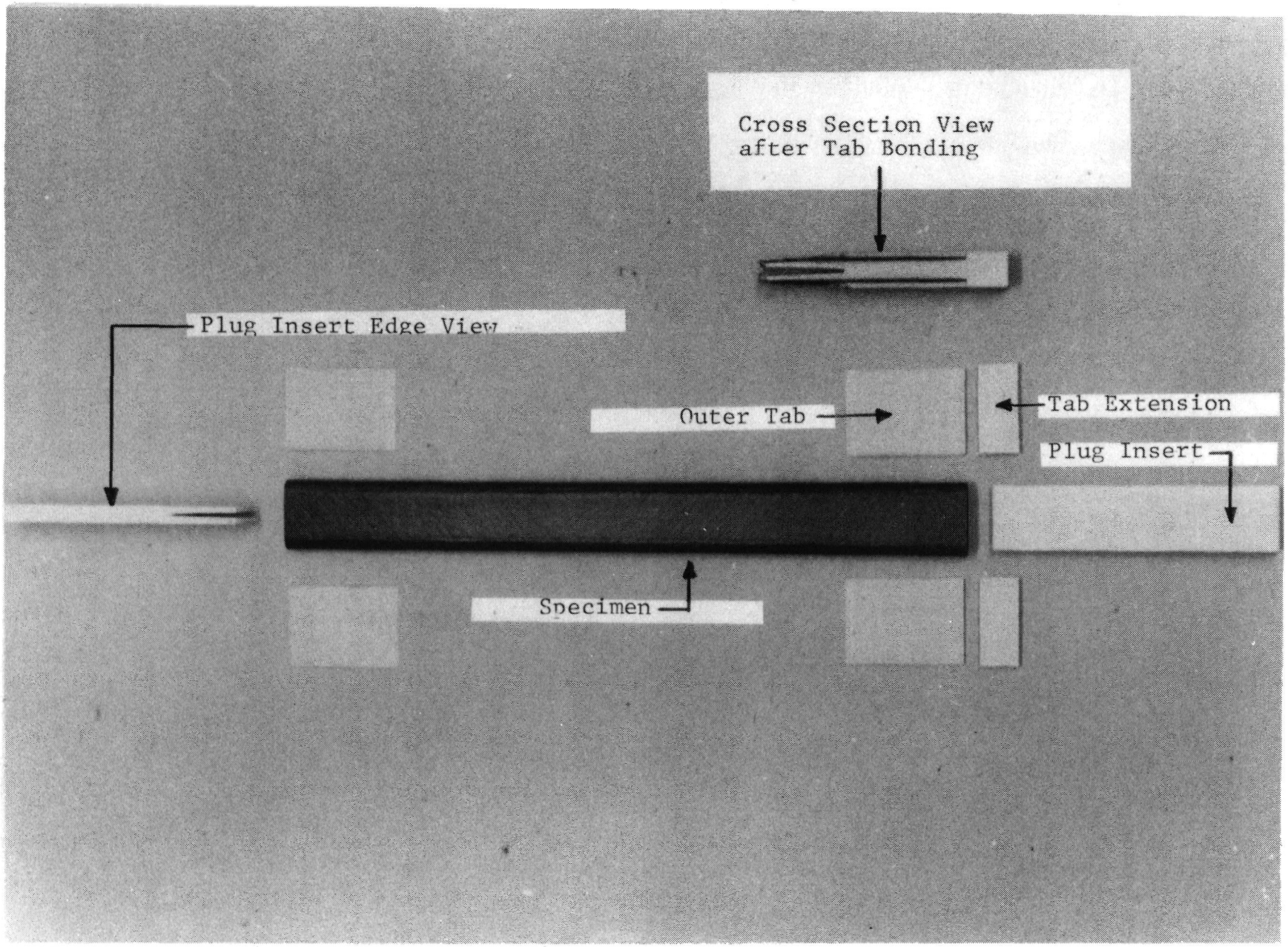

Figure 2.8 Specimen Tabs and Inserts

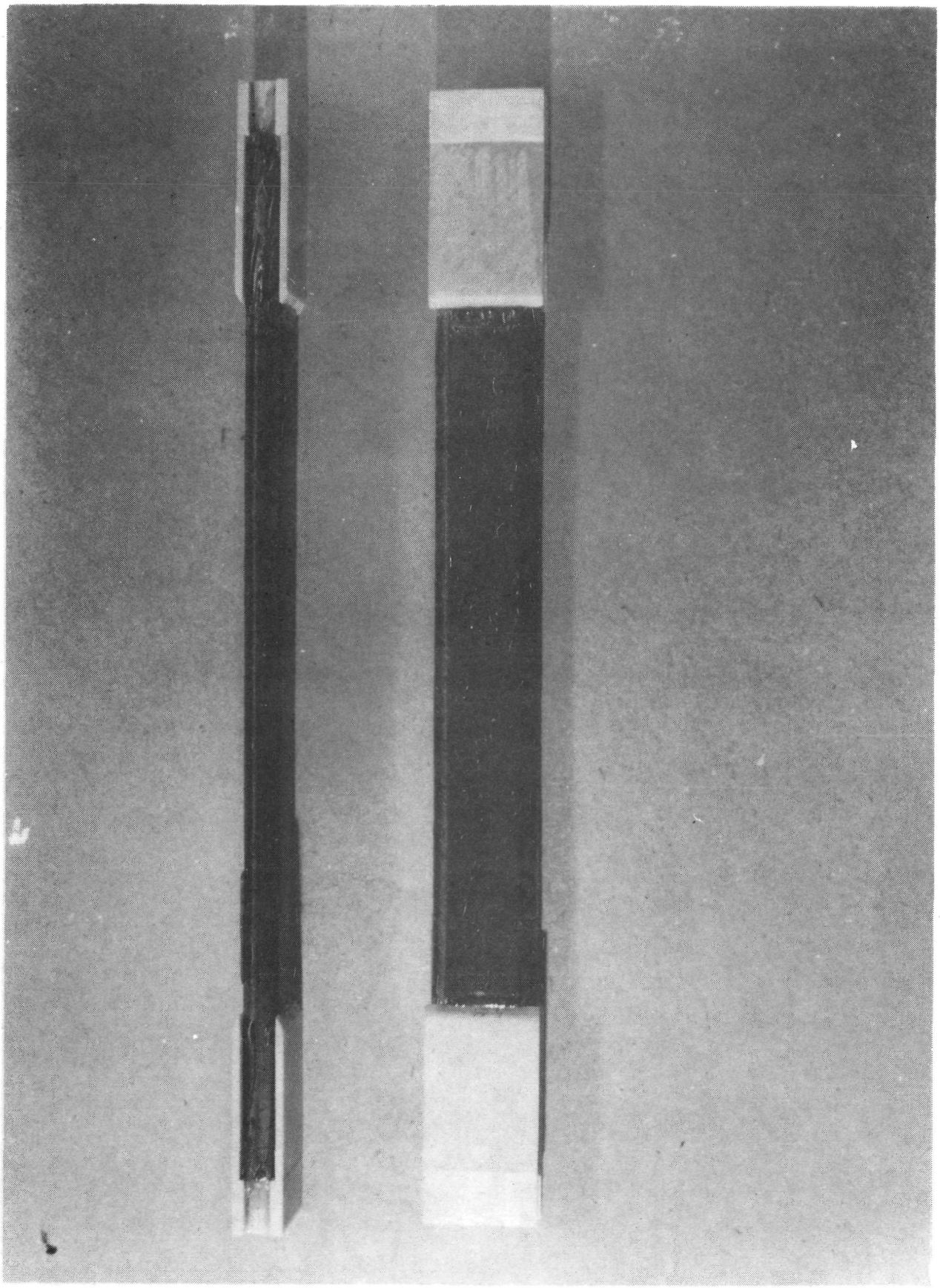

Figure 2.9 Finished Specimen with Tabs

3.0 TEST PROGRAM

The requirements of the test program were to evaluate flattened tubular specimens of angle-ply construction under tensile static and fatigue loading at ambient room temperature, and compare the results with those obtained by testing corresponding flat coupon specimens. The program included determination of tensile residual properties of specimens which survived 10 million fatigue cycles.

Table 3.1 shows the specimens called for by the test program and the number of static and fatigue specimens to be tested for each material and each specimen type. As Table 3.1 indicates, all specimens in the test program were eight-ply angle-ply laminates of $[\pm 45/0_2]_s$ and $[0_2/\pm 45]_s$ construction fabricated from graphite/epoxy, S-glass/epoxy, Kevlar 49/epoxy and hybrid graphite/S-glass/epoxy materials.

The program required that each batch of prepreg material be subjected to standard acceptance qualification tests. These include longitudinal flexure and interlaminar shear tests at room temperature. Subsequently, standard characterization tests are conducted to determine static properties of the unidirectional material.

3.1 Materials and Qualification Tests

The three materials used in the program were purchased in prepreg form from the 3M Company, St. Paul, Minnesota. The same epoxy resin system, PR-286, was used in all three materials. The prepreg materials are designated as follows:

Graphite/Epoxy:	SP-286T300
S-Glass/Epoxy :	SP-304/S-glass
Kevlar 49/Epoxy:	SP-306/Kevlar 49

Table 3.1

TEST PROGRAM SPECIMENS

Material	Layup	Type of Specimen	Number of Tests	
			Static	Fatigue
Graphite/Epoxy	$[\pm 45/0_2]_s$	Flat Coupon	4	10
	$[\pm 45/0_2]_s$	Flattened Tube	4	10
	$[0_2/\pm 45]_s$	Flat Coupon	4	6
	$[0_2/\pm 45]_s$	Flattened Tube	4	6
S-Glass/Epoxy	$[\pm 45/0_2]_s$	Flat Coupon	4	10
	$[\pm 45/0_2]_s$	Flattened Tube	4	10
Kevlar 49/Epoxy	$[\pm 45/0_2]_s$	Flat Coupon	4	10
	$[\pm 45/0_2]_s$	Flattened Tube	4	10
Graphite/S-Glass/ Epoxy	$[\pm 45^C/0_2{}^G]_s$	Flat Coupon	3	6
	$[\pm 45^C/0_2{}^G]_s$	Flattened Tube	3	6

The graphite/epoxy prepreg was received in two batches. The S-glass/epoxy and Kevlar 49/epoxy prepregs came in single batches. All batches of material received were qualified by determining their flexural and interlaminar shear strengths from unidirectional coupons.

Unidirectional plates, 15.2 cm x 15.2 cm (6 in. x 6 in.) and 15-plies thick were fabricated for qualification testing. Flexural strength coupons were 10.2 cm (4 in.) long, 1.3 cm (0.5 in.) wide with a 6.3 cm (2.5 in.) span length for the graphite/epoxy and Kevlar 49/epoxy materials and a 5.1 cm (2 in.) span for the S-glass/epoxy material. The use of a shorter span for the S-glass/epoxy was required due to excessive deflections encountered during testing of this lower-modulus material. Interlaminar shear strength coupons were 1.5 cm (0.6 in.) long, 0.6 cm (0.25 in.) wide with a 1 cm (0.4 in.) span length. These specimens were subjected to three-point bending. Results of the qualification tests are shown in Tables 3.2 through 3.9.

The results for the graphite/epoxy were judged satisfactory since they exceed the highest data available from the manufacturer for the comparable material SP-286T2. No data were available from the manufacturer for the S-glass/epoxy and Kevlar 49/epoxy materials, however, the data obtained for the S-glass/epoxy are higher than comparable data for other S-glass/epoxy systems. Likewise, for the Kevlar 49/epoxy the data obtained are higher then comparable data for another Kevlar 49/epoxy system.[7]

Table 3.2

QUALIFICATION FLEXURE TESTS FOR GRAPHITE/EPOXY SP-286T300

FIRST BATCH

Specimen Number	Thickness cm	(in.)	Width cm	(in.)	Flexural Strength MPa	(ksi)
1	0.196	(0.077)	1.257	(0.495)	1639	(238)
2	0.196	(0.077)	1.267	(0.499)	1660	(241)
3	0.196	(0.077)	1.275	(0.502)	1633	(237)
4	0.193	(0.076)	1.257	(0.495)	1664	(241)
5	0.196	(0.077)	1.278	(0.503)	1777	(258)
6	0.198	(0.078)	1.283	(0.505)	1624	(236)
				Average:	1666	(242)

Table 3.3

QUALIFICATION INTERLAMINAR SHEAR TESTS FOR GRAPHITE/EPOXY SP-286T300

FIRST BATCH

Specimen Number	Thickness cm	(in.)	Width cm	(in.)	Shear Strength MPa	(ksi)
1	0.191	(0.075)	0.607	(0.239)	103.3	(15.0)
2	0.185	(0.073)	0.612	(0.241)	114.6	(16.6)
3	0.191	(0.075)	0.607	(0.239)	104.4	(15.1)
4	0.188	(0.074)	0.610	(0.240)	106.3	(15.4)
5	0.191	(0.075)	0.605	(0.238)	106.6	(15.5)
6	0.188	(0.074)	0.615	(0.242)	101.9	(14.8)
				Average:	106.3	(15.4)

Table 3.4

QUALIFICATION FLEXURE TESTS FOR GRAPHITE/EPOXY SP-286T300

SECOND BATCH

Specimen Number	Thickness cm	(in.)	Width cm	(in.)	Flexural Strength MPa	(ksi)
1	0.191	(0.075)	1.257	(0.495)	1684	(244)
2	0.188	(0.074)	1.252	(0.493)	1696	(246)
3	0.191	(0.075)	1.260	(0.496)	1606	(233)
4	0.188	(0.074)	1.255	(0.494)	1649	(239)
5	0.188	(0.074)	1.252	(0.493)	1674	(243)
6	0.188	(0.074)	1.255	(0.494)	1660	(241)
				Average:	1662	(241)

Table 3.5

QUALIFICATION INTERLAMINAR SHEAR TESTS FOR GRAPHITE/EPOXY SP-286T300

SECOND BATCH

Specimen Number	Thickness cm	(in.)	Width cm	(in.)	Shear Strength MPa	(ksi)
1	0.185	(0.073)	0.635	(0.250)	101.0	(14.6)
2	0.185	(0.073)	0.640	(0.252)	102.6	(14.9)
3	0.188	(0.074)	0.638	(0.251)	103.6	(15.0)
4	0.183	(0.072)	0.638	(0.251)	101.5	(14.7)
5	0.188	(0.074)	0.635	(0.250)	101.9	(14.8)
6	0.185	(0.073)	0.630	(0.248)	103.3	(15.0)
				Average:	102.3	(14.8)

Table 3.6

QUALIFICATION FLEXURE TESTS FOR S-GLASS/EPOXY (SP-304)

Specimen Number	Thickness cm	(in.)	Width cm	(in.)	Flexural Strength MPa	(ksi)
1	0.180	(0.071)	1.270	(0.500)	1734	(251)
2	0.173	(0.068)	1.273	(0.501)	1857	(269)
3	0.173	(0.068)	1.270	(0.500)	1906	(276)
4	0.175	(0.069)	1.270	(0.500)	1868	(271)
5	0.178	(0.070)	1.270	(0.500)	1900	(276)
6	0.175	(0.069)	1.265	(0.498)	1788	(259)
				Average:	1842	(267)

Table 3.7

QUALIFICATION INTERLAMINAR SHEAR TESTS FOR S-GLASS/EPOXY (SP-304)

Specimen Number	Thickness cm	(in.)	Width cm	(in.)	Shear Strength MPa	(ksi)
1	0.163	(0.064)	0.627	(0.247)	71.6	(10.4)
2	0.163	(0.064)	0.622	(0.245)	82.4	(12.0)
3	0.163	(0.064)	0.625	(0.246)	69.0	(10.0)
4	0.163	(0.064)	0.627	(0.247)	74.3	(10.8)
5	0.163	(0.064)	0.627	(0.247)	72.0	(10.4)
6	0.163	(0.064)	0.627	(0.247)	73.3	(10.6)
				Average:	75.0	(10.9)

Table 3.8

QUALIFICATION FLEXURE TESTS FOR KEVLAR 49/EPOXY SP-306

Specimen Number	Thickness cm	(in.)	Width cm	(in.)	Flexural Strength MPa	(ksi)
1	0.216	(0.085)	1.283	(0.505)	673	(97.6)
2	0.216	(0.085)	1.295	(0.510)	758	(109.9)
3	0.216	(0.085)	1.250	(0.492)	676	(98.1)
4	0.216	(0.085)	1.255	(0.494)	775	(112.4)
5	0.211	(0.083)	1.265	(0.498)	671	(97.3)
6	0.211	(0.083)	1.257	(0.495)	720	(104.5)
				Average:	712	(103.3)

Table 3.9

QUALIFICATION INTERLAMINAR SHEAR TESTS FOR KEVLAR 49/EPOXY SP-306

Specimen Number	Thickness cm	(in.)	Width cm	(in.)	Shear Strength MPa	(ksi)
1	0.213	(0.084)	0.638	(0.251)	68.2	(9.9)
2	0.213	(0.084)	0.638	(0.251)	60.8	(8.8)
3	0.216	(0.085)	0.638	(0.251)	60.6	(8.8)
4	0.216	(0.085)	0.640	(0.252)	68.8	(10.0)
5	0.213	(0.084)	0.648	(0.255)	64.5	(9.3)
6	0.208	(0.082)	0.648	(0.255)	68.0	(9.3)
				Average:	65.1	(9.4)

3.2 Material Curing

All specimens in this program were made using the following curing cycle specified by the manufacturers for the prepreg materials:

1. Insert bagged layup into cold autoclave and apply full vacuum.
2. Pressurize autoclave to 690 kPa (100 psi).
3. Raise temperature at 2.8 degK (5°F) per minute to 393 degK (250°F).
4. Release vacuum.
5. Raise temperature at 2.8 degK (5°F) per minute to 448 degK (350°F) and hold for 2 hours.
6. Allow to cool to room temperature.
7. Postcure at 478 degK (400°F) for 6 hours in air circulating oven.

3.3 Characterization of Unidirectional Material

To characterize the three materials unidirectional tensile properties were obtained by testing 2.54 cm x 22.9 cm (1 in. x 9 in.) coupons which had a 15.2 cm (6 in.) long test section and 3.81 cm (1.5 in.) long crossplied fiberglass/epoxy gripping tabs at each end. The 0-degree specimens were 6-ply coupons and the 90-degree specimens were 8-ply coupons except for the Kevlar 49/epoxy specimens which because of their fragility were 15-ply coupons. At least two specimens were used for each test for each material. The average tensile moduli, Poisson's ratios, tensile strengths and ultimate tensile strains obtained from the tests are shown in Tables 3.10, 11 and 12.

Stress-strain curves for the characterization tests of the unidirectional graphite/epoxy material are shown in Figs. 3.1

Table 3.10

MEASURED PROPERTIES OF UNIDIRECTIONAL GRAPHITE/EPOXY SP-286T300

Property	Value
Nominal Ply Thickness	0.127 mm (0.0050 in.)
Longitudinal Tensile Modulus, E_{11}	154 GPa (22.4 x 10^6 psi)
Transverse Tensile Modulus, E_{22}	11.0 GPa (1.60 x 10^6 psi)
Major Poisson's Ratio, ν_{12}	0.30
Minor Poisson's Ratio, ν_{21}	0.014
Longitudinal Tensile Strength, S_{11T}	1528 MPa (222 ksi)
Longitudinal Ultimate Tensile Strain, ε^u_{11T}	0.00973
Transverse Tensile Strength, S_{22T}	55 MPa (8.0 ksi)
Transverse Ultimate Tensile Strain, ε^u_{22T}	0.00519

Table 3.11

MEASURED PROPERTIES OF UNIDIRECTIONAL S-GLASS/EPOXY SP-304

Property	Value
Nominal Ply Thickness	0.1194 mm (0.0047 in.)
Longitudinal Tensile Modulus, E_{11}	59.2 GPa (8.59 x 10^6 psi)
Transverse Tensile Modulus, E_{22}	25.4 GPa (3.69 x 10^6 psi)
Major Poisson's Ratio, ν_{12}	0.25
Minor Poisson's Ratio, ν_{21}	0.090
Longitudinal Tensile Strength, S_{11T}	1845 MPa (268 ksi)
Longitudinal Ultimate Tensile Strain, ε^u_{11T}	0.03284
Transverse Tensile Strength, S_{22T}	49 MPa (7.1 ksi)
Transverse Ultimate Tensile Strain, ε^u_{22T}	0.00206

Table 3.12

MEASURED PROPERTIES OF UNIDIRECTIONAL KEVLAR 49/EPOXY SP-306

Property	Value
Nominal Ply Thickness	0.152 mm (0.006 in.)
Longitudinal Tensile Modulus, E_{11}	81.1 GPa (11.8 x 10^6 psi)
Transverse Tensile Modulus, E_{22}	5.9 GPa (0.86 x 10^6 psi)
Major Poisson's Ratio, ν_{12}	0.36
Minor Poisson's Ratio, ν_{21}	0.021
Longitudinal Tensile Strength, S_{11T}	1308 MPa (190 ksi)
Longitudinal Ultimate Tensile Strain, ε^u_{11T}	0.0129
Transverse Tensile Strength, S_{22T}	12.0 MPa (1.74 ksi)
Transverse Ultimate Tensile Strain, ε^u_{22T}	0.0021

through 3.4. Strains in the 0-degree specimens are linear up to approximately 689 to 827 MPa (100 to 120 ksi). At this level they show a small increase in modulus and continue to behave linearly to failure. Both specimens failed at loads within 4 percent of each other. The 90-degree specimens behave linearly up to approximately 41 MPa (6 ksi) where they exhibit a small decrease in modulus and continue linearly to failure at 55 MPa (8 ksi).

Stress-strain curves for the characterization tests of the unidirectional S-glass/epoxy material are shown in Figs. 3.5 through 3.8. Strains in the 0-degree specimens are linear up to approximately 1379 to 1517 MPa (200 to 220 ksi), and become nonlinear with a decreasing modulus thereafter. Both specimens failed at loads within 16 percent of each other. The 90-degree specimens are linear up to approximately 28 MPa (4 ksi) and become nonlinear thereafter with a decreasing modulus to failure at an average stress

of 49 MPa (7.1 ksi). The two specimens failed at loads within 7 percent of each other.

Stress-strain curves for the characterization tests of the unidirectional Kevlar 49/epoxy material are shown in Figs. 3.9 through 3.13. Strains in the 0-degree specimens are linear up to approximately 827 to 965 MPa (120 to 140 ksi). At this level they show a small increase in modulus and continue to behave linearly to failure. All three specimens failed at loads within $\pm$5 percent of their average. The longitudinal strains of the 90-degree specimens behave nonlinearly, with a slowly decreasing modulus to failure at an average stress of 12.0 MPa (1.74 ksi). The two specimens failed at loads of within less than 1 percent of each other.

3.4 Test Procedures for Angle-Ply Specimens

The flattened tube specimens were fabricated individually using the dimensions, techniques and fixturing described in Section 2.

For each material all flat coupon specimens were cut from a single plate fabricated using standard procedures. The coupon dimensions were 2.54 cm x 22.9 cm (1 in. x 9 in.) with a 15.2 cm (6 in.) long test section and 3.81 cm (1.5 in.) long crossplied fiberglass/epoxy gripping tabs at each end. The 0-degree plies of the specimens were oriented in the longitudinal direction.

For all specimens used in the program, wall thickness used in stress calculations were based on nominal ply thicknesses as obtained from cured flat laminates for the three basic materials. The ply thicknesses are:

graphite/epoxy -- 0.127 mm (0.0050 in.)
S-glass/epoxy -- 0.119 mm (0.0047 in.)
Kevlar 49/epoxy -- 0.152 mm (0.0060 in.)

To satisfy static test requirements, to determine stress-strain curves and to detect extraneous bending, each static specimen was instrumented with two two-gage strain gage rosettes located centrally, one on each flat side of the specimen.

Each static specimen was tested to failure in an Instron testing machine. Strains were monitored and recorded throughout the test at each load increment. Abnormal behavior and failure modes, when noticeable, were recorded by appropriate remarks. Stress-strain curves were plotted from the recorded data and the following properties determined from them:

Initial axial modulus, E_{xx}

Poisson's ratio, ν_{xy}

Axial tensile strength, S_{xxT}

Axial ultimate strain, ε^{u}_{xx}

Fatigue testing was done on a Sonntag Universal Fatigue Test Machine. Each fatigue specimen was subjected to tensile load cycling at the standard rate of 30 cycles per second, at a stress ratio R = 0.1 and a constant maximum load amplitude. The maximum load amplitude for each test was selected in accordance with the requirement that the specimen fail within the range of approximately 5×10^5 to 10^7 cycles. The load selections were based on past experience with fatigue testing of similar materials. Thermocouples were clipped to the surface of some of these specimens to determine and record specimen heating which occurs during fatigue loading and may contribute to specimen degradation. Each fatigue test was run continuously to failure or 10^7 cycles, whichever occurred first. Maximum stress amplitudes and cycles to failure were recorded, tabulated and S-N curves drawn from the data. Those specimens which survived 10^7 cycles were tested statically to failure to determine residual properties. Instrumentation, testing and data analysis for these tests were the same as for the static specimens.

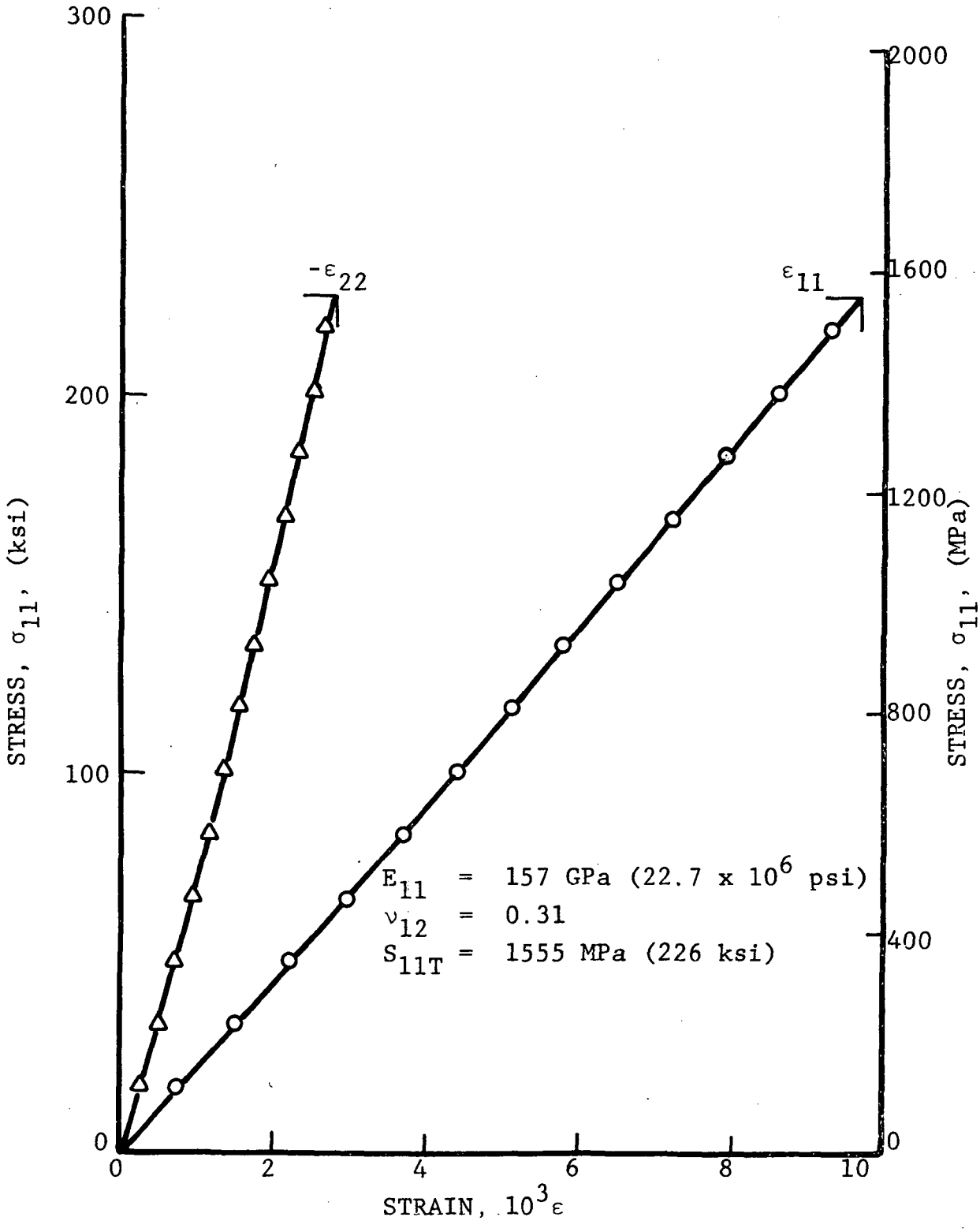

Figure 3.1 STRESS-STRAIN CURVES FOR UNIDIRECTIONAL 0-DEGREE GRAPHITE/EPOXY SPECIMEN UNDER TENSILE LOADING

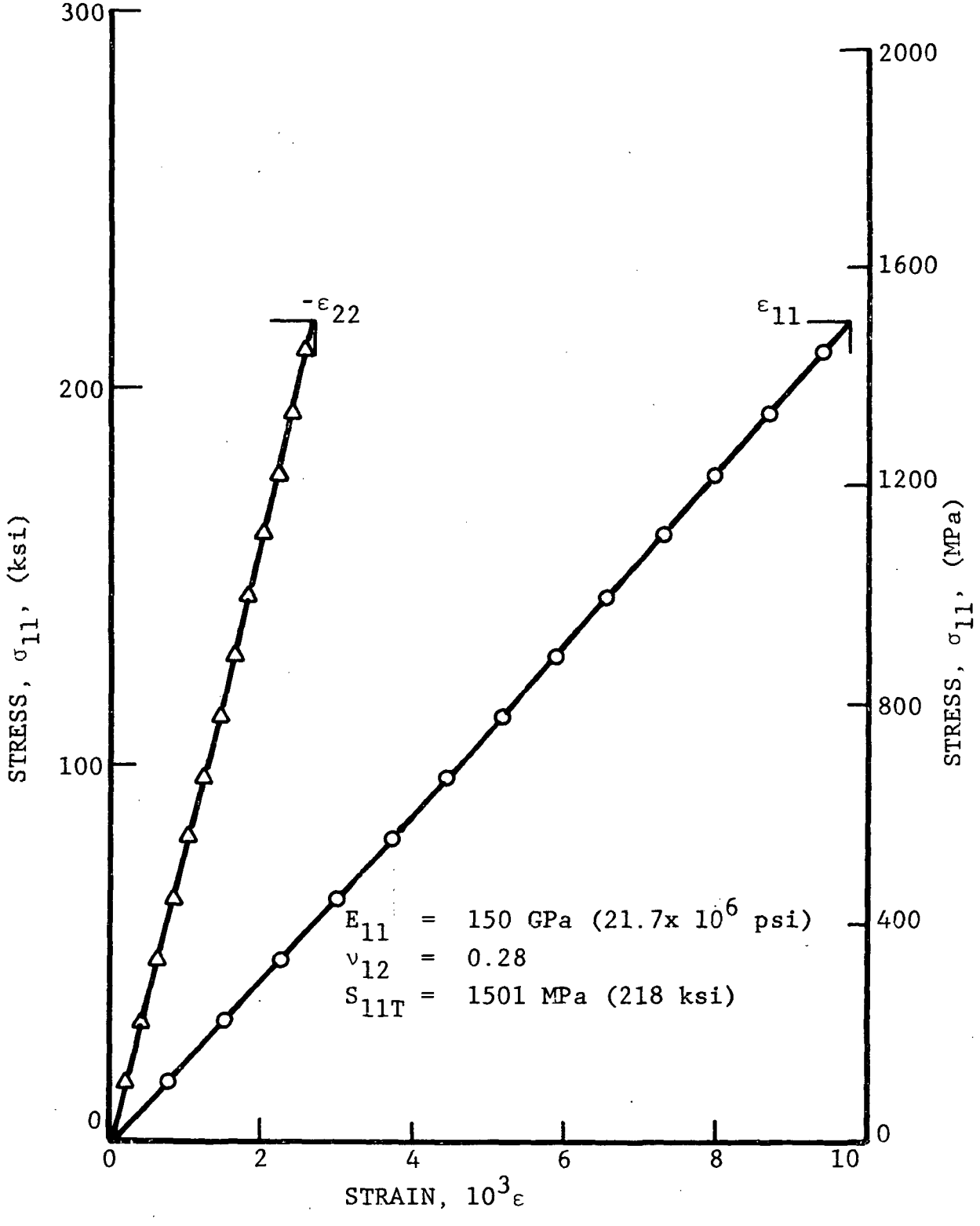

Figure 3.2 STRESS-STRAIN CURVES FOR UNIDIRECTIONAL 0-DEGREE GRAPHITE/EPOXY SPECIMEN UNDER TENSILE LOADING

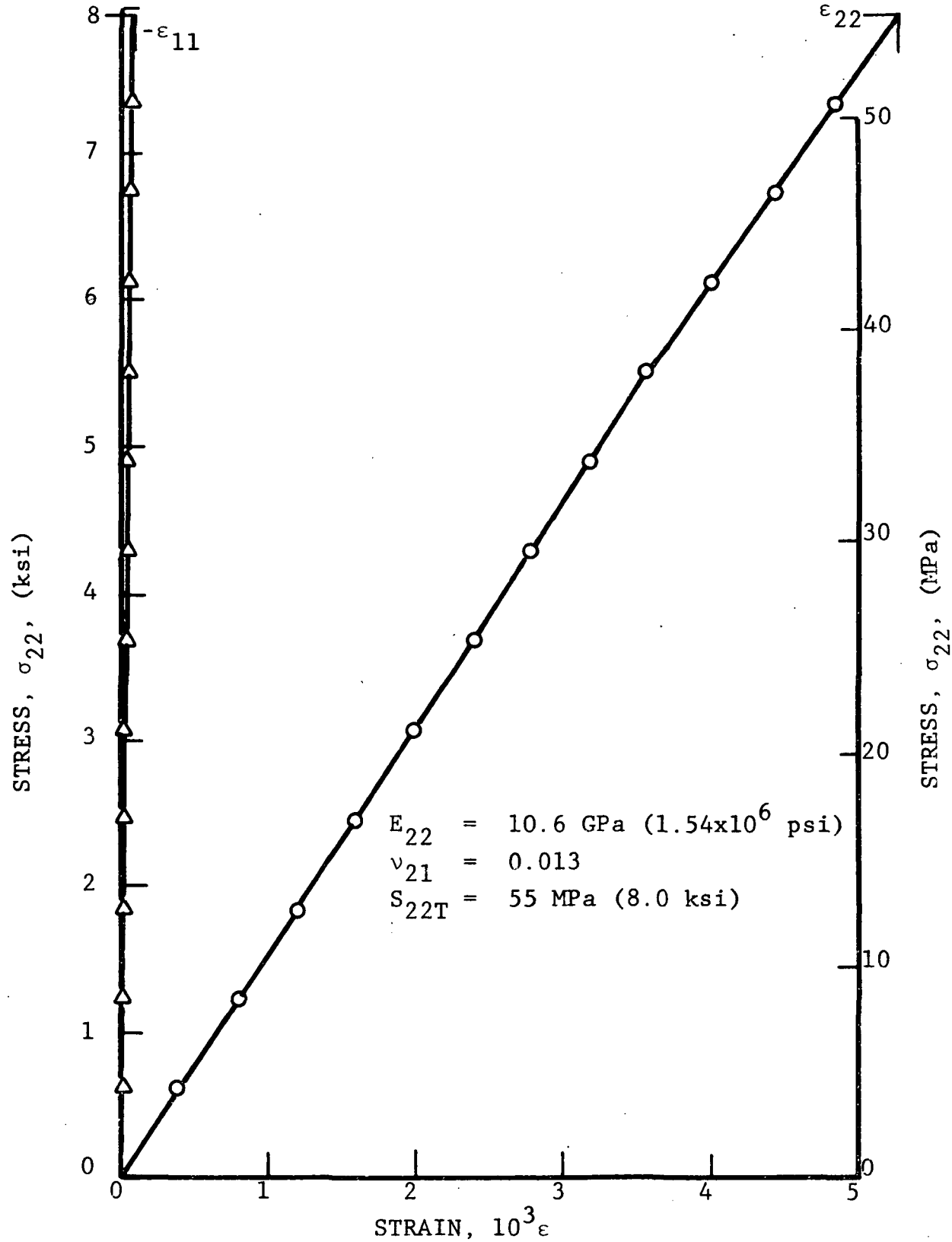

Figure 3.3 STRESS-STRAIN CURVES FOR UNIDIRECTIONAL 90-DEGREE GRAPHITE/EPOXY SPECIMEN UNDER TENSILE LOADING

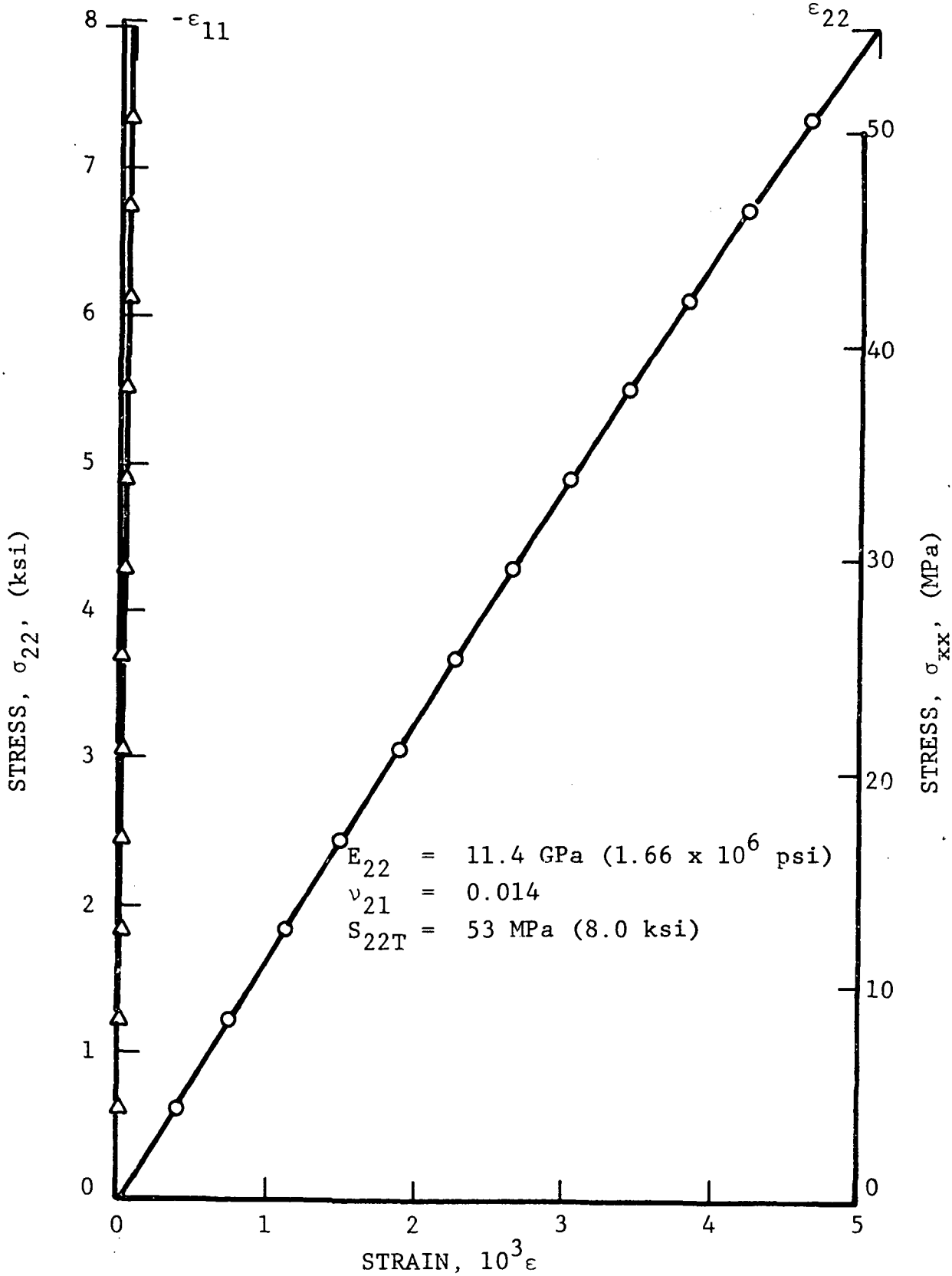

Figure 3.4 STRESS-STRAIN CURVES FOR UNIDIRECTIONAL 90-DEGREE GRAPHITE/EPOXY SPECIMEN UNDER TENSILE LOADING

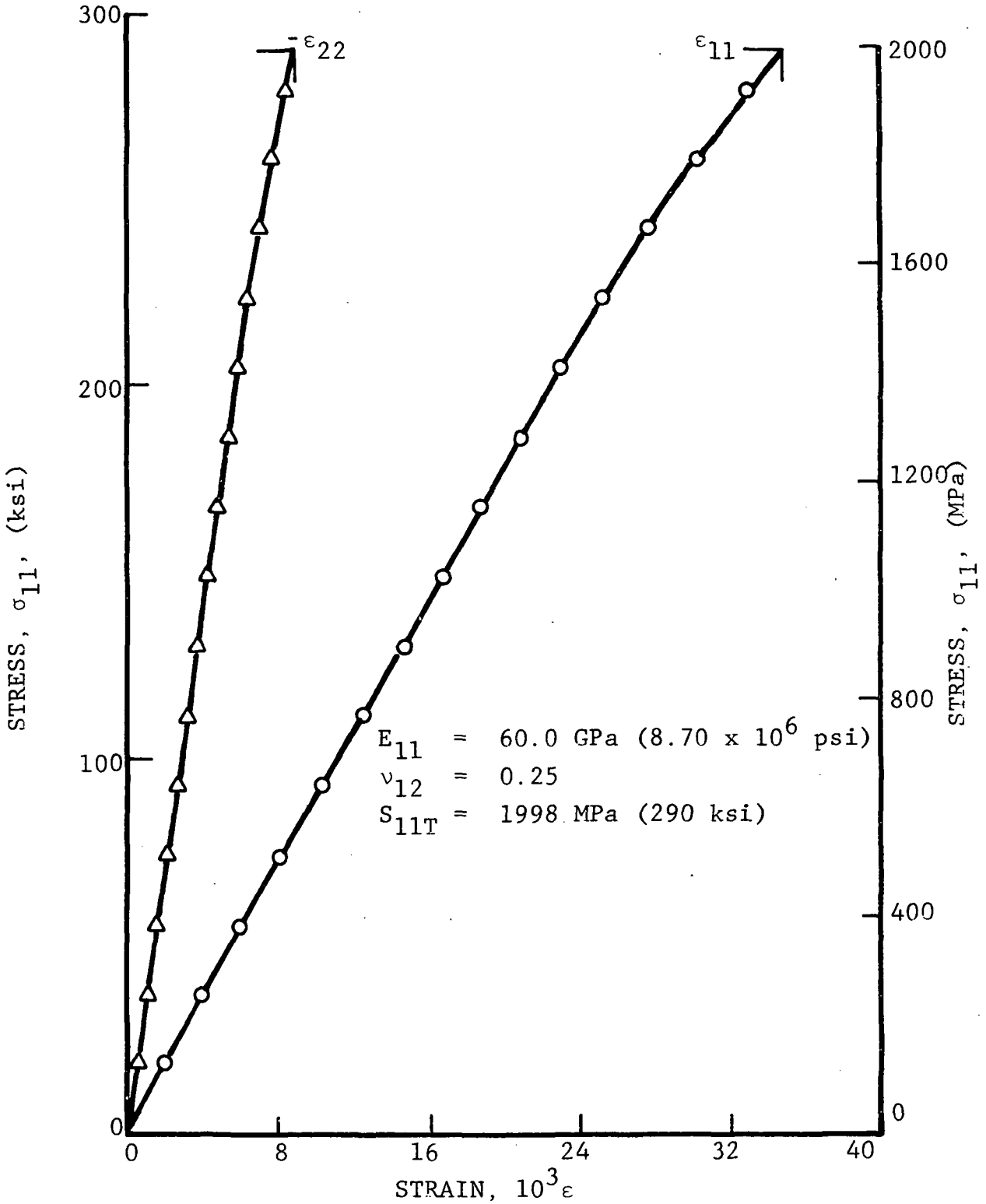

Figure 3.5 STRESS-STRAIN CURVES FOR UNIDIRECTIONAL 0-DEGREE S-GLASS/EPOXY SPECIMEN UNDER TENSILE LOADING

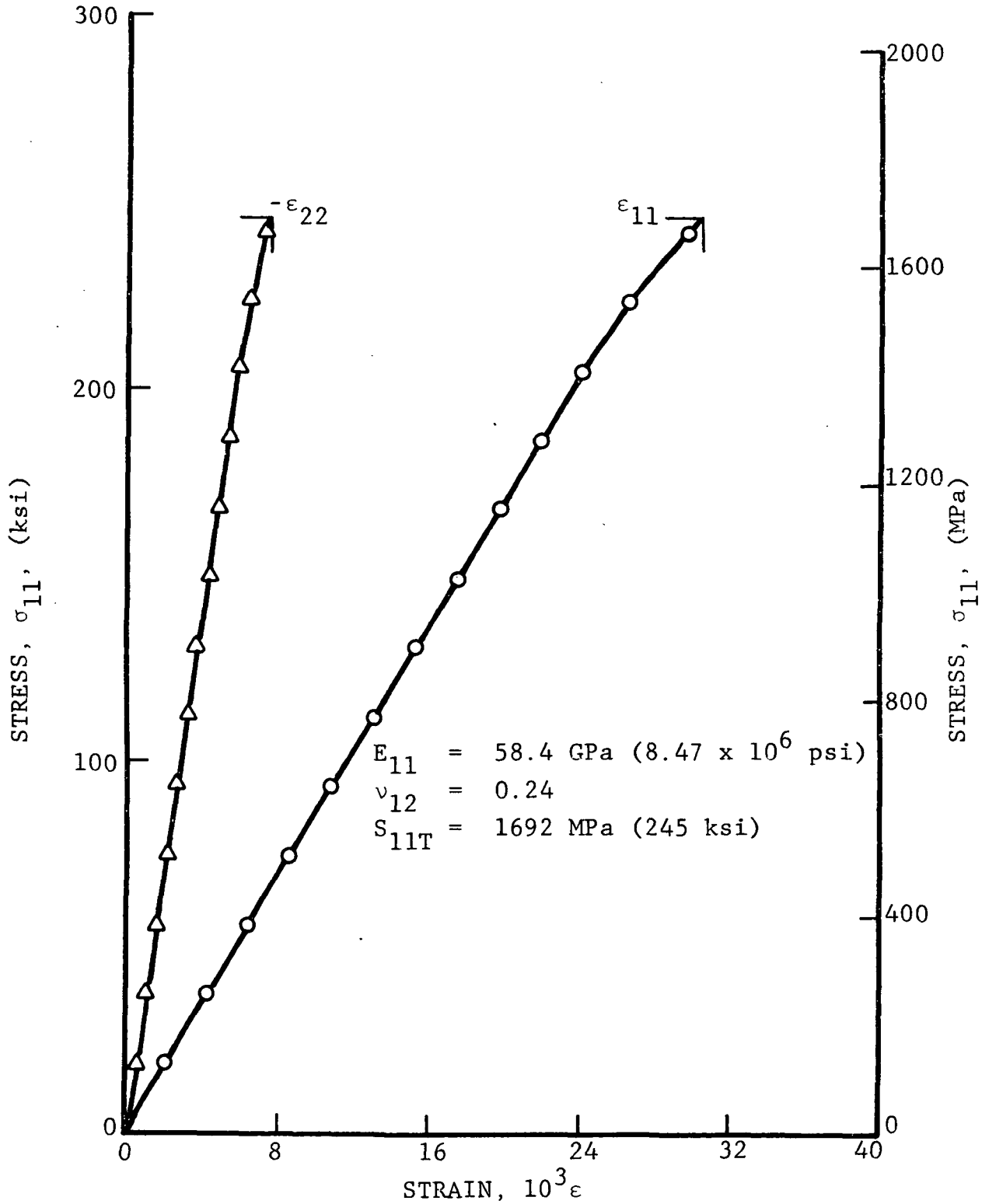

Figure 3.6 STRESS-STRAIN CURVES FOR UNIDIRECTIONAL 0-DEGREE S-GLASS/EPOXY SPECIMEN UNDER TENSILE LOADING

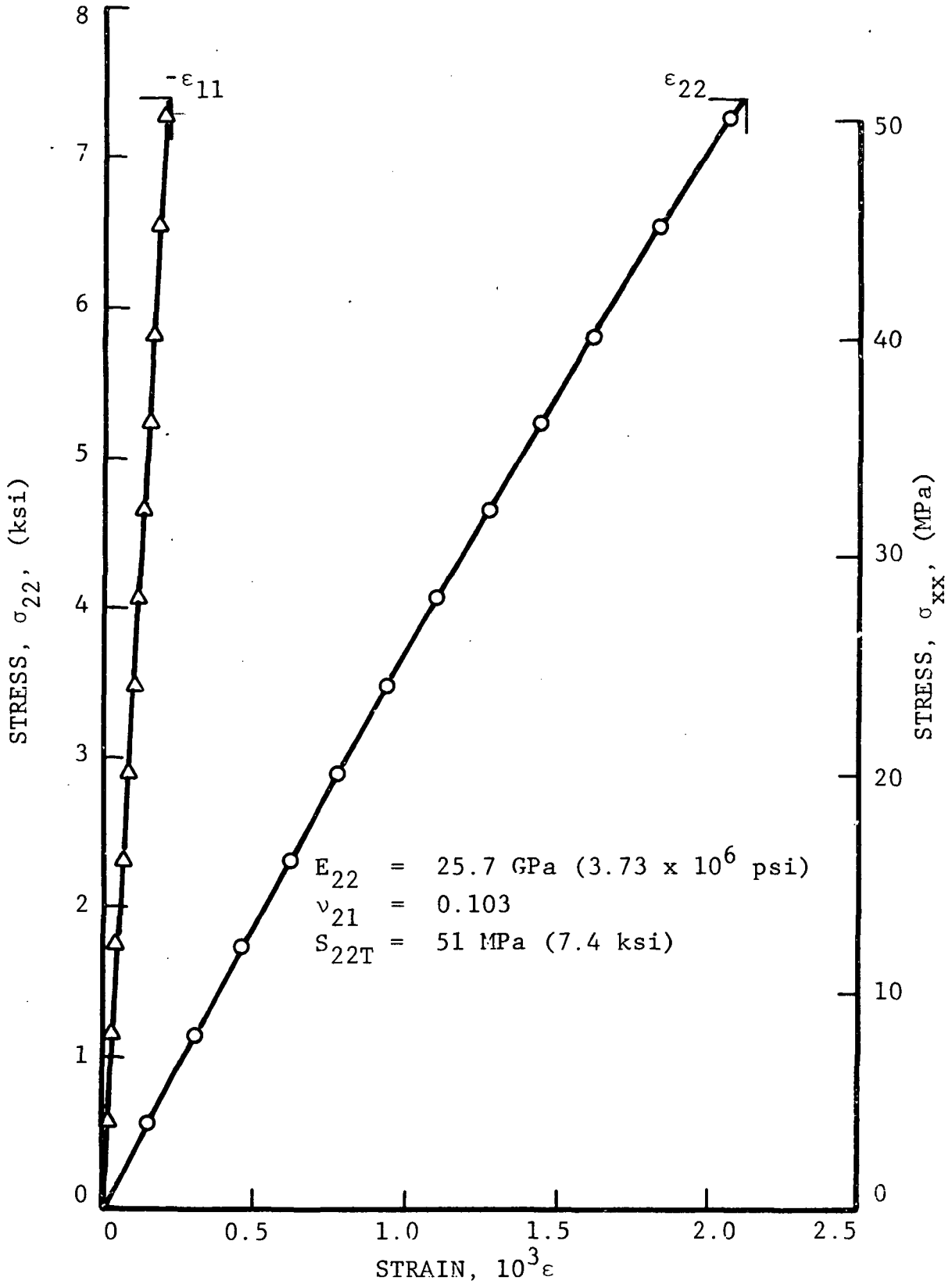

Figure 3.7 STRESS-STRAIN CURVES FOR UNIDIRECTIONAL 90-DEGREE S-GLASS/EPOXY SPECIMEN UNDER TENSILE LOADING

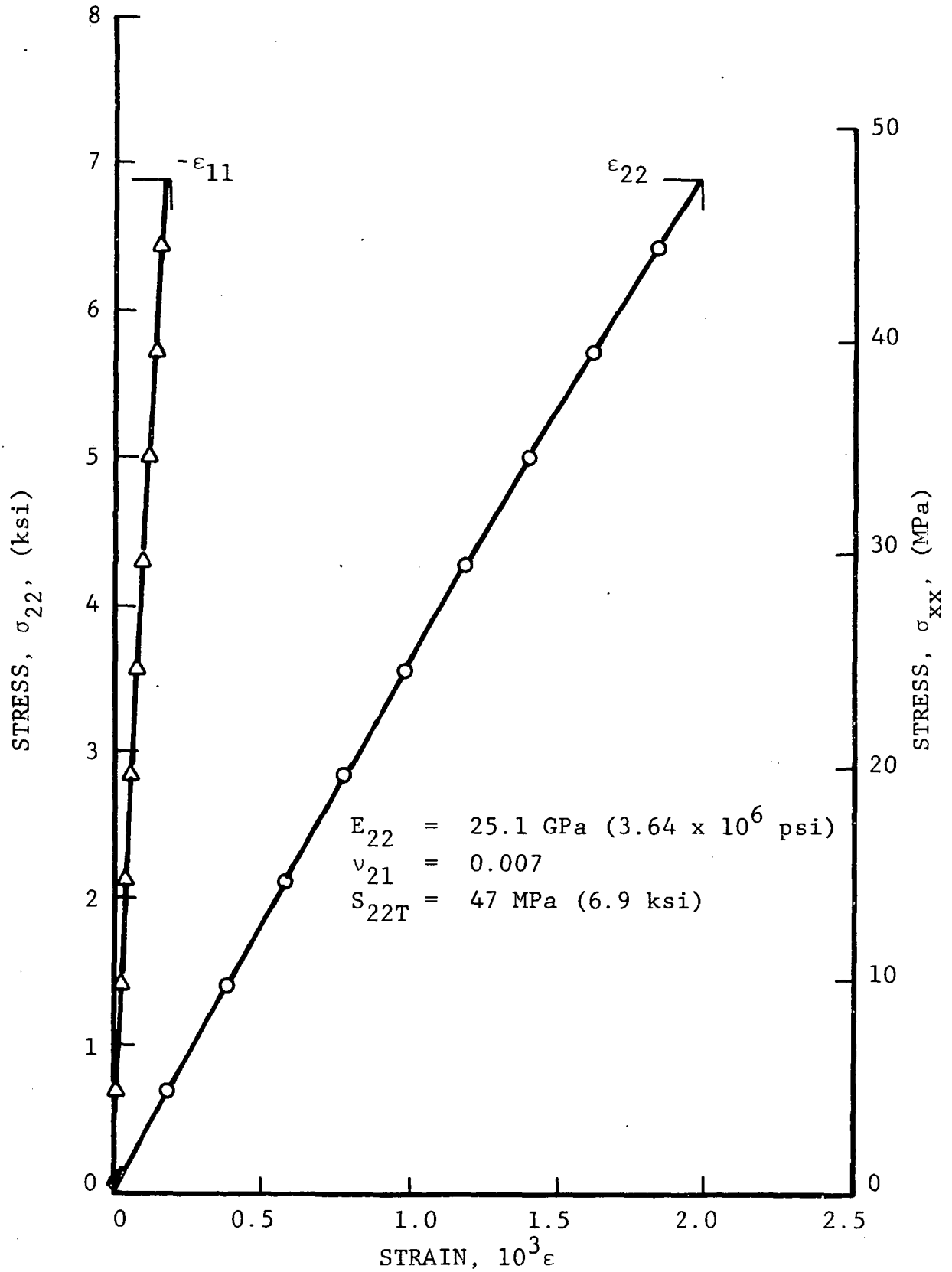

Figure 3.8 STRESS-STRAIN CURVES FOR UNIDIRECTIONAL 90-DEGREES S-GLASS/EPOXY SPECIMEN UNDER TENSILE LOADING

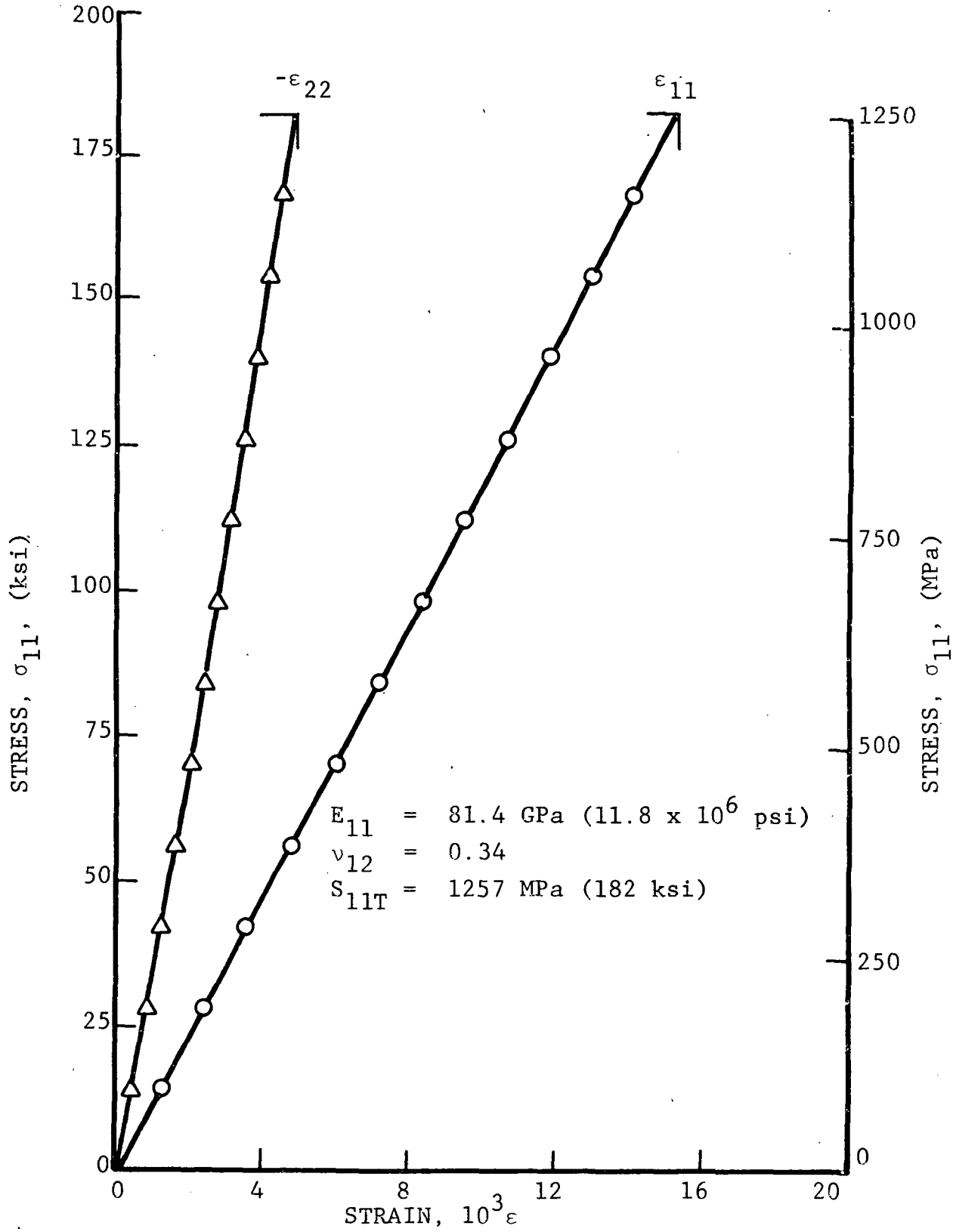

Figure 3.9 STRESS-STRAIN CURVES FOR UNIDIRECTIONAL 0-DEGREE KEVLAR 49/EPOXY SPECIMEN UNDER UNIAXIAL TENSION

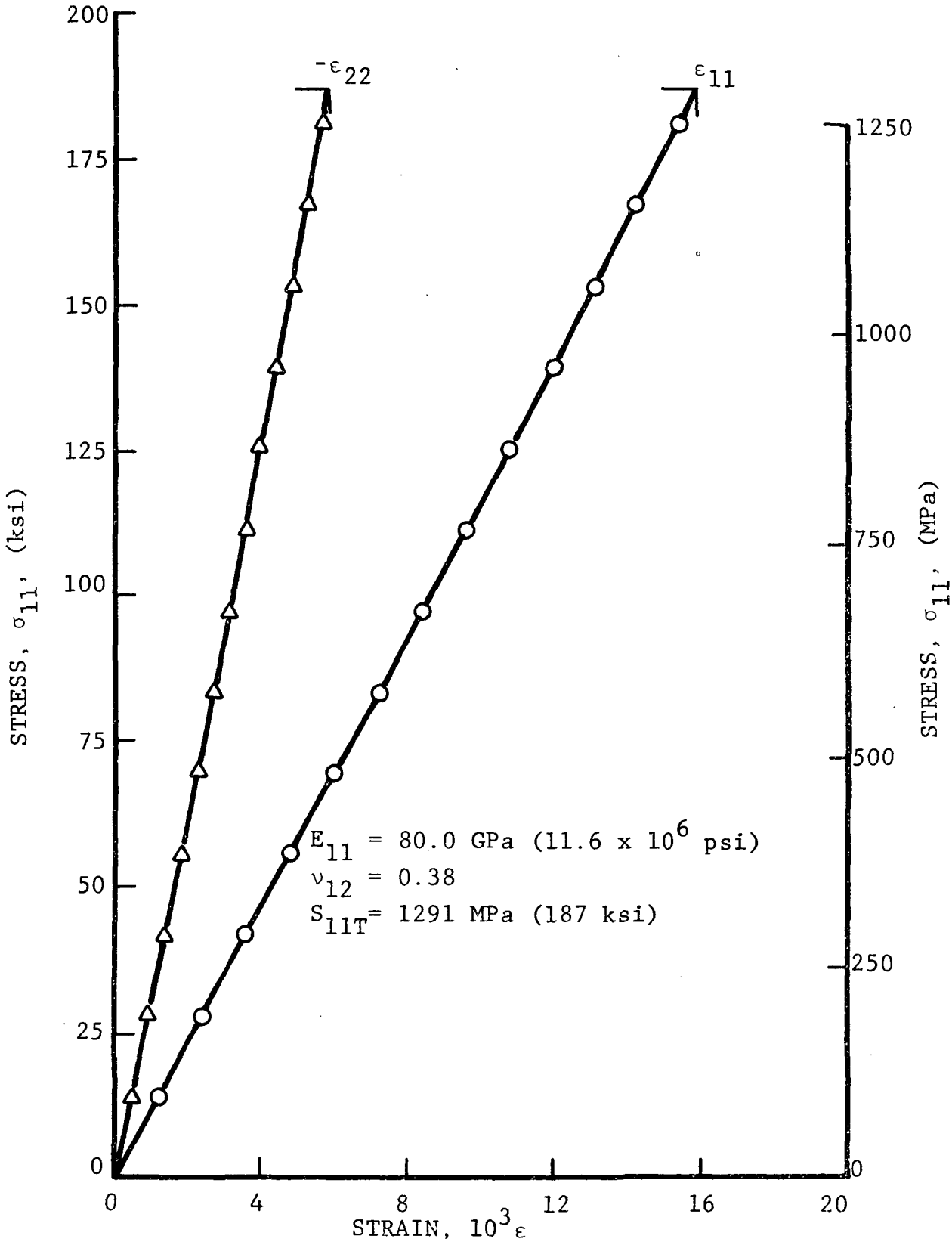

Figure 3.10 STRESS-STRAIN CURVES FOR UNIDIRECTIONAL 0-DEGREE KEVLAR 49/EPOXY SPECIMEN UNDER UNIAXIAL TENSION

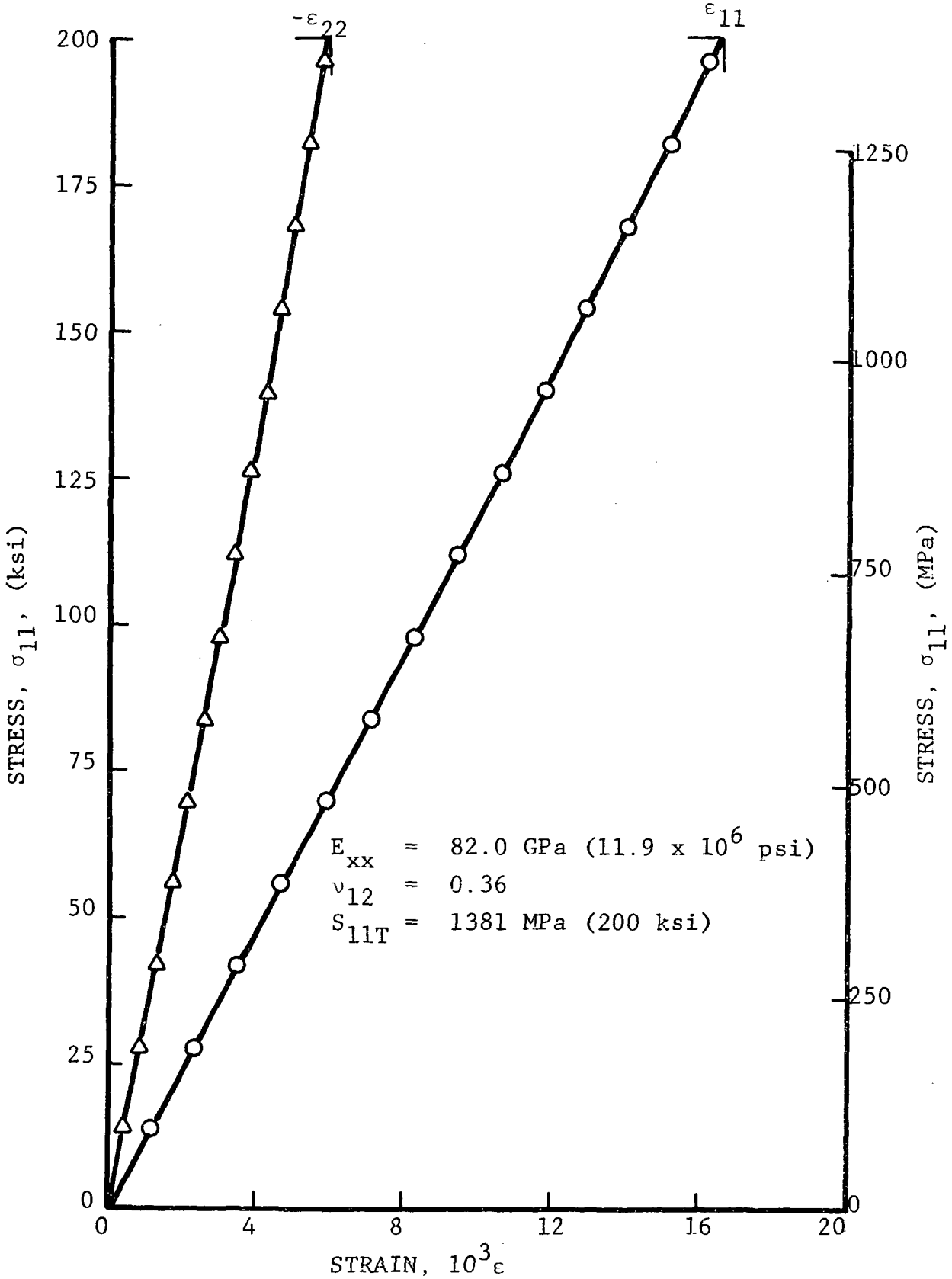

Figure 3.11 STRESS-STRAIN CURVES FOR UNIDIRECTIONAL 0-DEGREE KEVLAR 49/EPOXY SPECIMEN UNDER UNIAXIAL TENSION

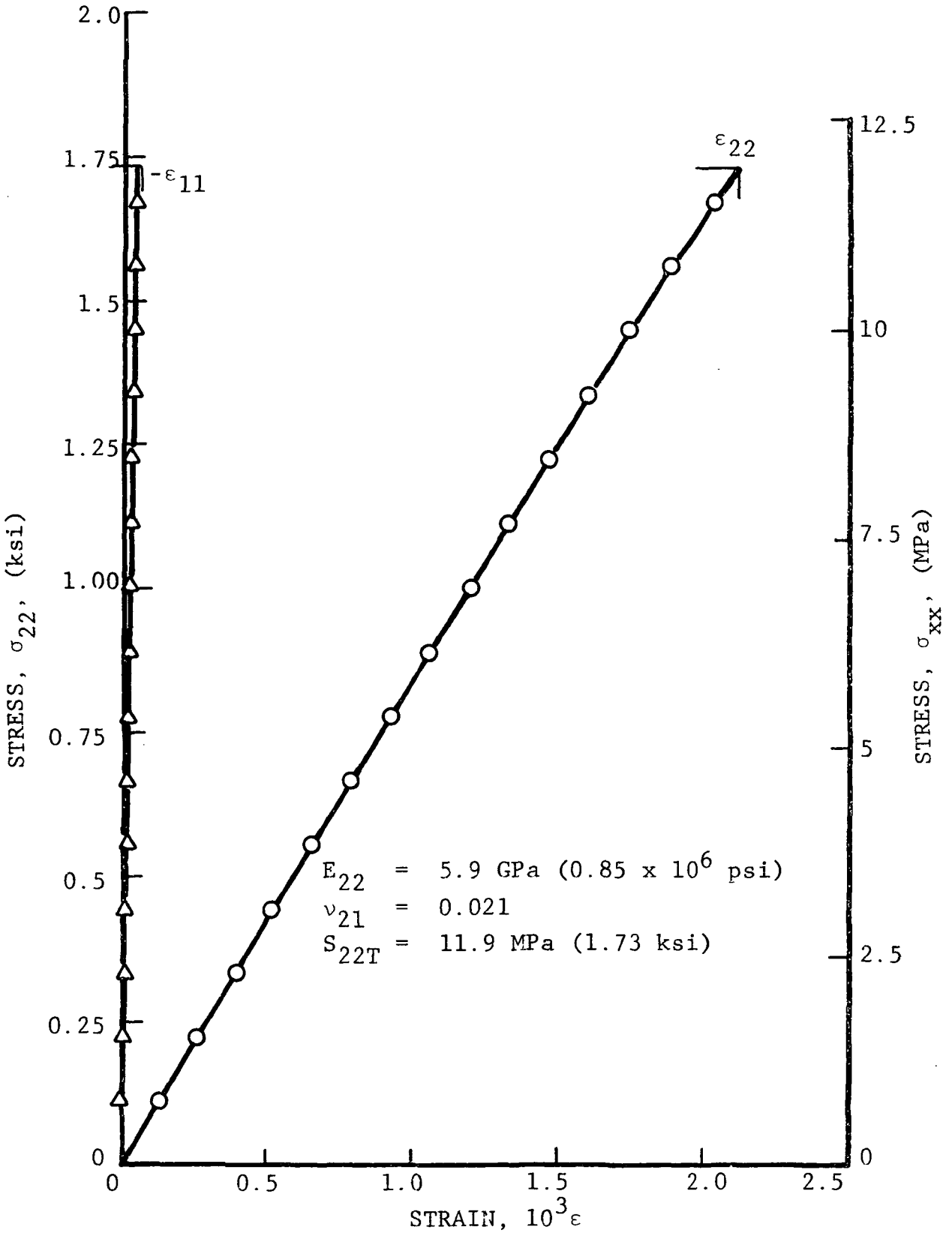

Figure 3.12 STRESS-STRAIN CURVES FOR UNIDIRECTIONAL 90-DEGREE KEVLAR 49/EPOXY SPECIMEN UNDER UNIAXIAL TENSION

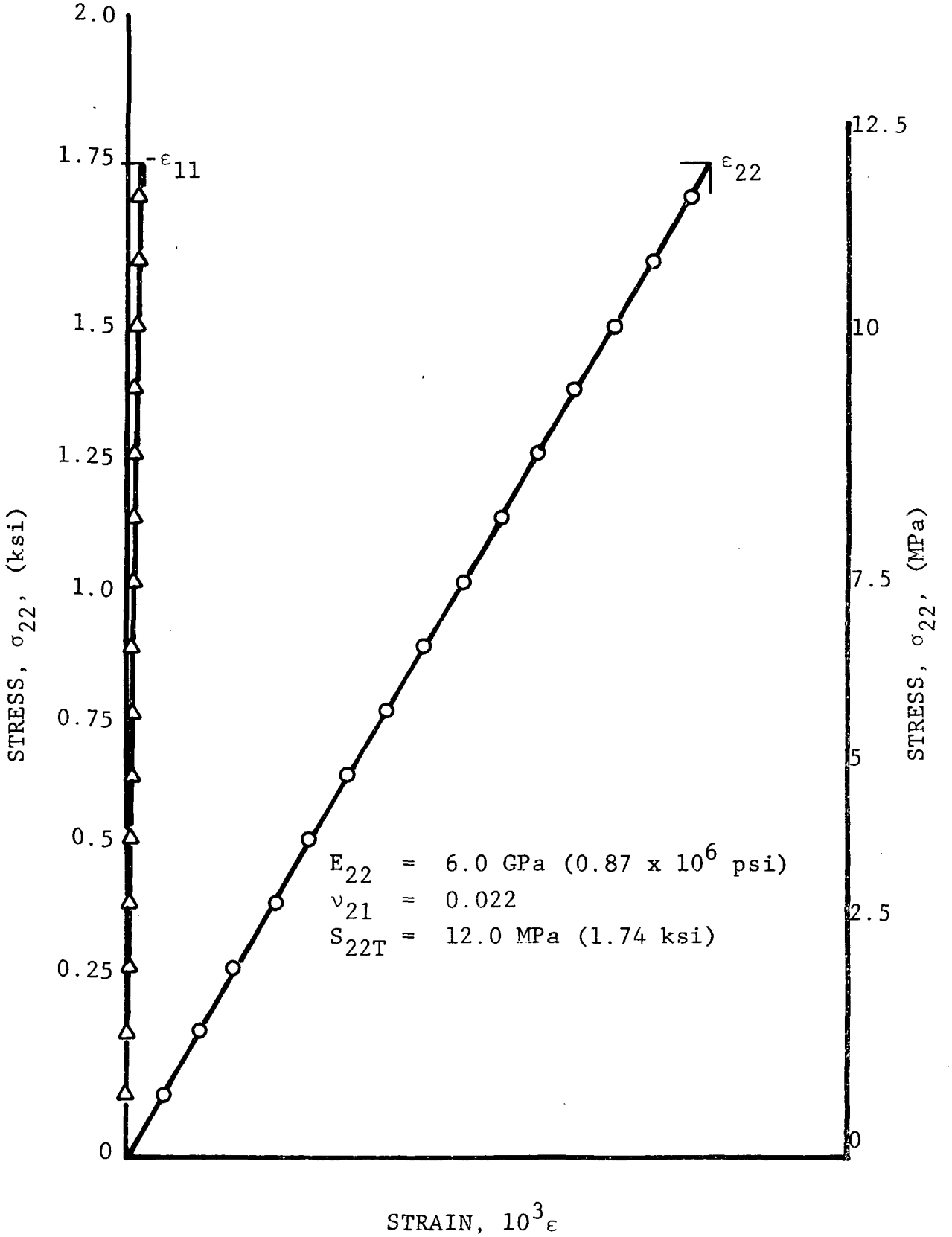

Figure 3.13 STRESS-STRAIN CURVES FOR UNIDIRECTIONAL 90-DEGREE KEVLAR 49/EPOXY SPECIMEN UNDER UNIAXIAL TENSION

4.0 RESULTS AND DISCUSSION

Graphite/epoxy flattened tube and flat coupon specimens of $[\pm 45/0_2]_s$ construction were the first ones fabricated. Comparison of static test results between the two types of specimens served as the basis for improvements in the fabrication and tabbing techniques for the flattened tube specimens. Before compaction of the rounded sides by means of the expanding silicon rubber strips was introduced in the fabrication process (Section 2) the flattened tube specimens showed tensile moduli and Poisson's ratios corresponding to those of the flat coupons but significantly lower strengths. The introduction of the lateral compaction technique eliminated this trend. The compacted flattened tube specimen was therefore adapted as the standard specimen for the remainder of the study. It served well for the static tests but not in fatigue. This will be discussed in greater detail below.

4.1 Static Tests

4.1.1 Graphite/Epoxy $[\pm 45/0_2]_s$ Specimens

Table 4.1 shows the results obtained for the graphite/epoxy $[\pm 45/0_2]_s$ flattened tubes and flat coupons. The average longitudinal tensile modulus for the flattened tubes is 86 GPa (12.5×10^6 psi) identical to that of flat coupons. The corresponding average Poisson's ratios are 0.65 and 0.68 and the ultimate strains are 0.01097 and 0.01062. Deviations of individual specimen results from their averages are relatively small, all less than 10 percent. The average strengths are 942 MPa (137 ksi) for the flattened tubes and 909 MPa (132 ksi) for the flat coupons. Although the higher average strength of the flattened tubes is numerically not significant it does indicate a trend reflected in the strengths of the individual specimens. A representative failure mode for the statically tested flattened tubes is shown in Fig. 4.1 and for the flat coupons in Fig. 4.2. The failure

Table 4-1

RESULTS OF STATIC UNIAXIAL TENSILE TESTS OF GRAPHITE/EPOXY $[\pm 45/0_2]_s$ SPECIMENS

Tensile Modulus E_{xx} GPa	(10^6 psi)	Poisson's Ratio ν_{xy}	Failure Stress, S_{xxT} MPa	(ksi)	Failure Strain, ϵ^u_{xxT} 10^{-3} m/m
Flat Coupons					
87.6	(12.7)	0.69	931	(135)	10.62
86.4	(12.5)	0.70	901	(131)	10.45
86.7	(12.7)	0.70	896	(130)	10.50
83.8	(12.2)	0.64	896	(130)	10.90
-	-	-	922	(134)	-
Average					
86.1	(12.5)	0.68	909	(132)	10.62
Flattened Tubes					
89.6	(13.0)	0.67	930	(135)	10.46
82.7	(12.0)	0.65	935	(135)	11.26
87.2	(12.7)	0.64	967	(140)	10.88
84.3	(12.2)	0.65	942	(137)	11.28
-	-	-	937	(136)	-
Average					
86.0	(12.5)	0.65	942	(137)	10.97

modes are valid test section failures.

Figures 4.3 through 4.10 show the stress-strain curves for the graphite/epoxy $[\pm 45/0_2]_s$ specimens. As expected, the curves for the flattened tubes and flat coupons are quite similar. The longitudinal strains are basically linear to failure. The transverse strains are nonlinear to failure showing a continuous small decrease in slope with load.

4.1.2 S-glass/Epoxy $[\pm 45/0_2]_s$ Specimens

Table 4.2 shows the results obtained for the S-glass/epoxy flattened tubes and flat coupons. The average longitudinal tensile modulus for the flattened tubes is 41 GPa (5.9×10^6 psi) compared with 44 GPa (6.4×10^6 psi) for the flat coupons. The lower modulus for the flattened tube is probably a reflection of scatter in fabrication quality since one of the tubes tested did show a modulus of 44 GPa (6.4×10^6 psi), equal to that of the flat coupons. The average Poisson's ratios are 0.41 for the flattened tubes and 0.43 for the flat coupons. The corresponding ultimate strains are 0.03301 and 0.03138, and strengths are 1043 MPa (151 ksi) and 1026 MPa (149 ksi). The somewhat higher average strength of the flattened tubes is not significant since it does not reflect a corresponding trend among the individual specimens. A typical failure mode for the statically tested flattened tubes is shown in Fig. 4.1. It exhibits a characteristic necking of the test section. The failure mode for the flat coupons is shown in Fig. 4.2. Both types of specimens show valid test section failures.

Figures 4.11 through 4.17 show the stress-strain curves for the S-glass/epoxy specimens. The curves for the flattened tubes and flat coupons show the same characteristics. Both the longitudinal and transverse strains are nonlinear showing a gradually

Table 4-2

RESULTS OF STATIC UNIAXIAL TENSILE TESTS OF S-GLASS/EPOXY $[\pm 45/0_2]_s$ SPECIMENS

Tensile Modulus E_{xx} GPa	(10^6 psi)	Poisson's Ratio ν_{xy}	Failure Stress, S_{xxT} MPa	(ksi)	Failure Strain, ε^u_{xxT} 10^{-3} m/m
Flat Coupons					
44.0	(6.4)	0.43	998	(145)	29.44
43.5	(6.3)	0.42	1017	(148)	30.00
44.1	(6.4)	0.44	1032	(150)	32.80
43.9	(6.4)	0.43	1058	(154)	33.28
Average					
43.9	(6.4)	0.43	1026	(149)	31.38
Flattened Tubes					
39.5	(5.7)	0.33	1021	(148)	33.68
38.0	(5.5)	0.49	1053	(153)	32.36
44.0	(6.4)	0.40	1054	(153)	33.00
Average					
40.5	(5.9)	0.41	1043	(151)	33.01

decreasing slope as stress level increases. The sudden slope change seen in the curves of Figs. 4.11 and 4.12 at high load is most likely due to failure initiation at that load.

4.1.3 Kevlar 49/Epoxy $[\pm 45/0_2]_s$ Specimens

Table 4.3 presents the results obtained for the Kevlar 49/epoxy specimens. The average longitudinal tensile modulus for the flattened tubes is 45 GPa (6.6×10^6 psi) equal to that for the flat coupons. The corresponding average Poisson's ratios are 0.76 and 0.77, the ultimate strains are 0.01797 and 0.01621 and strengths are 796 MPa (115 ksi) and 717 MPa (104 ksi). The higher average strength of the flattened tubes is numerically significant and is reflected as a definite trend observed in the strengths of the individual specimens. Deviations of the individual specimen results from their respective averages are relatively small. A typical failure mode for the statically tested flattened tubes is shown in Fig. 4.1. The characteristic necking of the test section is similar to that of the S-glass specimens. The typical failure modes for the flat coupons is shown in Fig. 4.2. Both the flattened tubes and flat coupons failed with valid test section failures.

Figures 4.18 through 4.27 show the stress-strain curves for the Kevlar 49/epoxy specimens. The curves for the flattened tubes and flat coupons are similar as expected. Both the longitudinal and transverse strains are nonlinear manifested by a small decrease in slope of the curves with increasing stress up to failure.

4.1.4 Graphite/S-glass/Epoxy $[\pm 45^C/0_2{}^G]_s$ Specimens

Table 4.4 presents the results obtained for the hybrid graphite/S-glass/epoxy specimens (superscript C designates graphite and superscript G designates S-glass). The average longitudinal

Table 4-3

RESULTS OF STATIC UNIAXIAL TENSILE TESTS OF KEVLAR 49/EPOXY $[\pm 45/0_2]_s$ SPECIMENS

Tensile Modulus E_{xx} GPa	(10^6 psi)	Poisson's Ratio ν_{xy}	Failure Stress, S_{xxT} MPa	(ksi)	Failure Strain, ε^u_{xxT} 10^{-3} m/m
Flat Coupons					
45.0	(6.5)	0.79	703	(102)	15.90
45.6	(6.6)	0.76	744	(108)	16.60
44.4	(6.4)	0.80	701	(102)	16.20
46.6	(6.8)	0.77	690	(100)	15.44
44.7	(6.5)	0.75	745	(108)	16.92
Average					
45.3	(6.6)	0.77	717	(104)	16.21
Flattened Tubes					
48.2	(7.0)	0.76	716	(104)	15.08
43.4	(6.3)	0.77	767	(111)	18.00
44.2	(6.4)	0.73	820	(119)	18.84
46.9	(6.8)	0.78	834	(121)	18.36
44.2	(6.4)	0.77	841	(122)	19.56
Average					
45.4	(6.6)	0.76	796	(115)	17.97

Table 4-4

RESULTS OF STATIC UNIAXIAL TENSILE TESTS OF GRAPHITE/S-GLASS/EPOXY $[\pm 45^{C}/0_2{}^{G}]_s$ SPECIMENS

(C = graphite, G = S-glass)

Tensile Modulus E_{xx} GPa	(10^6 psi)	Poisson's Ratio ν_{xy}	Failure Stress, S_{xxT} MPa	(ksi)	Failure Strain, ε^{u}_{xxT} 10^{-3} m/m
Flat Coupons					
41.6	(6.0)	0.61	985	(143)	30.72
45.4	(6.6)	0.61	1008	(146)	31.28
41.4	(6.0)	0.62	1015	(147)	33.04
Average					
42.8	(6.2)	0.61	1003	(145)	31.68
Flattened Tubes					
42.1	(6.1)	0.59	945	(137)	28.40
41.4	(6.0)	0.59	986	(143)	29.40
41.4	(6.0)	0.59	1014	(147)	31.20
Average					
41.6	(6.0)	0.59	982	(142)	29.67

tensile modulus for the flattened tubes is 42 GPa (6.0×10^6 psi) which is not significantly different from the value of 43 GPa (6.2×10^6 psi) for the flat coupons. This same trend is evident in the other mechanical properties. Thus, the corresponding average Poisson's ratios are 0.59 for the flattened tubes and 0.61 for the flat coupons, the strengths are 982 MPa (142 ksi) and 1003 MPa (145 ksi) and the ultimate strains are 0.02967 and 0.03168, respectively. The flattened tubes show a somewhat lower strength than the flat coupons. It is not numerically significant and is primarily due to one specimen out of the three tested failing at a low strength.

Figure 4.1 shows a typical failure mode for the statically tested flattened tube specimens of hybrid construction. It reveals failure occurring not only in the test section but also near the gripping tab. Even in the test section failure occurred by splitting of the outer $\pm$45-deg. graphite plies along the transition between the rounded and flat sections of the specimen. These additional failure modes contribute to strength reduction. Therefore, the true tensile strength of the material is probably greater than indicated by the data in Table 4.4. Figure 4.2 shows a typical failure mode for the flat coupons. In contrast to the flattened tubes it is a valid test section failure.

The stress-strain curves for the statically tested hybrid specimens are shown in Figs. 4.28 through 4.33. The stress-strain behavior is similar for both types of specimens, flattened tubes and flat coupons. Both the longitudinal and transverse strains are nonlinear to failure showing a decrease of slope up to failure. The stress-strain behavior of the hybrids, their moduli, strengths and ultimate strains show characteristics and values close to those of the S-glass/epoxy specimens. This indicates that the behavior of the hybrids is strongly dominated by the 0-degree S-glass plies.

4.1.5 Graphite/Epoxy $[0_2/\pm45]_s$ Specimens

Ten graphite/epoxy flat coupon specimens of $[0_2/\pm45]_s$ construction were fabricated for static testing. Of these, seven were tested for strength determinations only and three were tested with strain gage instrumentation to determine modulus and Poisson's ratio as well as strength and ultimate strain. The results are shown in Table 4.5. The average longitudinal modulus is 85.7 GPa (12.4 x 10^6 psi), Poisson's ratio is 0.66 and ultimate strain is 0.00985. The strengths range from 786 MPa (114 ksi) to 951 MPa (138 ksi). The average strength is 855 MPa (124 ksi). This is lower than the average strength for the graphite/epoxy flat coupon specimens of $[\pm45/0_2]_s$ construction, which is shown in Table 4.1 as 909 MPa (132 ksi).

Figures 4.34 through 4.36 show the stress-strain curves for the instrumented specimens. The strains are essentially linear to failure showing minimal decrease in modulus with increase in stress.

Flattened tubular graphite/epoxy specimens of $[0_2/\pm45]_s$ construction were fabricated and tested statically in tension. Consistently, because of parasitic failure modes they showed substantially lower strengths than the flat coupons. Their strengths ranged from 620 MPa (90 ksi) to 696 MPa (101 ksi). The parasitic failure modes manifested themselves as ripping of the outer 0-degree plies along the length of the specimen at the crown of the rounded sides. Attempts to modify specimen fabrication to eliminate this phenomenon were unsuccessful. As a consequence the fabrication and testing of the flattened tube graphite/epoxy specimens of the $[0_2/\pm45]_s$ construction was subsequently discontinued.

Table 4.5

RESULTS OF STATIC UNIAXIAL TENSILE TESTS OF GRAPHITE/EPOXY $[0_2/\pm45]_s$ SPECIMENS

Tensile Modulus E_{xx} GPa	(10^6 psi)	Poisson's Ratio xy	Failure Stress, S_{xxT} MPa	(ksi)	Failure Strain, ε^u_{xxT} 10^{-3} m/m
Flat Coupons					
80.7	(11.7)	0.61	790	(114)	9.76
86.9	(12.6)	0.66	864	(125)	10.10
89.6	(13.0)	0.67	863	(125)	9.70
			814	(118)	
			834	(121)	
			834	(121)	
			848	(123)	
			855	(124)	
			903	(131)	
			951	(138)	
Average					
85.7	(12.4)	0.66	855	(124)	9.85

4.2 Fatigue Tests

4.2.1 Graphite/Epoxy $[\pm 45/0_2]_s$ Specimens

The fatigue test results for the graphite/epoxy $[\pm 45/0_2]_s$ flattened tube specimens and flat coupons are summarized in Table 4.6 and Fig. 4.37. The figure shows the actual data points as well as a straight line drawn to indicate approximately the trend of the data.

The fatigue data for the flattened tube specimens fall in the range of 3.8×10^4 to 1.2×10^7 cycles. In this range the data points span a fatigue strength of 58.0 percent to 70.0 percent of static strength. Two specimens survived the runout of 10^7 cycles. They were tested statically in tension to failure to determine their residual properties. Their stress-strain curves are shown in Figs. 4.38 and 4.39.

The specimen which survived cycling to 58.0 percent of static strength had the following residual properties:

E_{xx} = 80.7 GPa (11.7×10^6 psi)
ν_{xy} = 0.64
S_{xxT} = 966 MPa (140 ksi)
ε^u_{xxT} = 0.01210

The specimen which survived cycling to 60.0 percent of static strength had the following residual properties:

E_{xx} = 72.4 GPa (10.5×10^6 psi)
ν_{xy} = 0.71
S_{xxT} = 896 MPa (130 ksi)
ε^u_{xxT} = 0.01234

Both specimens show a significant decrease in tensile modulus as compared with initial static properties listed in Table 4.1. One

Table 4-6

RESULTS OF TENSILE CYCLING FATIGUE TESTS OF $[\pm 45/0_2]_s$ GRAPHITE/EPOXY SPECIMENS

Maximum Cyclic Stress				
MPa	ksi	Percent of Average Static Strength	Cycles to Failure	
Flat Coupon				
676.4	(98.1)	74.3	1.244×10^7	Runout
696.4	(101)	76.3	7.730×10^6	
699.1	(101)	76.8	1.498×10^6	
701.9	(102)	77.1	4.974×10^6	
701.5	(102)	77.1	5.89×10^5	
703.9	(102)	77.3	3.55×10^5	
706.0	(102)	77.6	7.240×10^6	
719.1	(104)	79.0	6.77×10^5	
737.7	(107)	81.1	6.52×10^5	
Flattened Tube				
547.9	(79.5)	58.0	1.000×10^7	Runout
566.7	(82.2)	60.0	1.230×10^7	Runout
566.7	(82.2)	60.0	4.604×10^6	
576.2	(83.6)	61.0	4.500×10^6	
580.9	(84.3)	61.5	1.132×10^7	
585.6	(84.9)	62.0	8.304×10^6	
585.6	(84.9)	62.0	2.907×10^6	
595.1	(86.3)	63.0	1.89×10^5	
604.5	(87.7)	64.0	1.232×10^6	
623.4	(90.4)	66.0	3.26×10^5	
661.2	(95.9)	70.0	3.8×10^4	

specimen also shows a drop in strength and an increase in Poisson's ratio.

Fatigue results for the graphite/epoxy flat coupons are in the range of 3.6×10^5 to 1.2×10^7 cycles. In this range the data encompass fatigue strengths from 74.3 percent to 81.1 percent of static strength. The specimen cycled to 74.3 percent of static strength survived the runout of 10^7 cycles. Visual inspection revealed edge delaminations of the $\pm$45-degree plies. The specimen was tested in tension to failure to determine its residual properties. It showed a strength reduction to 854 MPa (124 ksi). The tensile modulus decreased but Poisson's ratio showed no significant difference in comparison with initial static properties listed in Table 4.1. The residual stress-strain curves are shown in Fig. 4.40 and the properties are listed below.

E_{xx} = 82.3 GPa (11.9×10^6 psi)
ν_{xy} = 0.70
S_{xxT} = 854 MPa (124 ksi)
ε^u_{xxT} = 0.01050

The trend lines in Fig. 4.37 indicate that the flattened tube data, although exhibiting the same trends as the flat coupons, show a significantly lower fatigue strength. Most likely this is due to parasitic stresses occurring at the transition between the rounded and flat sections of the specimen forcing the failure modes to occur by splitting of the $\pm$45-degree plies along this transition. This splitting can be observed in the typical failure mode shown in Fig. 4.1. By further refining the specimen fabrication technique a smoother transition between the rounded and flat sections of the specimen could likely be achieved eliminating this parasitic failure. A typical failure mode for the flat coupon specimens is shown in Fig. 4.2.

Another possible cause of the lower fatigue strength of the lfattened tubes is heating due to cycling. Temperatures during cycling were monitored on some of the specimens using clipped-on thermocouples. The flattened tubes become substantially hotter during cycling than flat coupons. This is due to the tubular shape. It encloses a trapped air volume in contact with half the specimen surface, not subject to convective cooling by ambient air as is the case with the outside specimen surface and as is the case with the surfaces of the flat coupon. During cycling the specimen reaches an approximately constant plateau temperature of up to 40 degK (72°F) above ambient, and shows a rapid rise above the plateau just before failure. Failure temperatures of up to 46 degK (83°F) above ambient have been recorded. Generally the longer the cycle life the greater was the temperature rise at failure. This is not surprising. Since the difference in maximum load levels for the various life lengths was relatively small, the heat generating damage accumulation due to cycling duration dominated over that due to maximum load level. The heating phenomenon may be either a contributing cause to specimen failure or a symptom of gradual specimen degradation or both. If it is a contributing cause it can be eliminated by air cooling of the specimen during cycling using an air blower.

4.2.2 S-Glass/Epoxy $[\pm 45/0_2]_s$ Specimens

Fatigue results for the S-glass/epoxy specimens are presented in Table 4.7 and Fig. 4.41. For the flattened tube specimens the data fall in the range of 4.4×10^5 to 1.2×10^7 cycles. As expected for glass/epoxy laminates the fatigue strength is quite low spanning only 17.5 to 20.0 percent of static strength. The specimen cycled to 17.5 percent of static strength survived the runout to 1.2×10^7 cycles. It was tested statically in tension to determine its residual properties. The residual test stress-strain curves are shown in Fig. 4.42 and the properties derived from them are listed below:

Table 4-7

RESULTS OF TENSILE CYCLING FATIGUE TESTS OF $[\pm 45/0_2]_s$ S-GLASS/EPOXY SPECIMENS

Maximum Cyclic Stress		Percent of Average Static Strength	Cycles to Failure	
MPa	(ksi)			
Flat Coupon				
164.1	(23.8)	16.0	1.000×10^7	Runout
168.9	(24.5)	16.4	1.000×10^7	Runout
178.6	(25.9)	17.4	8.070×10^6	
188.9	(27.4)	18.4	3.989×10^6	
208.9	(30.3)	20.3	2.410×10^6	
213.7	(31.0)	20.8	1.062×10^6	
219.3	(31.8)	21.3	1.046×10^6	
228.9	(33.2)	22.3	1.117×10^6	
233.7	(33.9)	22.8	7.06×10^5	
238.6	(34.6)	23.2	3.69×10^5	
Flattened Tube				
182.0	(26.4)	17.5	1.239×10^7	Runout
182.0	(26.4)	17.5	9.085×10^6	
184.1	(26.7)	17.7	2.937×10^6	
186.2	(27.0)	17.9	2.386×10^6	
187.5	(27.2)	18.0	2.866×10^6	
187.5	(27.2)	18.0	3.363×10^6	
192.4	(27.9)	18.5	1.662×10^6	
197.9	(28.7)	19.0	1.35×10^6	
202.7	(29.4)	19.5	8.50×10^5	
208.2	(30.2)	20.0	4.42×10^5	

E_{xx} = 44.7 GPa (6.49 x 10^6 psi)
ν_{xy} = 0.43
S_{xxT} = 913 MPa (132 ksi)
ε^u_{xxT} = 0.02320

The residual modulus and Poisson's ratio show no significant differences from corresponding initial static properties listed in Table 4.2. The residual strength, however, shows a reduction to 913 MPa (132 ksi).

Results for the S-glass/epoxy flat coupons are in the range of 3.7 x 10^5 to 1.0 x 10^7 cycles. The fatigue strength for this range is quite low as expected, spanning only 16.0 to 23.3 percent of static strength. The two specimens cycled to 16.0 and 16.4 percent of static strength survived the runout to 1.0 x 10^7 cycles and were subsequently tested in tension to failure to determine their residual properties. The stress-strain curves are shown in Figs. 4.43 and 4.44.

The specimen which survived cycling to 16.0 percent of static strength had the following residual properties:

E_{xx} = 39.6 GPa (5.75 x 10^6 psi)
ν_{xy} = 0.40
S_{xxT} = 835 MPa (121 ksi)
ε^u_{xxT} = 0.02500

The specimen which survived cycling to 16.4 percent of static strength had the following residual properties:

E_{xx} = 38.7 GPa (5.62 x 10^6 psi)
ν_{xy} = 0.42
S_{xxT} = 763 MPa (111 ksi)
ε^u_{xxT} = 0.02360

Both specimens show a decrease in tensile modulus to 40 GPa (5.75×10^6 psi) and 39 GPa (5.62×10^6 psi) respectively, and a substantial decrease in strength to 835 MPa (121 ksi) and 763 MPa (111 ksi). Poisson's ratios show no significant changes.

It can be observed from the trend lines in Fig. 4.41 that in general the fatigue strength of the flattened tube specimens is somewhat lower than that of the flat coupons except near 10^7 cycles where the trend reverses. Most likely this is again due to parasitic stresses occurring at the transition between the rounded and flat sections of the specimen. The telltale splitting mode of failure of the $\pm$45-degree plies can be observed in Fig. 4.1. The failure mode for the flat coupon specimens is illustrated in Fig. 4.2.

The difference in fatigue strength between the flattened tubes and the flat coupons in the case of the S-glass/epoxy specimens is substantially smaller than in the case of the graphite/epoxy specimens. This may be due to the contributing effect of heating during cycling. Because of the lower fatigue loads, the plateau temperature of the S-glass/epoxy specimens during cycling was of the order of 20 degK (36°F) above ambient, which is significantly lower than for the graphite/epoxy specimens. Just before failure the S-glass/epoxy specimens did exhibit a very substantial rise in temperature of the order of 56 degK (100°F) above ambient.

4.2.3 Kevlar 49/Epoxy $[\pm 45/0_2]_s$ Specimens

Fatigue results for the Kevlar 49/epoxy specimens are shown in Table 4.8 and Fig. 4.45. The data for the flattened tube specimens fall in the range of 1.3×10^5 to 1.3×10^7 cycles. In this range the data encompass fatigue strengths from 36.0 to 52.0 percent of static strength. The specimen cycled to 36.0 percent of static strength survived the runout to

Table 4-8

RESULTS OF TENSILE CYCLING FATIGUE TESTS OF $[\pm 45/0_2]_s$ KEVLAR-49/EPOXY SPECIMENS

Maximum Cyclic Stress			
MPa	(ksi)	Percent of Average Static Strength	Cycles to Failure
Flat Coupon			
329.6	(47.8)	46.0	1.231×10^7 Runout
337.2	(48.9)	47.0	1.000×10^7
344.0	(49.9)	48.0	6.765×10^6
358.5	(52.0)	50.0	3.028×10^6
365.4	(53.0)	51.0	5.617×10^7
376.5	(54.6)	52.5	1.020×10^7 Runout
387.5	(56.2)	54.0	1.0819×10^7
397.8	(57.7)	55.5	3.302×10^6
405.4	(58.8)	56.5	2.433×10^6
412.3	(59.8)	57.5	1.016×10^6
Flattened Tube			
285.4	(41.4)	36.0	1.025×10^7 Runout
290.0	(42.0)	36.5	1.298×10^7
293.7	(42.6)	37.0	5.937×10^6
301.3	(43.7)	38.0	2.106×10^6
309.6	(44.9)	39.0	1.035×10^6
317.2	(46.0)	40.0	2.456×10^6
333.0	(48.3)	42.0	3.074×10^6
348.9	(50.6)	44.0	1.651×10^6
380.6	(55.2)	48.0	4.16×10^5
412.3	(59.8)	52.0	1.34×10^5

1.0×10^7 cycles and was subsequently tested statically in tension to determine its residual properties. Figure 4.46 shows the stress-strain curves obtained. The residual properties are listed below:

E_{xx} = 49 GPa (7.10×10^6 psi)
ν_{xy} = 0.89
S_{xxT} = 627 MPa (91 ksi)
ε^u_{xxT} = 0.01280

Both the tensile modulus and Poisson's ratio are on the high side as compared with initial static properties listed in Table 4.3. The strength shows a significant reduction to 627 MPa (91 ksi).

Fatigue results for the Kevlar 49/epoxy flat coupons fall in the range of 1.0×10^5 to 1.2×10^7 cycles. The data encompass fatigue strengths from 46.0 to 57.5 percent of static strength. Three out of the four specimens cycled to 10^7 cycles or more survived this runout. They were cycled to 46.0, 47.0 and 52.5 percent of static strength. These were subsequently tested in tension to failure to determine their residual properties. The stress-strain curves are shown in Figs. 4.47 through 4.49. The residual properties derived from them are

E_{xx} = 43.7 GPa (6.34×10^6 psi)
$_{xy}$ = 0.82
S_{xxT} = 696 MPa (101 ksi)
$^u_{xxT}$ = 0.01630

for the specimen which survived cycling to 46.0 percent of static strength

E_{xx} = 47.0 GPa (6.81×10^6 psi)
ν_{xy} = 0.73
S_{xxT} = 510 MPa (74 ksi)
ε^u_{xxt} = 0.01104

for the specimen which survived cycling to 47.0 percent of static strength, and

$$E_{xx} = 45.0 \text{ GPa } (6.53 \times 10^6 \text{ psi})$$
$$\nu_{xy} = 0.80$$
$$S_{xxT} = 655 \text{ MPa } (95 \text{ ksi})$$
$$\varepsilon^u_{xxt} = 0.01500$$

for the specimen which survived cycling to 52.5 percent of static strength. The residual moduli and Poisson's ratios show no significant differences from corresponding initial static properties listed in Table 4.3. The residual strengths, however, show a reduction in two out of the three specimens to 655 MPa (95 ksi) for the specimen cycled to 46.0 percent of static strength and to 510 MPa (74 ksi) for the specimen cycled to 47.0 percent of static strength.

It is evident from Fig. 4.45 that the fatigue data for both types of specimens exhibit significant scatter. The trend lines for both types of specimens run parallel but the fatigue strength for the flattened tubes is significantly lower. All of the flattened tube specimens exhibited the splitting mode of failure at the transition between the rounded and flat sections of the specimen and most of them also failed near the gripping tabs as illustrated by the typical failure mode shown in Fig. 4.1. These parasitic failure modes are the most likely reasons for the reduced fatigue strength of the flattened tube specimens. The failure modes for the flat coupons are illustrated in Fig. 4.2.

4.2.4 Graphite/S-Glass/Epoxy $[\pm 45^C/0_2^G]_s$ Specimens

Fatigue results for the graphite/S-glass/epoxy specimens are shown in Table 4.9 and Fig. 4.50. For the flattened tube specimens the data fall in the range of 2.1×10^5 to 1.3×10^7 cycles. The fatigue strengths for this range are quite low and span from 20.5 to 27.5 percent of static strength. The specimen

Table 4-9

RESULTS OF TENSILE CYCLING FATIGUE TESTS
OF $[\pm 45^{C}/0_2{}^{G}]_s$ GRAPHITE/S-GLASS/EPOXY SPECIMENS

Maximum Cyclic Stress				
MPa	(ksi)	Percent of Average Static Strength	Cycles to Failure	
Flat Coupon				
240.0	(34.8)	24.0	1.002×10^7	Runout
250.3	(36.3)	25.0	5.123×10^6	
260.0	(37.7)	26.0	5.154×10^6	
280.0	(40.6)	28.0	3.049×10^6	
300.0	(43.5)	30.0	2.103×10^6	
340.0	(49.3)	34.0	1.45×10^5	
Flattened Tube				
201.0	(29.2)	20.5	4.077×10^6	
210.8	(30.6)	21.5	1.264×10^7	Runout
220.6	(32.0)	22.5	4.436×10^6	
230.4	(33.4)	23.5	3.166×10^6	
240.0	(34.8)	24.5	2.054×10^6	
250.0	(36.3)	25.5	1.077×10^6	
269.6	(39.1)	27.5	2.14×10^5	

cycled to 21.5 percent of static strength survived the runout of 1.3×10^7 cycles and was tested in tension to failure to determine its residual properties. The stress-strain curves for this surviving specimen are shown in Fig. 4.51 and the residual properties are listed below:

E_{xx} = 42.0 GPa (6.1×10^6 psi)
ν_{xy} = 0.62
S_{xxT} = 648 MPa (94 ksi)
ε^u_{xxT} = 0.02060

No significant differences in tensile modulus or Poisson's ratio are observed compared with the initial static properties listed in Table 4.4. The residual strength shows a substantial decrease from the initial static strength of 982 MPa (142 ksi).

Fatigue results for the graphite/S-glass/epoxy flat coupons fall in the range of 1.5×10^5 cycles to 1.0×10^7 cycles. The fatigue strengths for this range are quite low and span only 24.0 to 34.0 percent of static strength. The specimen cycled to 24.0 percent of static strength survived the runout of 1.0×10^7 cycles and was tested statically in tension to failure to determine its residual properties. Figure 4.52 shows the stress-strain curves for this specimen and the residual properties are listed below:

E_{xx} = 41.7 GPa (6.0×10^6 psi)
ν_{xy} = 0.62
S_{xxT} = 728 MPa (106 ksi)
ε^u_{xxT} = 0.02168

The tensile modulus and Poisson's ratio are essentially the same as for the static specimens listed in Table 4.4. The residual strength, however, shows a substantial reduction to 728 MPa (106 ksi).

Since the strength of the hybrid laminate is governed mainly by the 0-degree S-glass/epoxy plies, it is of interest to compare the fatigue data of Fig. 4.50 with those of the S-glass/epoxy of Fig. 4.41. The comparison for both flattened tubes and flat coupons shows that their respective trend lines in the two figures follow approximately parallel paths but those for the hybrid laminates show consistently approximately 5 to 7 percent higher strength than for the S-glass/epoxy laminates. It may be concluded that this is due to the contribution provided by the higher fatigue strength $\pm$45-degree graphite/epoxy plies. Thus, such hybridization can be used to increase the fatigue strength of angle-ply S-glass/epoxy laminates without significantly decreasing their static strength as shown in Tables 4.4 and 4.2.

It can be seen from Fig. 4.50 that the fatigue data for the flattened tubes fall below the data for the flat coupons. Here again the reason for lowered strength are the parasitic failure modes consisting of failures occurring mostly at or near the gripping tabs and splitting of the $\pm$45-degree graphite/epoxy plies at the transition between the rounded and flat sections of the specimens, as illustrated in Fig. 4.1. The failure modes for the flat coupons are shown in Fig. 4.2.

4.2.5 Graphite/Epoxy $[0_2/\pm45]_s$ Specimens

Fatigue results for the graphite/epoxy flat coupon specimens of $[0_2/\pm45]_s$ construction are shown in Table 4.10 and Fig. 4.53. As indicated and explained in Section 4.1.5 static testing of the flattened tube graphite/epoxy specimens of this construction showed low strength due to parasitic failure modes which could not be eliminated by the steps undertaken for this purpose. The fabrication and testing of these specimens was then discontinued which is the reason why only flat coupon data are presented.

Table 4.10

RESULTS OF TENSILE CYCLING FATIGUE TESTS OF GRAPHITE/EPOXY $[0_2/\pm45]_s$ SPECIMENS

Maximum Cyclic Stress			
MPa	(ksi)	Percent of Average Static Strength	Cycles to Failure
Flat Coupon			
631.7	(91.6)	73.9	1.035×10^7 Runout
658.4	(95.5)	77.0	1.001×10^7 Runout
668.3	(96.9)	78.2	4.015×10^6
672.2	(97.5)	78.6	1.286×10^6
674.8	(97.9)	79.0	7.025×10^6
676.0	(98.0)	79.1	6.36×10^5
686.0	(99.5)	80.2	1.674×10^6
689.5	(100)	80.6	1.050×10^6
637.8	(92.5)	74.6	9.94×10^5
689.5	(100)	80.6	2.0×10^4

The data for the flat coupons fall in the range of 2.0×10^4 to 1.04×10^7 cycles. In this range the data encompass fatigue strengths from 73.9 to 80.6 percent of static strength. A comparison of these data with those of the $[\pm 45/0_2]_s$ graphite/epoxy flat coupon fatigue data presented in Section 4.1.1 shows that the strength ranges, data trends and scatter are very similar.

Two specimens survived the runout of 10^7 cycles but showed delamination damage at the edges. These were specimens cycled to 73.9 and 77.0 percent of static strength. They were tested in tension to failure to determine their residual properties. The stress-strain curves for these specimens are shown in Figs. 4.54 and 4.55.

The residual properties derived from them are

E_{xx} = 89.0 GPa (12.9 x 10^6 psi)
ν_{xy} = 0.69
S_{xxT} = 807 MPa (117 ksi)
ε^u_{xxT} = 0.00966

for the specimen which survived cycling to 73.9 percent of static strength, and

E_{xx} = 82.0 GPa (11.9 x 10^6 psi)
ν_{xy} = 0.69
S_{xxT} = 876 MPa (127 ksi)
ε^u_{xxT} = 0.01065

for the specimen which survived cycling to 77.0 percent of static strength. The residual properties show no significant change as compared with the initial static values shown in Table 4.5.

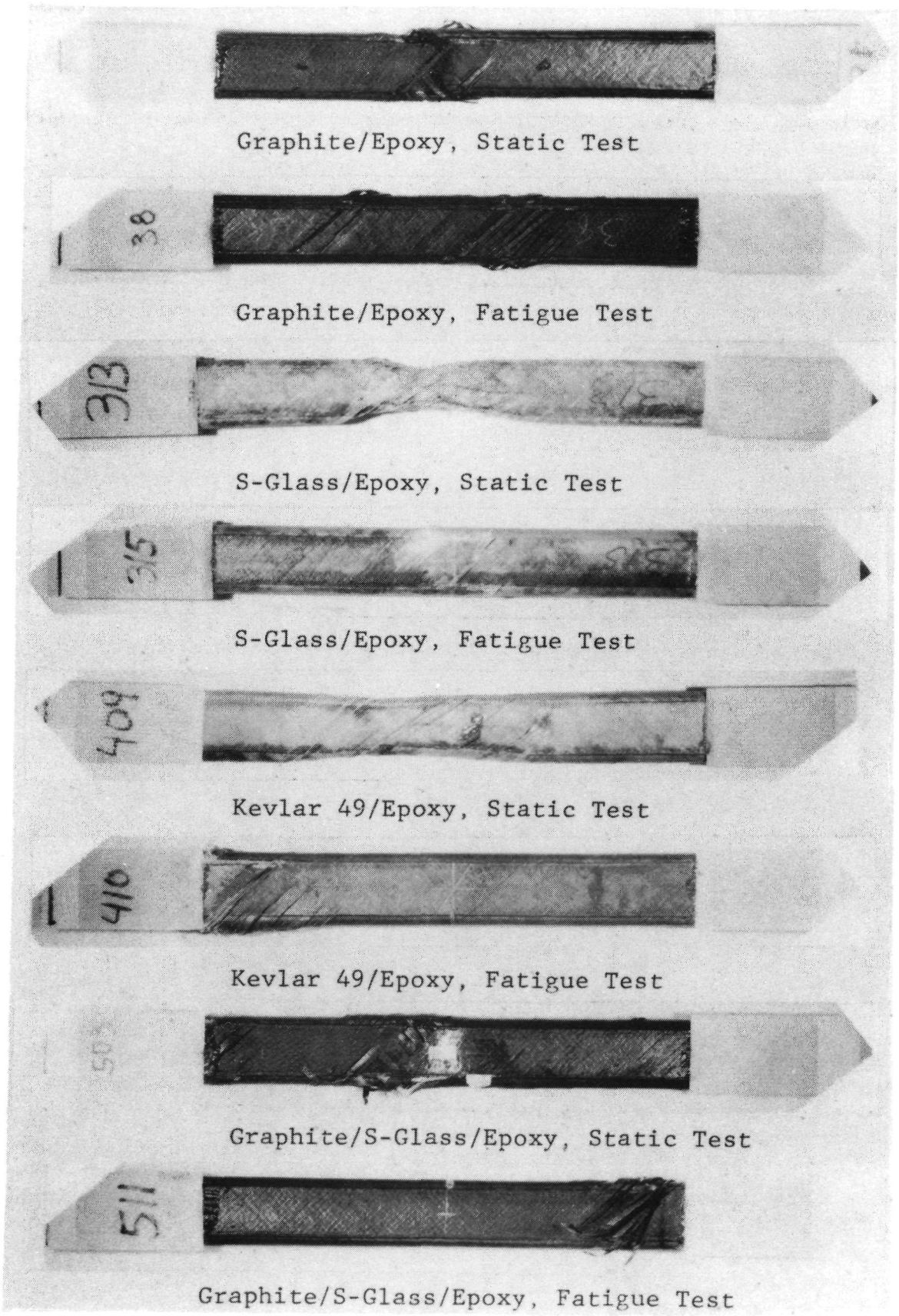

Figure 4.1 **Typical Failure Modes for** Flattened Tube Specimens for Tensile Static and Fatigue Testing

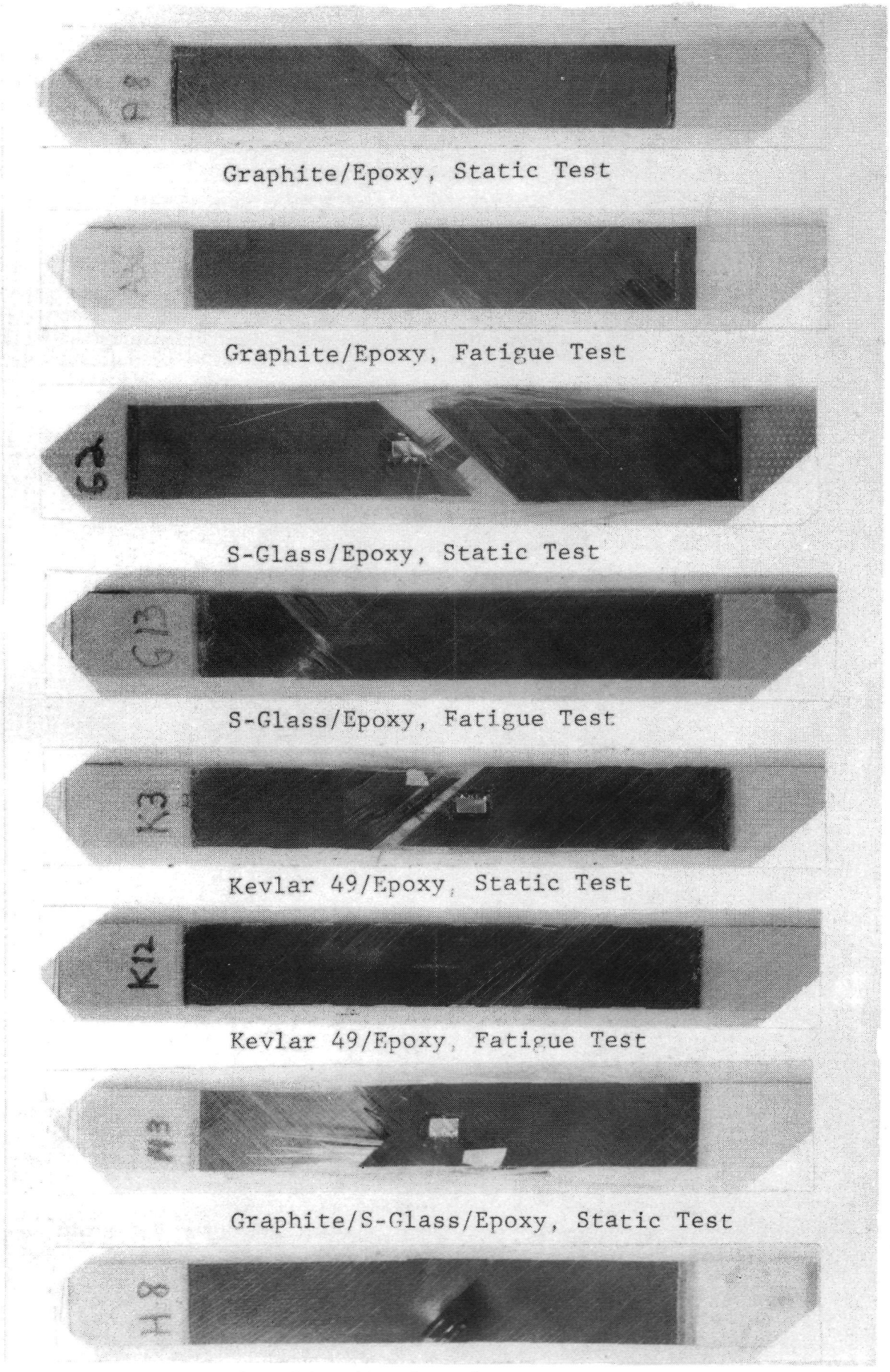

Graphite/Epoxy, Static Test

Graphite/Epoxy, Fatigue Test

S-Glass/Epoxy, Static Test

S-Glass/Epoxy, Fatigue Test

Kevlar 49/Epoxy, Static Test

Kevlar 49/Epoxy, Fatigue Test

Graphite/S-Glass/Epoxy, Static Test

Graphite/S-Glass/Epoxy, Fatigue Test

Figure 4.2 Typical Failure Modes for Flat Coupon Specimens for Tensile Static and Fatigue Testing

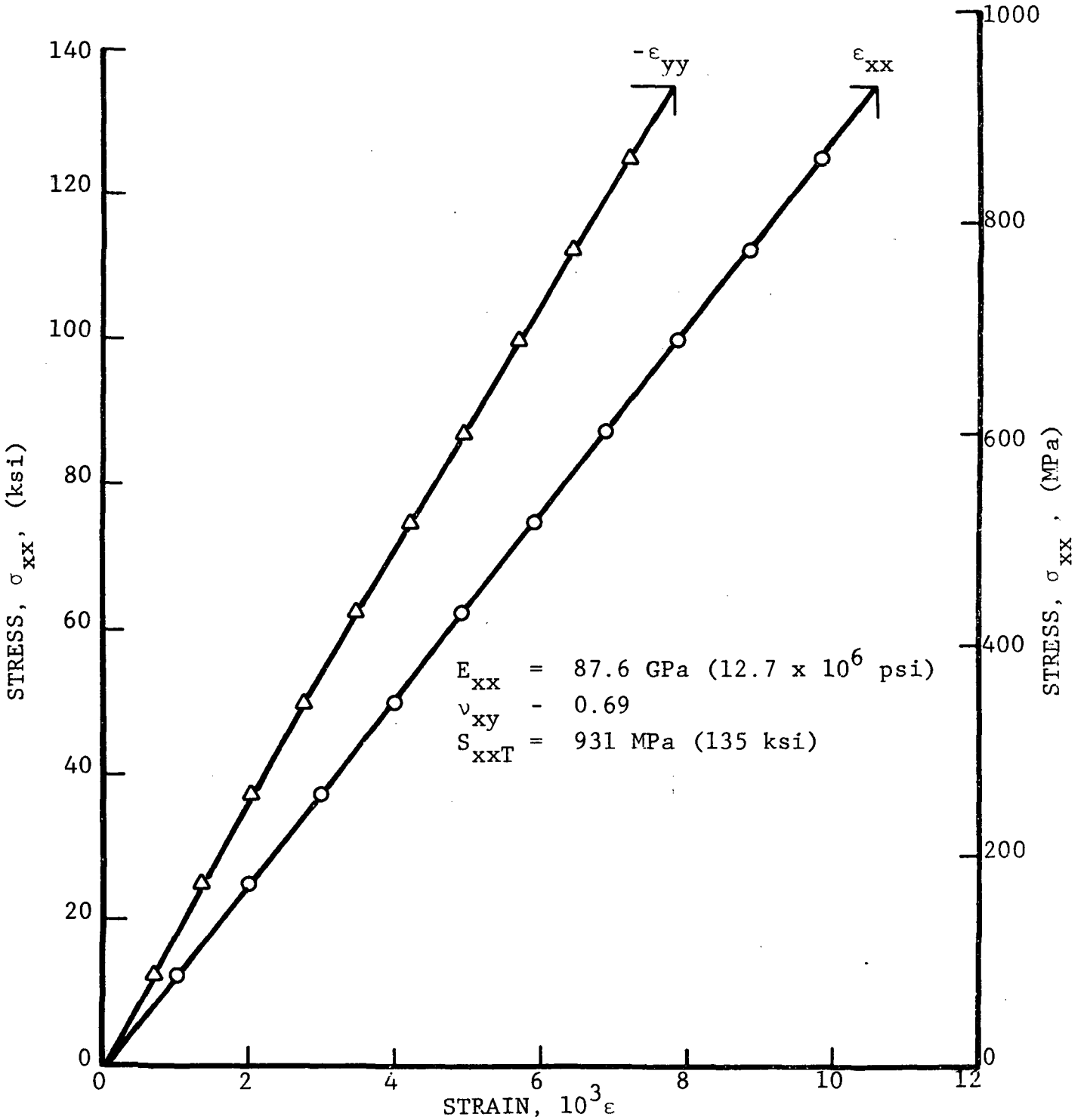

Figure 4.3 STRESS-STRAIN CURVES FOR $[\pm 45/0_2]_s$ GRAPHITE/EPOXY FLAT COUPON UNDER UNIAXIAL TENSILE LOADING

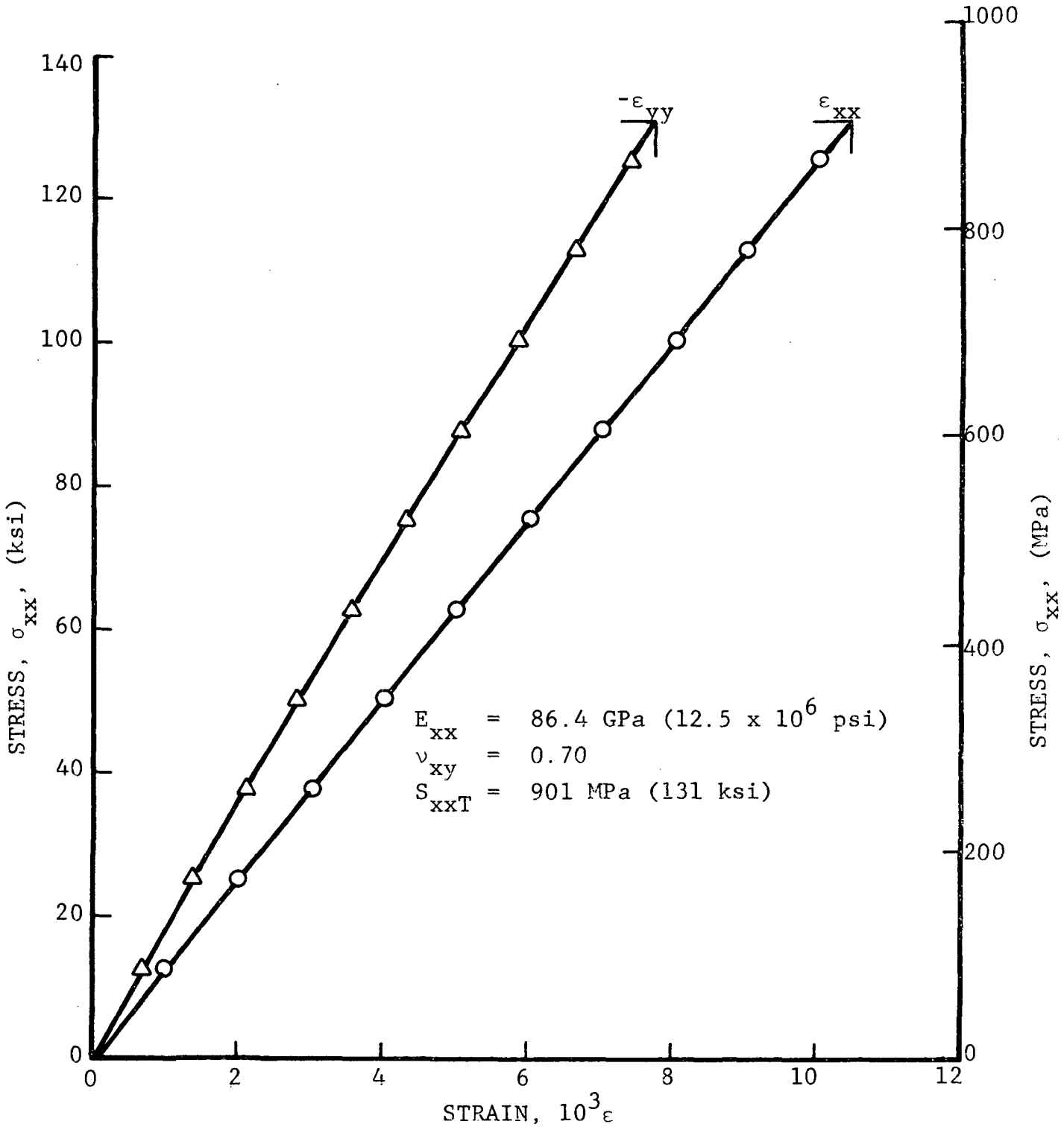

Figure 4-4 STRESS-STRAIN CURVES FOR $[+45/0_2]_s$ GRAPHITE/EPOXY FLAT COUPON UNDER UNIAXIAL TENSILE LOADING

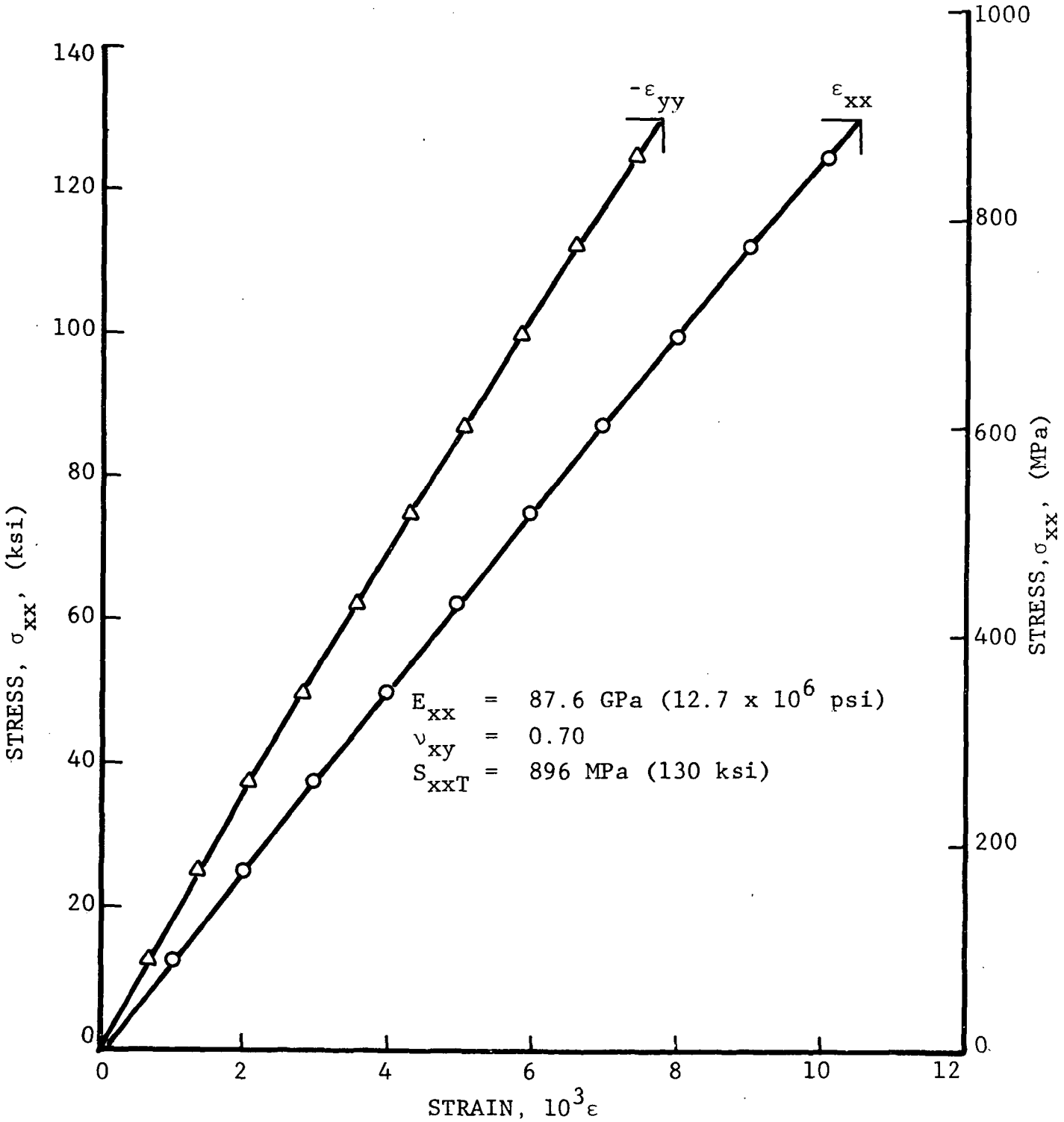

Figure 4.5 STRESS-STRAIN CURVES FOR $[\pm 45/0_2]_s$ GRAPHITE/EPOXY FLAT COUPON UNDER UNIAXIAL TENSILE LOADING

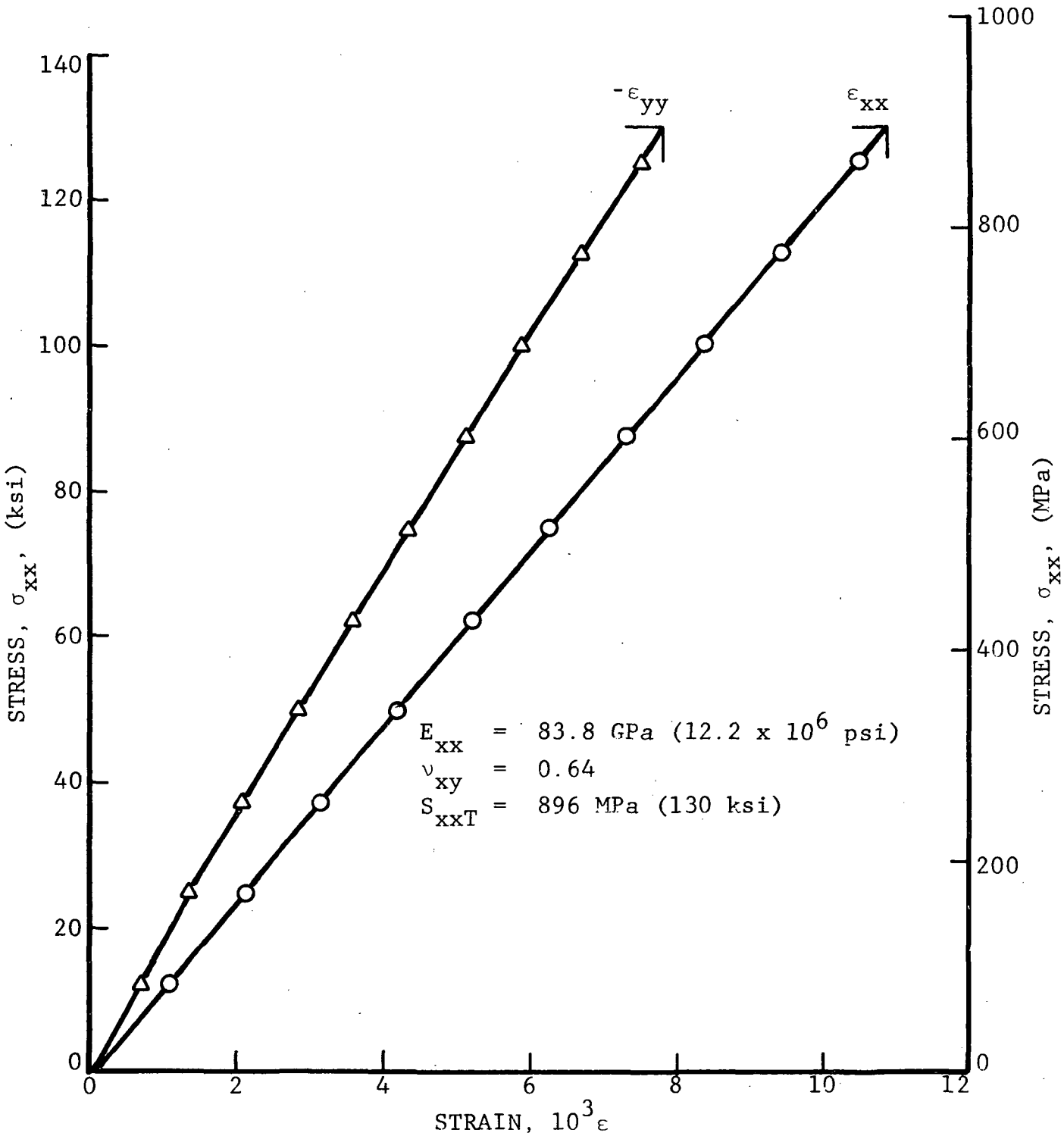

Figure 4.6 STRESS-STRAIN CURVES FOR $[\pm 45/0_2]_s$ GRAPHITE/EPOXY FLAT COUPON UNDER UNIAXIAL TENSILE LOADING

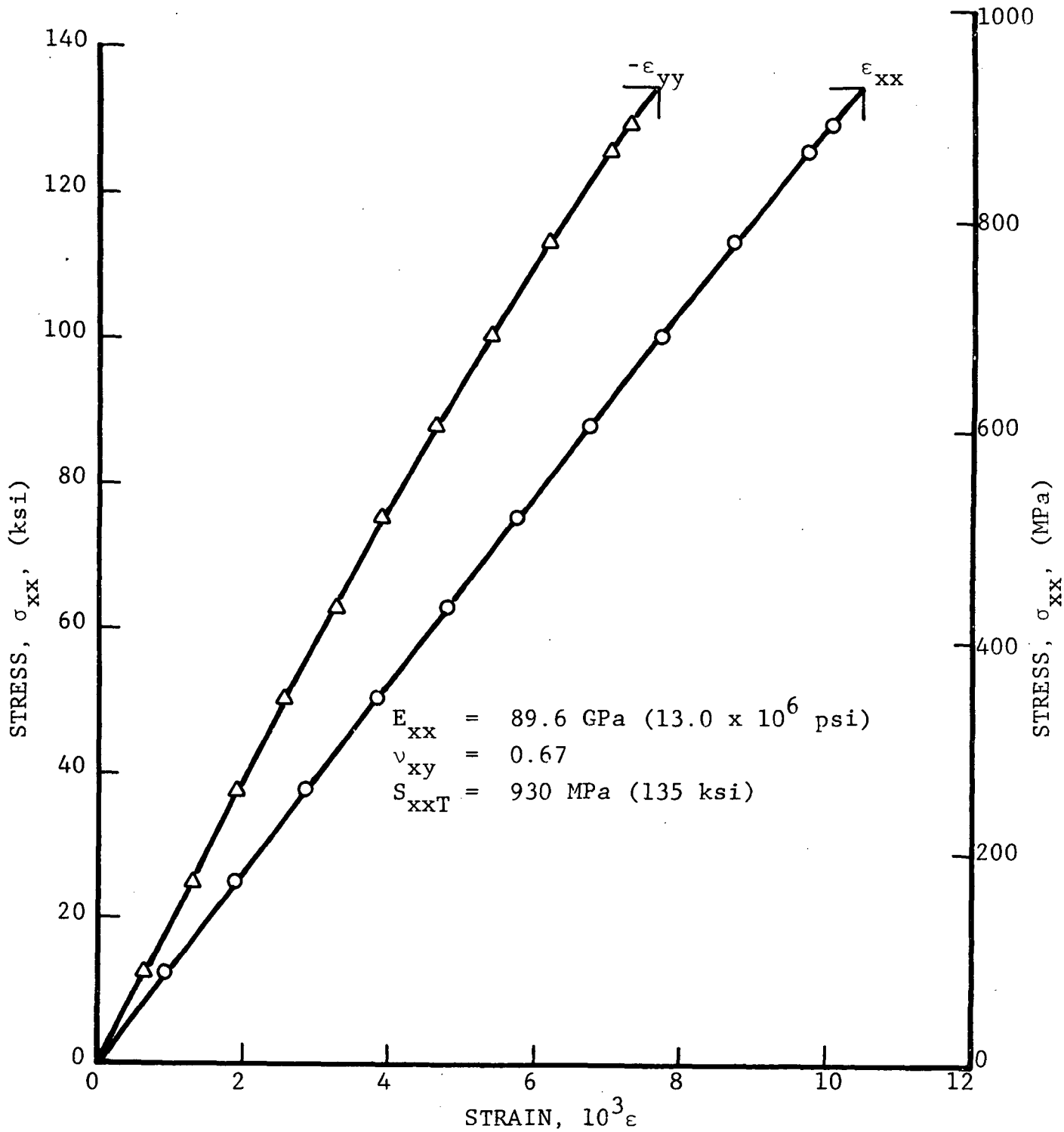

Figure 4.7 STRESS-STRAIN CURVES FOR $[+45/0_2]_s$ GRAPHITE/EPOXY FLATTENED TUBULAR SPECIMEN UNDER UNIAXIAL TENSILE LOADING

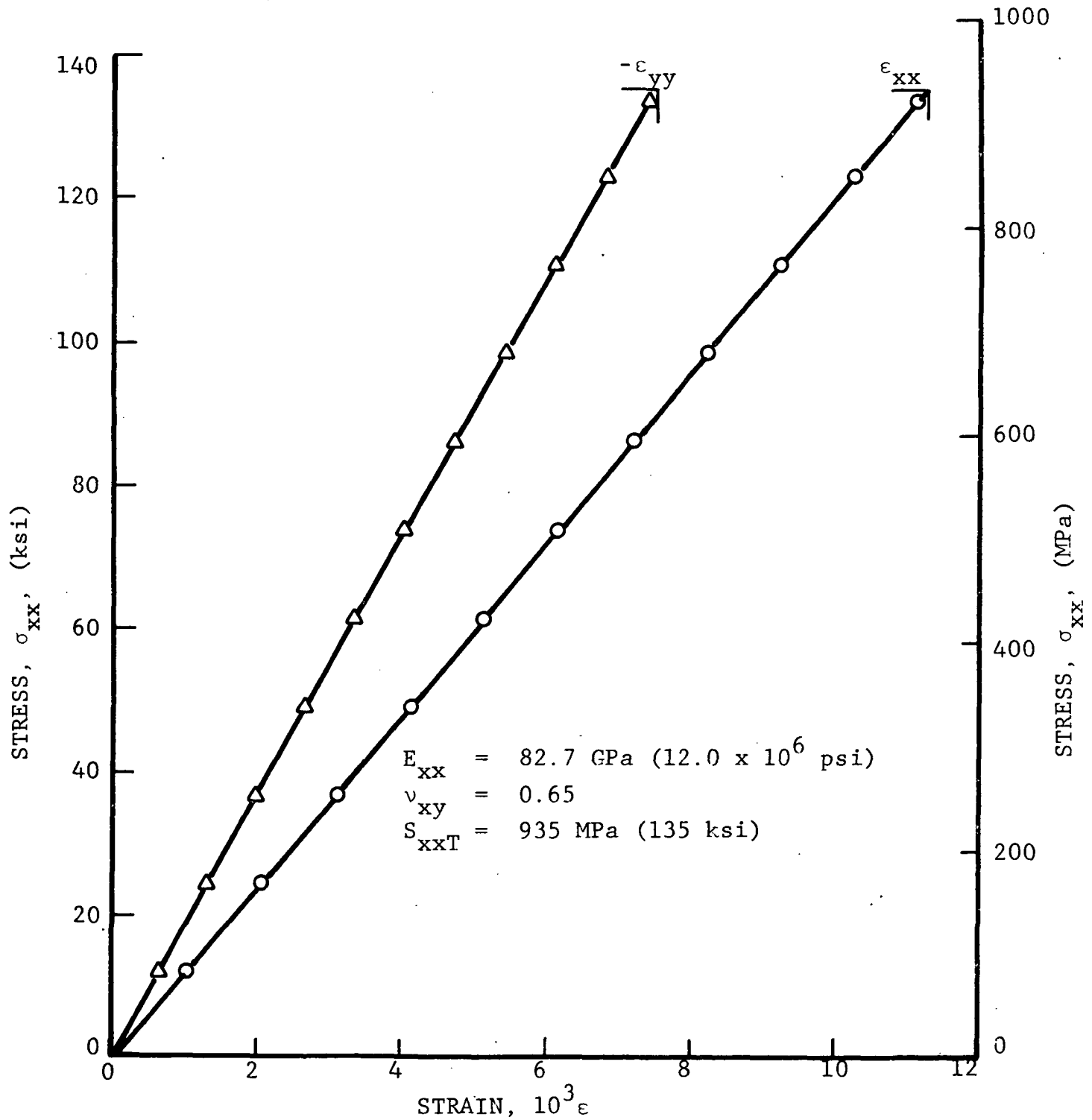

Figure 4.8 STRESS-STRAIN CURVES FOR $[\pm 45/0_2]_s$ GRAPHITE/EPOXY FLATTENED TUBULAR SPECIMEN UNDER UNIAXIAL TENSILE LOADING

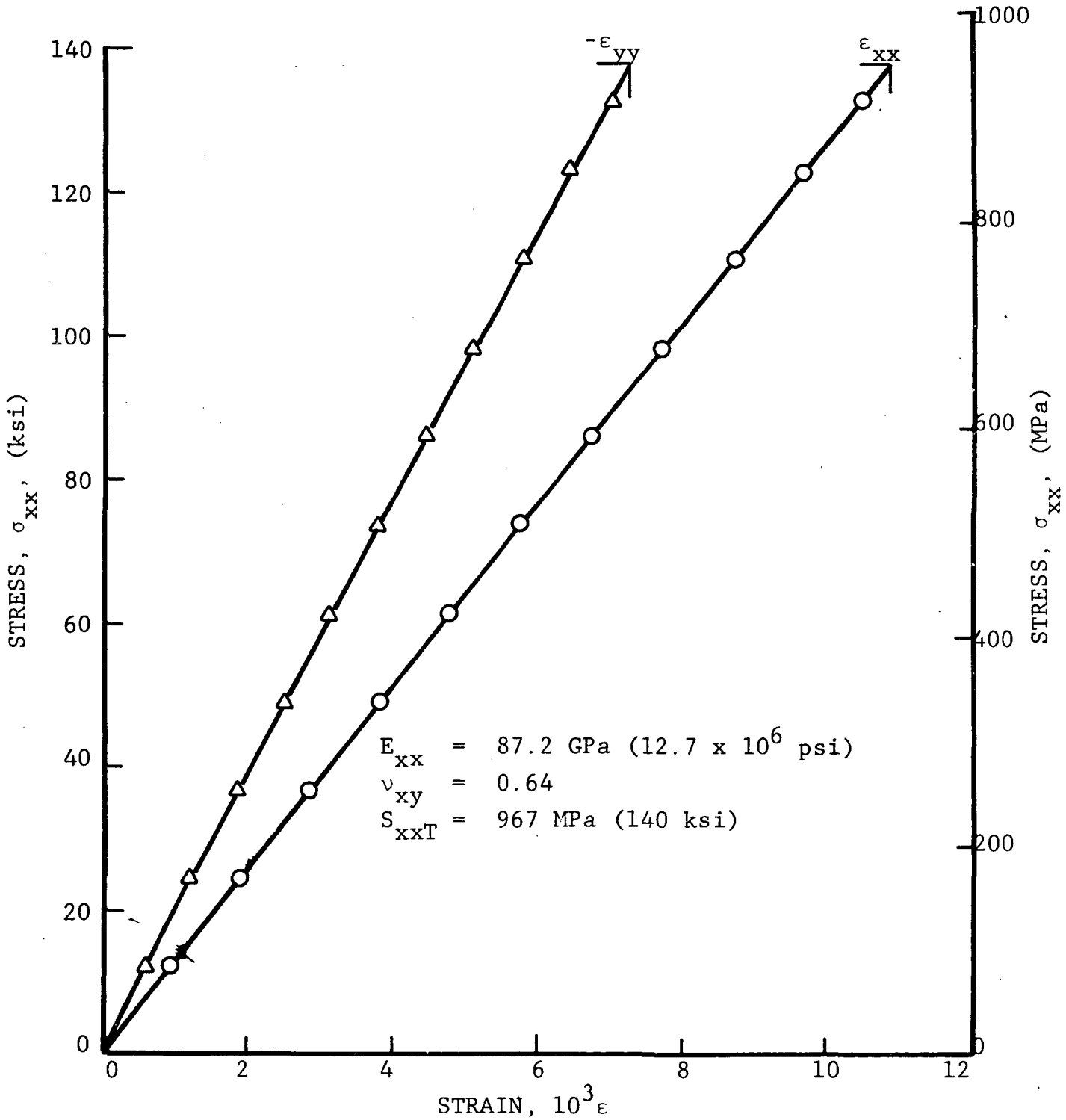

Figure 4.9 STRESS-STRAIN CURVES FOR $[\pm 45/0_2]_s$ GRAPHITE/EPOXY FLATTENED TUBULAR SPECIMEN UNDER UNIAXIAL TENSILE LOADING

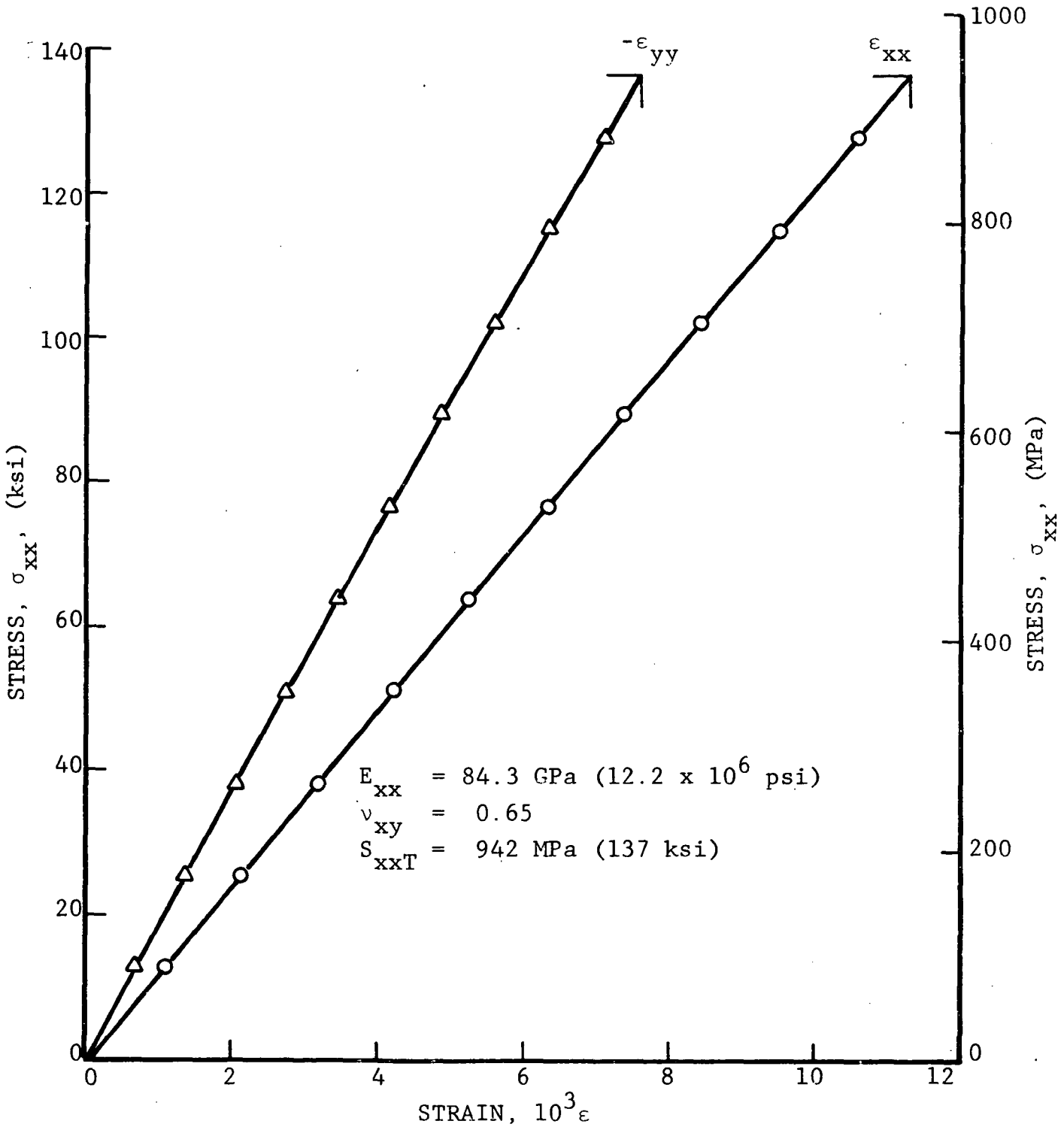

Figure 4-10 STRESS-STRAIN CURVES FOR $[\pm 45/0_2]_s$ GRAPHITE/EPOXY FLATTENED TUBULAR SPECIMEN UNDER UNIAXIAL TENSILE LOADING

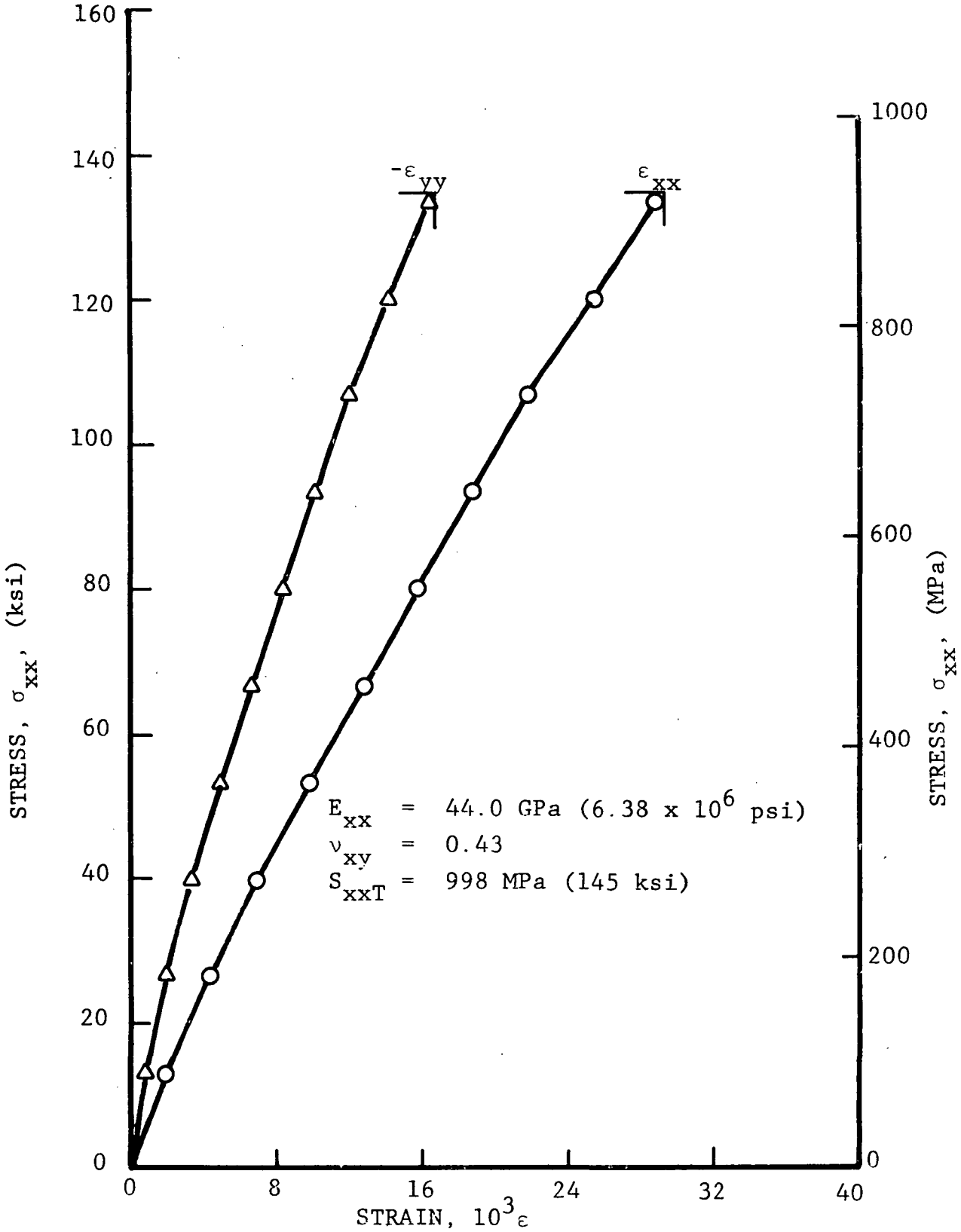

Figure 4.11 STRESS-STRAIN CURVES FOR $[\pm 45/0_2]_s$ S-GLASS/ EPOXY FLAT COUPON UNDER UNIAXIAL TENSILE LOADING

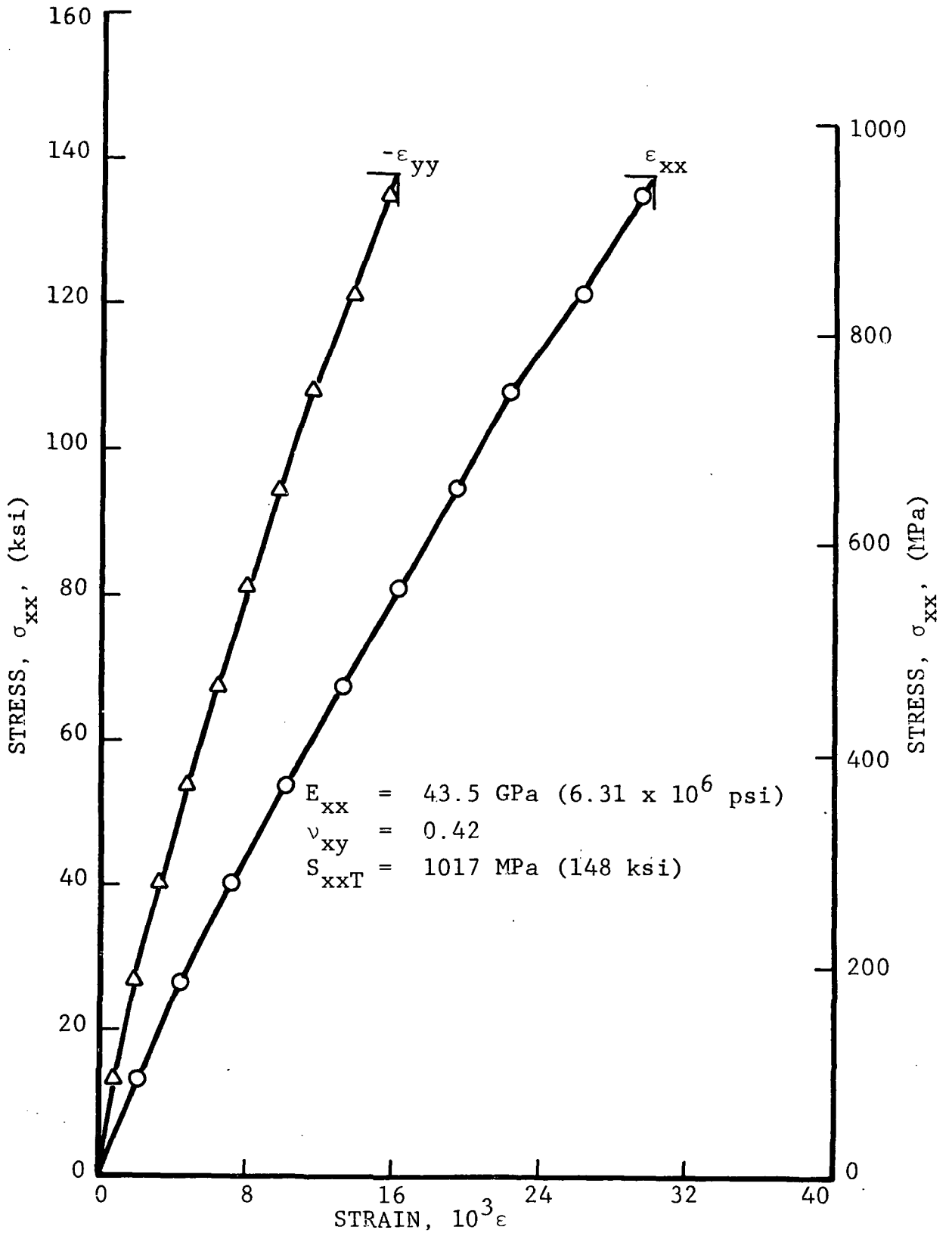

Figure 4.12 STRESS-STRAIN CURVES FOR $[+45/0_2]_s$ S-GLASS/ EPOXY FLAT COUPON UNDER UNIAXIAL TENSILE LOADING

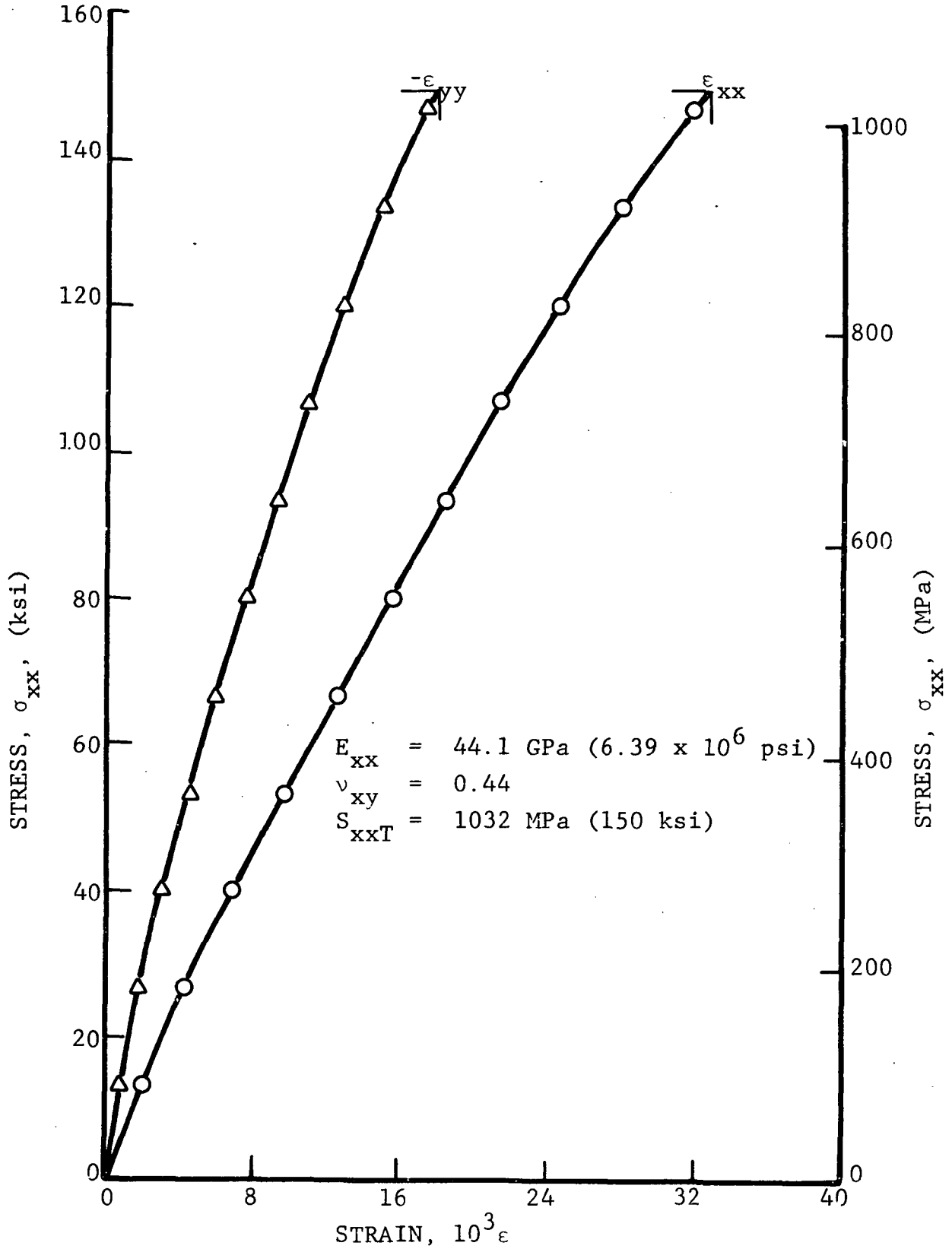

Figure 4.13 STRESS-STRAIN CURVES FOR $[+45/0_2]_s$ S-GLASS/ EPOXY FLAT COUPON UNDER UNIAXIAL TENSILE LOADING

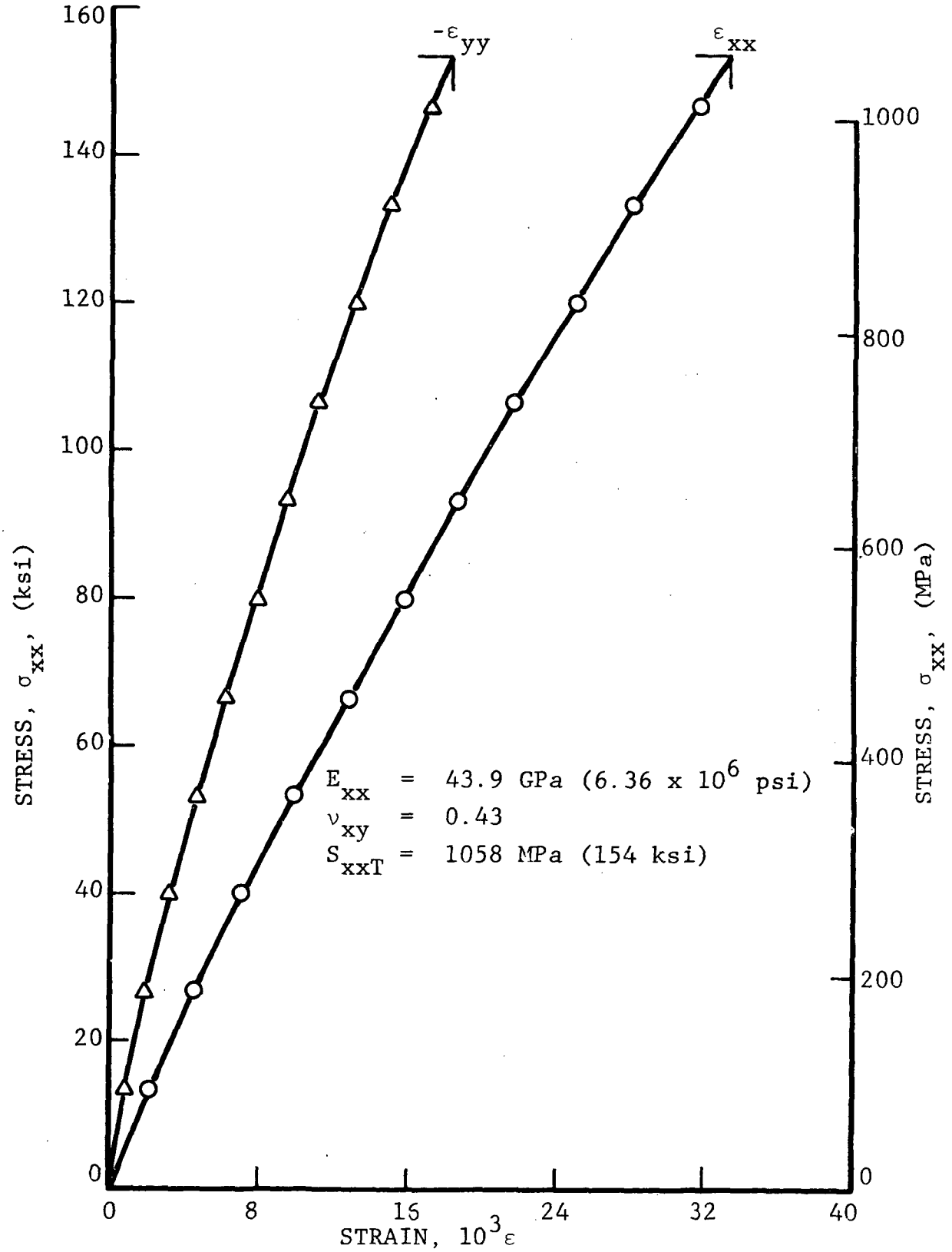

Figure 4.14 STRESS-STRAIN CURVES FOR $[+45/0_2]_s$ S-GLASS/ EPOXY FLAT COUPON UNDER UNIAXIAL TENSILE LOADING

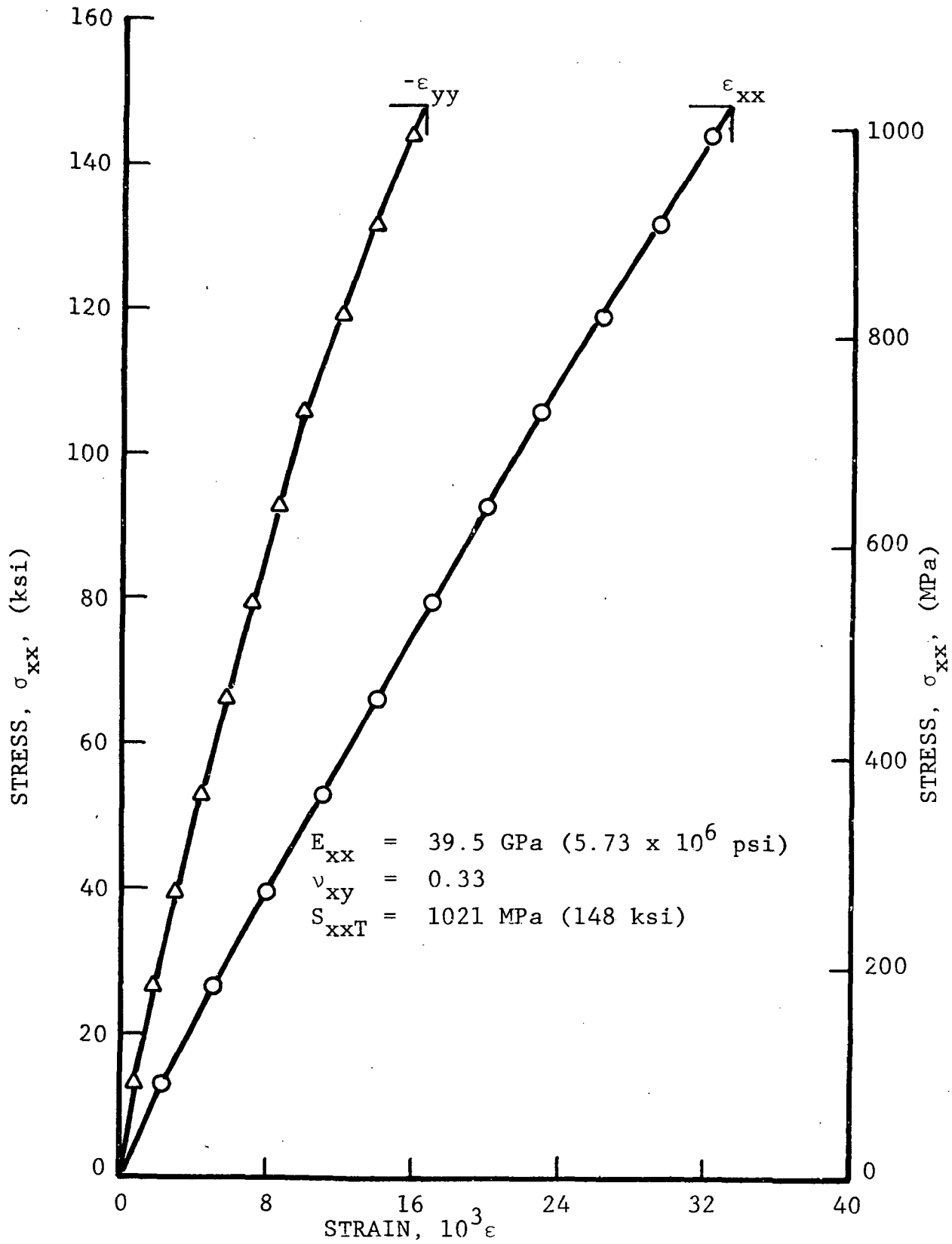

Figure 4.15 STRESS-STRAIN CURVES FOR $[\pm 45/0_2]_s$ S-GLASS/EPOXY FLATTENED TUBULAR SPECIMEN UNDER UNIAXIAL TENSILE LOADING

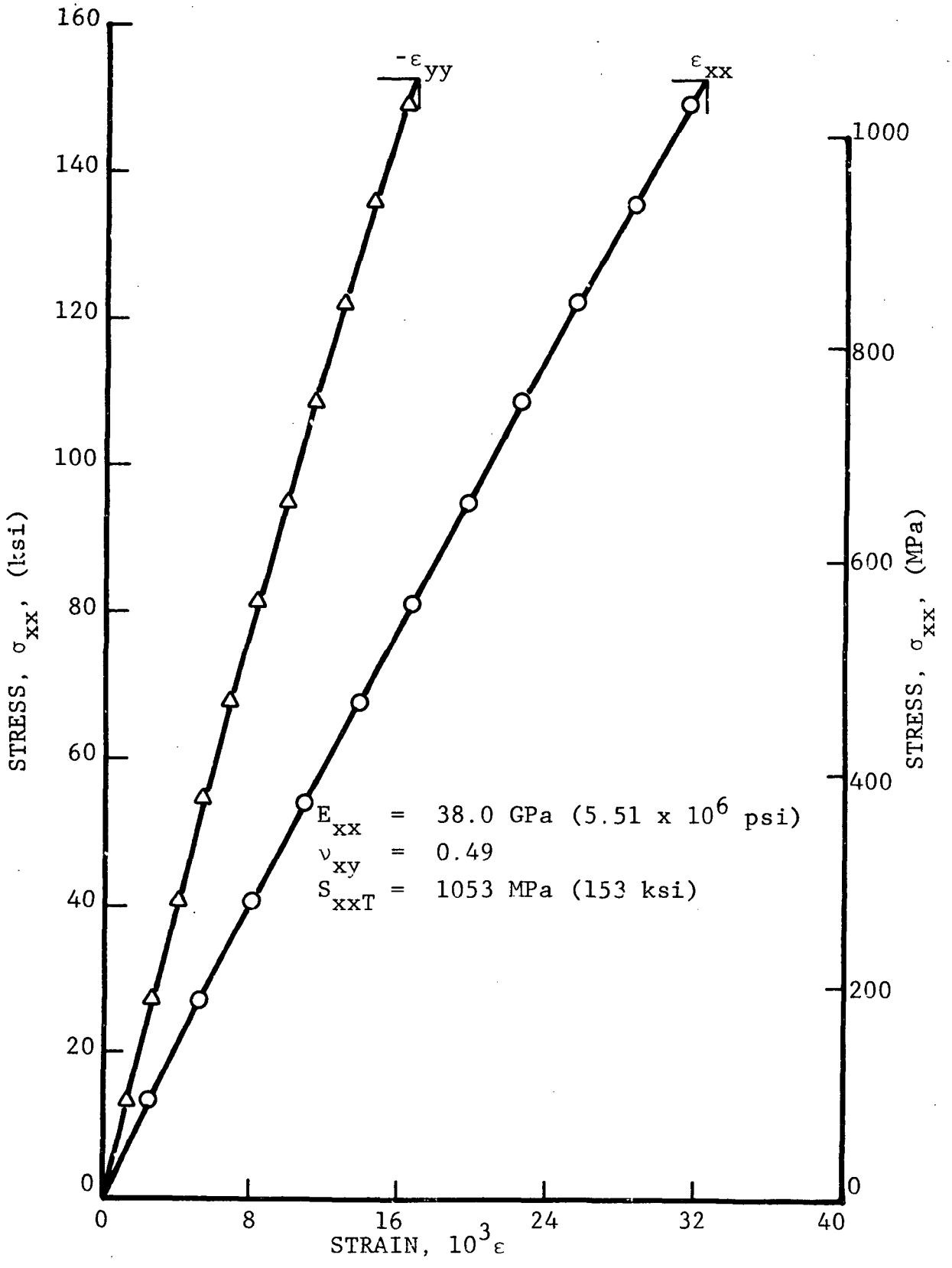

Figure 4.16 STRESS-STRAIN CURVES FOR $[+45/0_2]_s$ S-GLASS/ EPOXY FLATTENED TUBULAR SPECIMEN UNDER UNIAXIAL TENSILE LOADING

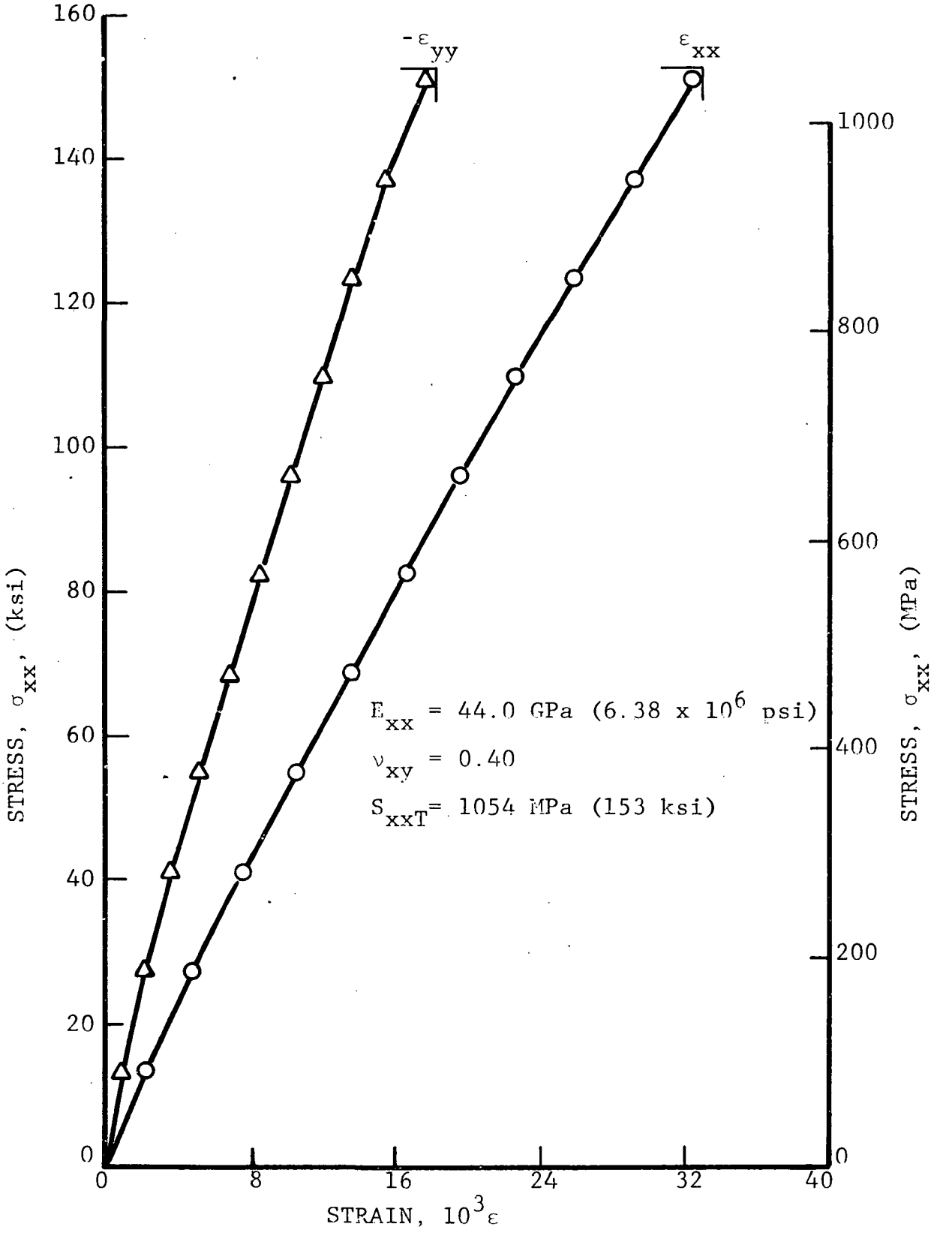

Figure 4.17 STRESS-STRAIN CURVES FOR $[\pm 45/0_2]_s$ S-GLASS/EPOXY FLATTENED TUBULAR SPECIMENS UNDER UNIAXIAL TENSILE LOADING

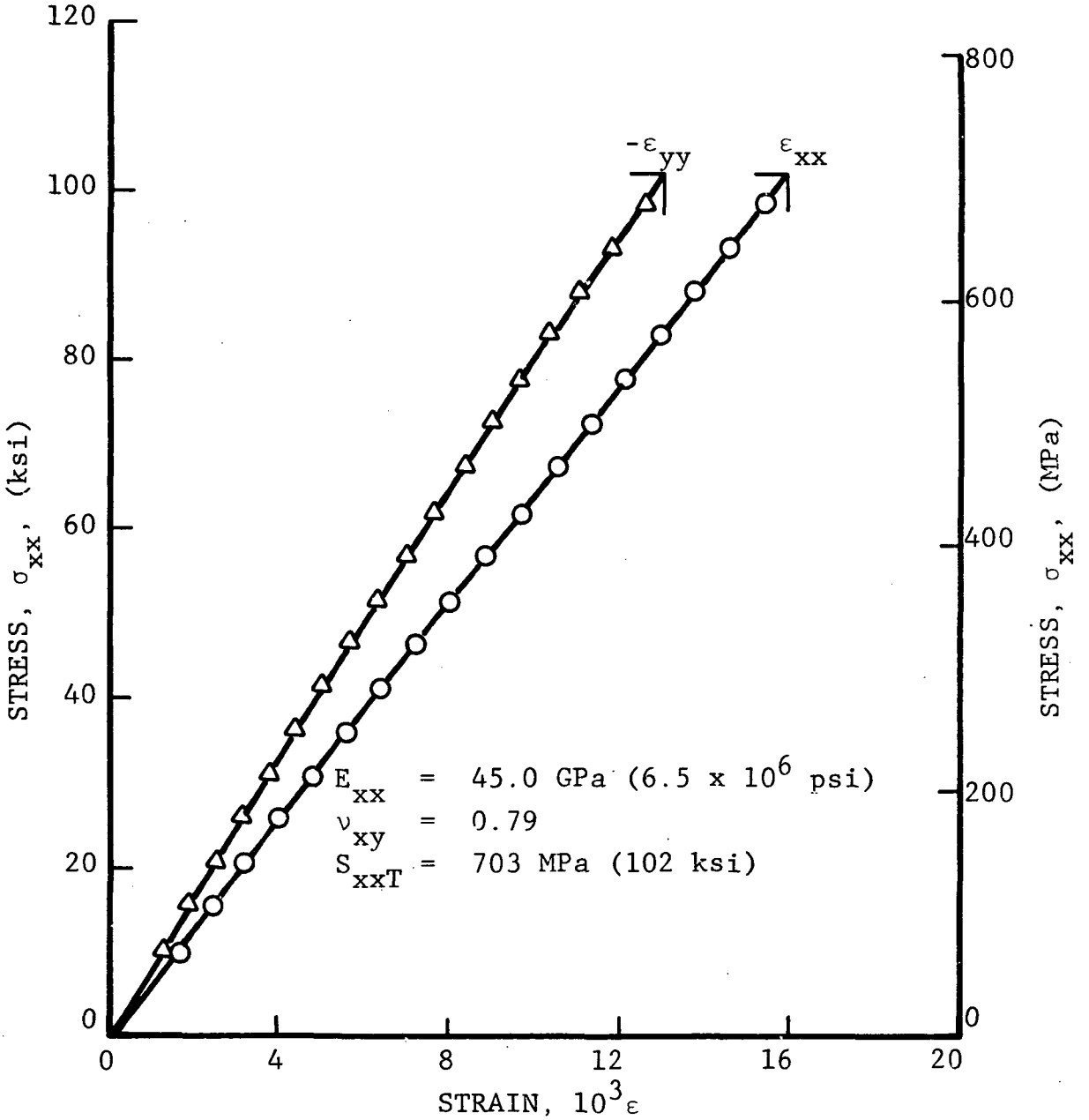

Figure 4.18 STRESS-STRAIN CURVES FOR $[\pm 45/0_2]_s$ KEVLAR 49/ EPOXY FLAT COUPON UNDER UNIAXIAL TENSILE LOADING

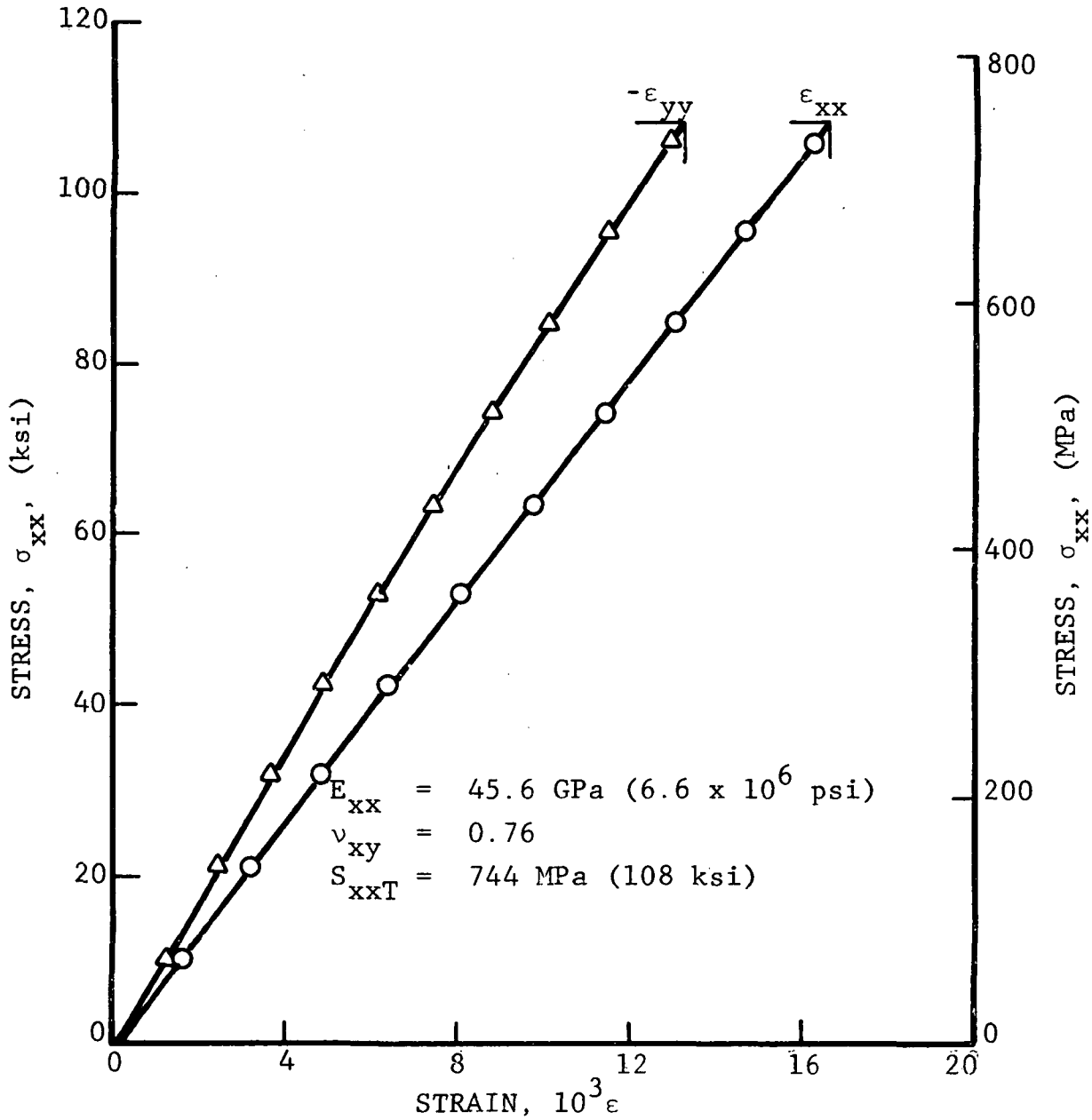

Figure 4.19 STRESS-STRAIN CURVES FOR $[+45/0_2]_s$ KEVLAR 49/ EPOXY FLAT COUPON UNDER UNIAXIAL TENSILE LOADING

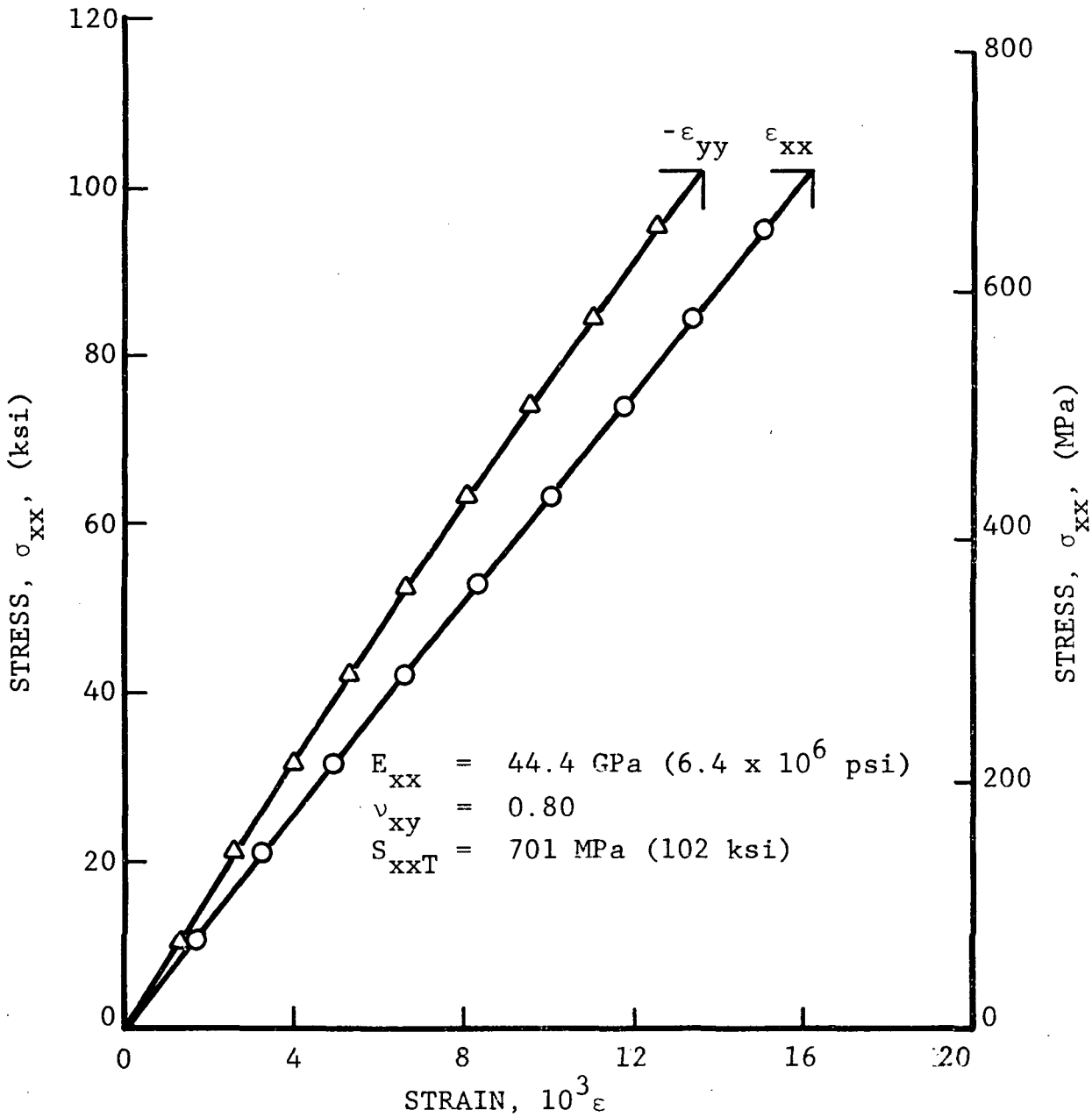

Figure 4.20 STRESS-STRAIN CURVES FOR $[+45/0_2]_s$ KEVLAR 49/ EPOXY FLAT COUPON UNDER UNIAXIAL TENSILE LOADING

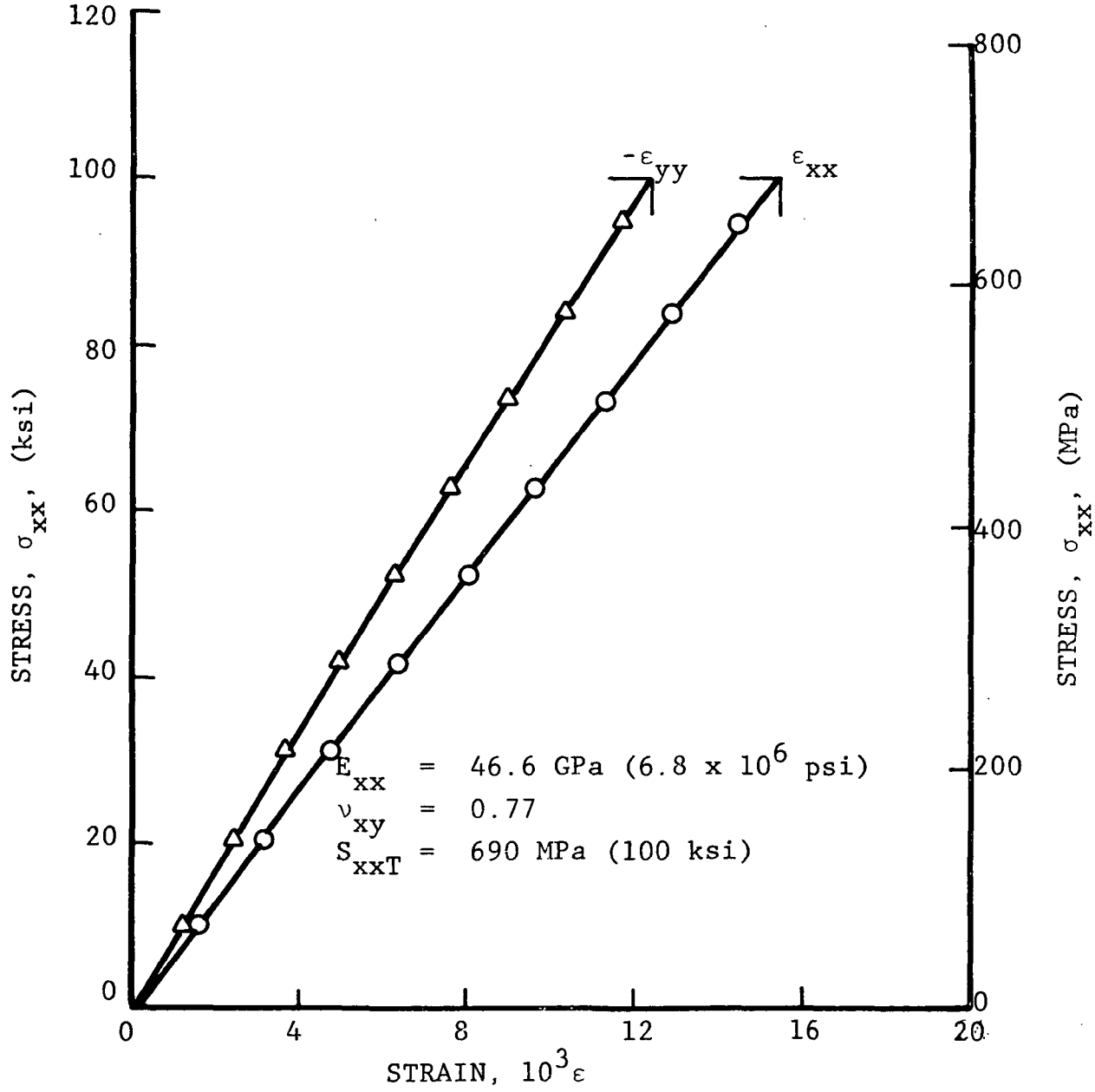

Figure 4.21 STRESS-STRAIN CURVES FOR $[+45/0_2]_s$ KEVLAR 49/ EPOXY FLAT COUPON UNDER UNIAXIAL TENSILE LOADING

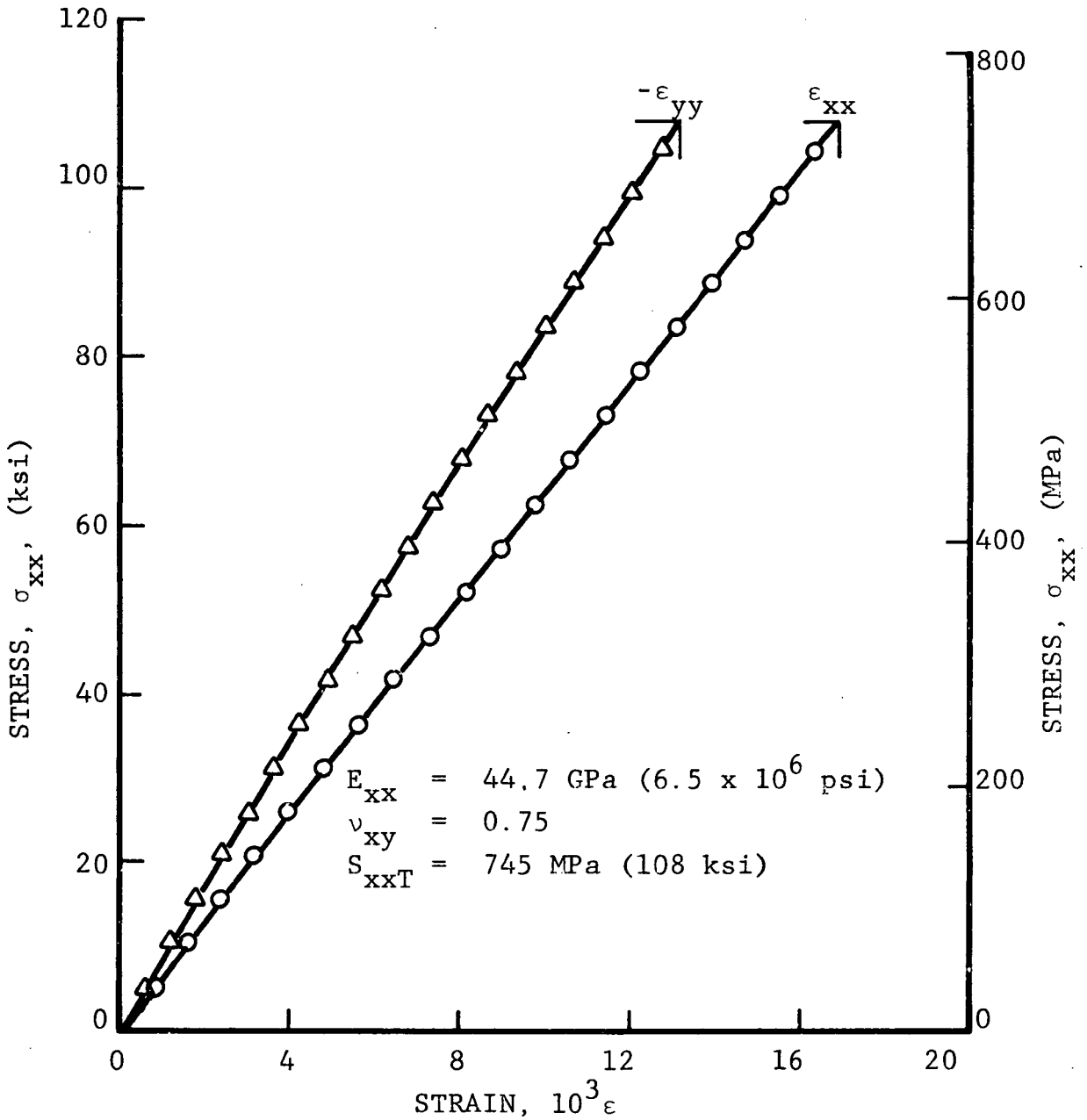

Figure 4.22 STRESS-STRAIN CURVES FOR $[\pm 45/0_2]_s$ KEVLAR 49/ EPOXY FLAT COUPON UNDER UNIAXIAL TENSILE LOADING

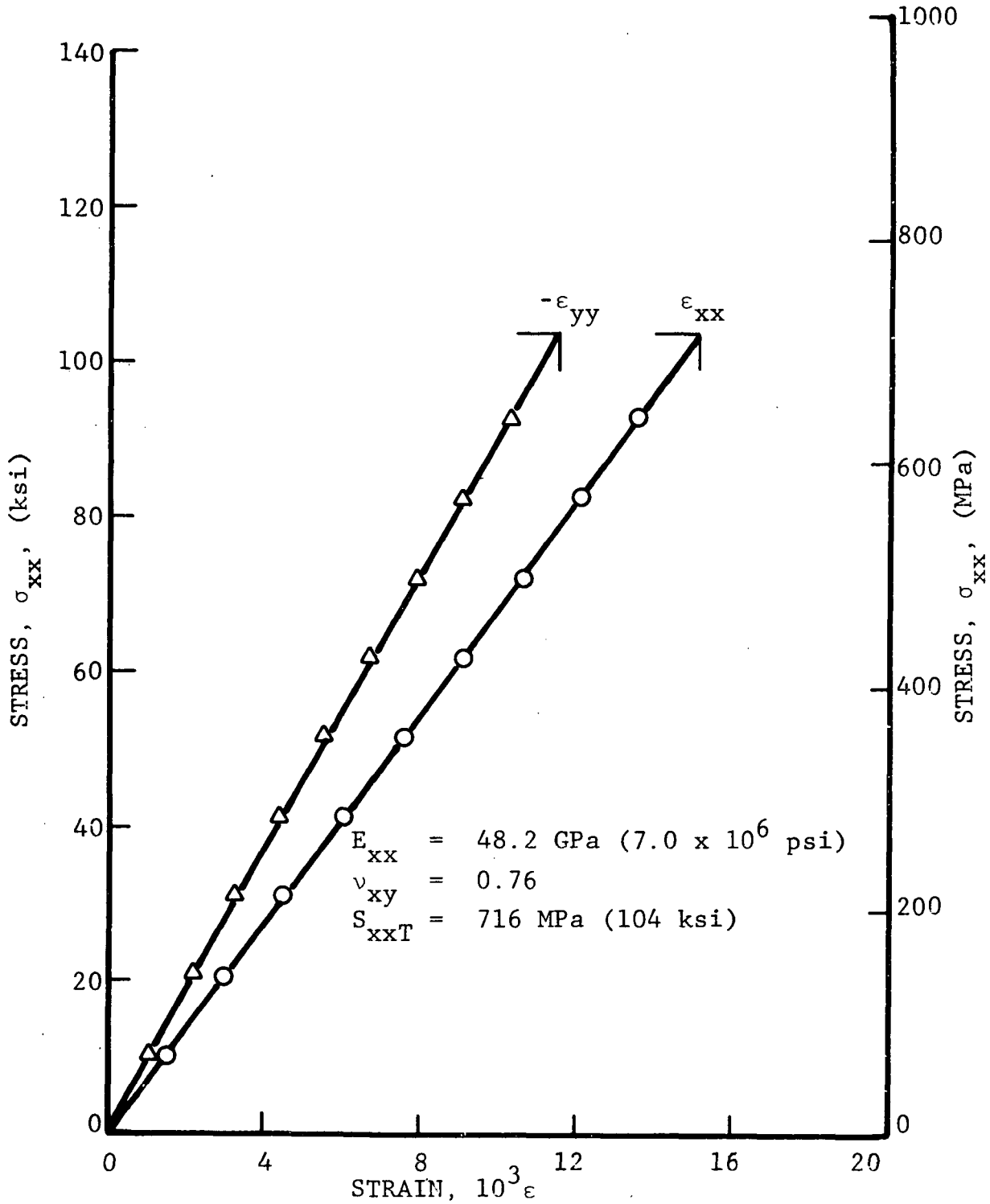

Figure 4.23 STRESS-STRAIN CURVES FOR $[\pm 45/0_2]_s$ KEVLAR 49/ EPOXY FLATTENED TUBULAR SPECIMEN UNDER UNIAXIAL TENSILE LOADING

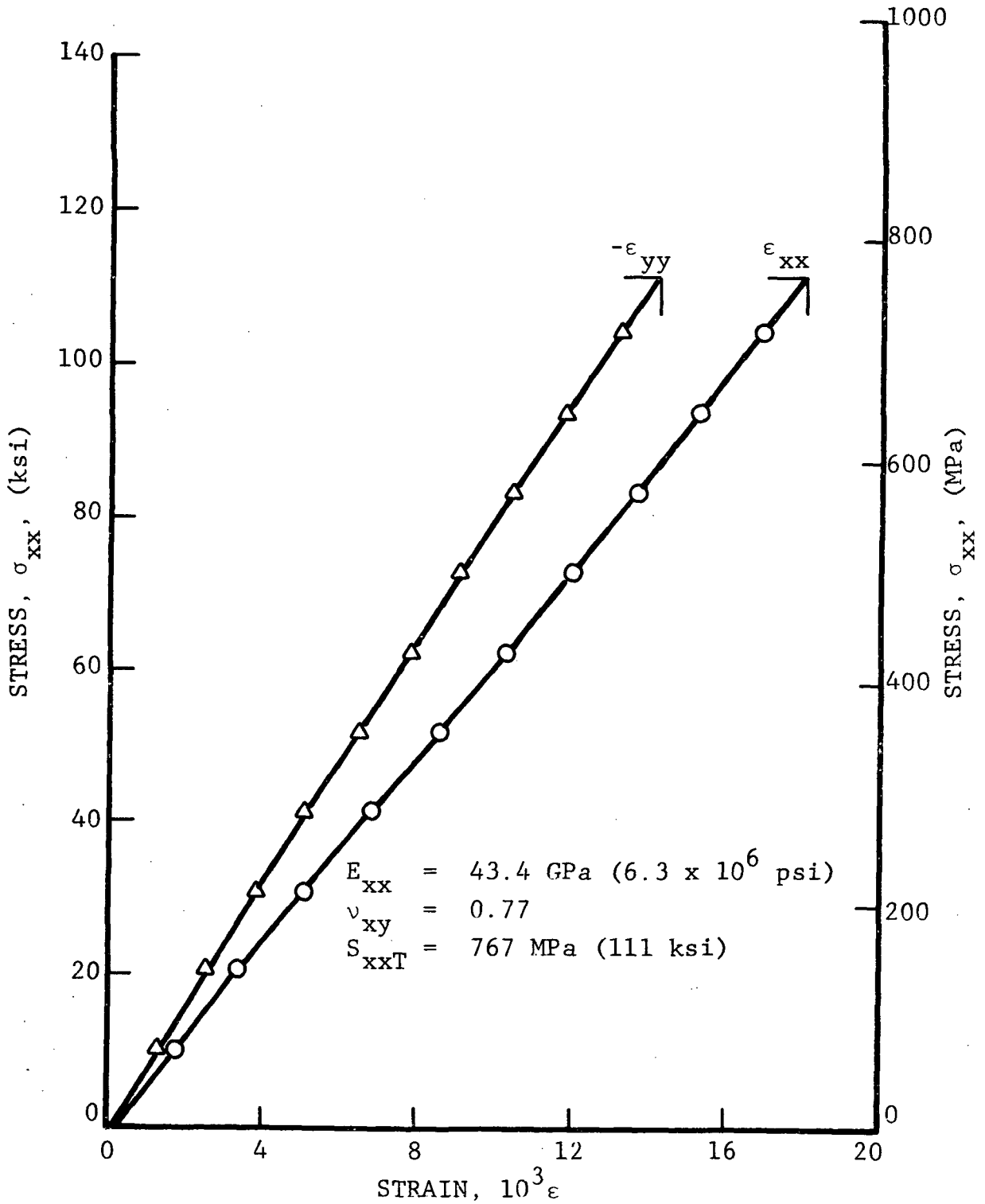

Figure 4.24 STRESS-STRAIN CURVES FOR $[+45/0_2]_s$ KEVLAR 49/ EPOXY FLATTENED TUBULAR SPECIMEN UNDER UNIAXIAL TENSILE LOADING

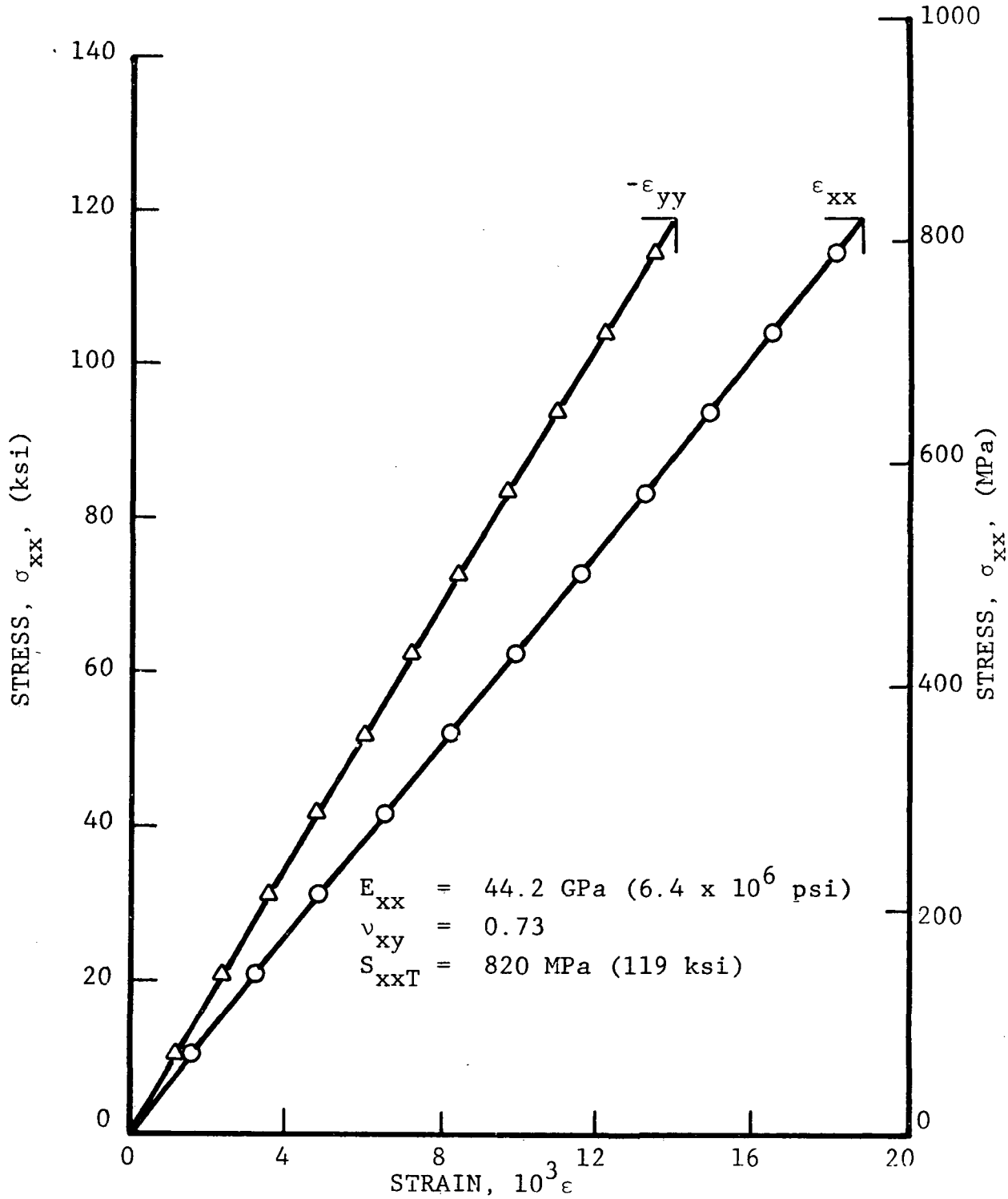

Figure 4.25 STRESS-STRAIN CURVES FOR $[+45/0_2]_s$ KEVLAR 49/ EPOXY FLATTENED TUBULAR SPECIMEN UNDER UNIAXIAL TENSILE LOADING

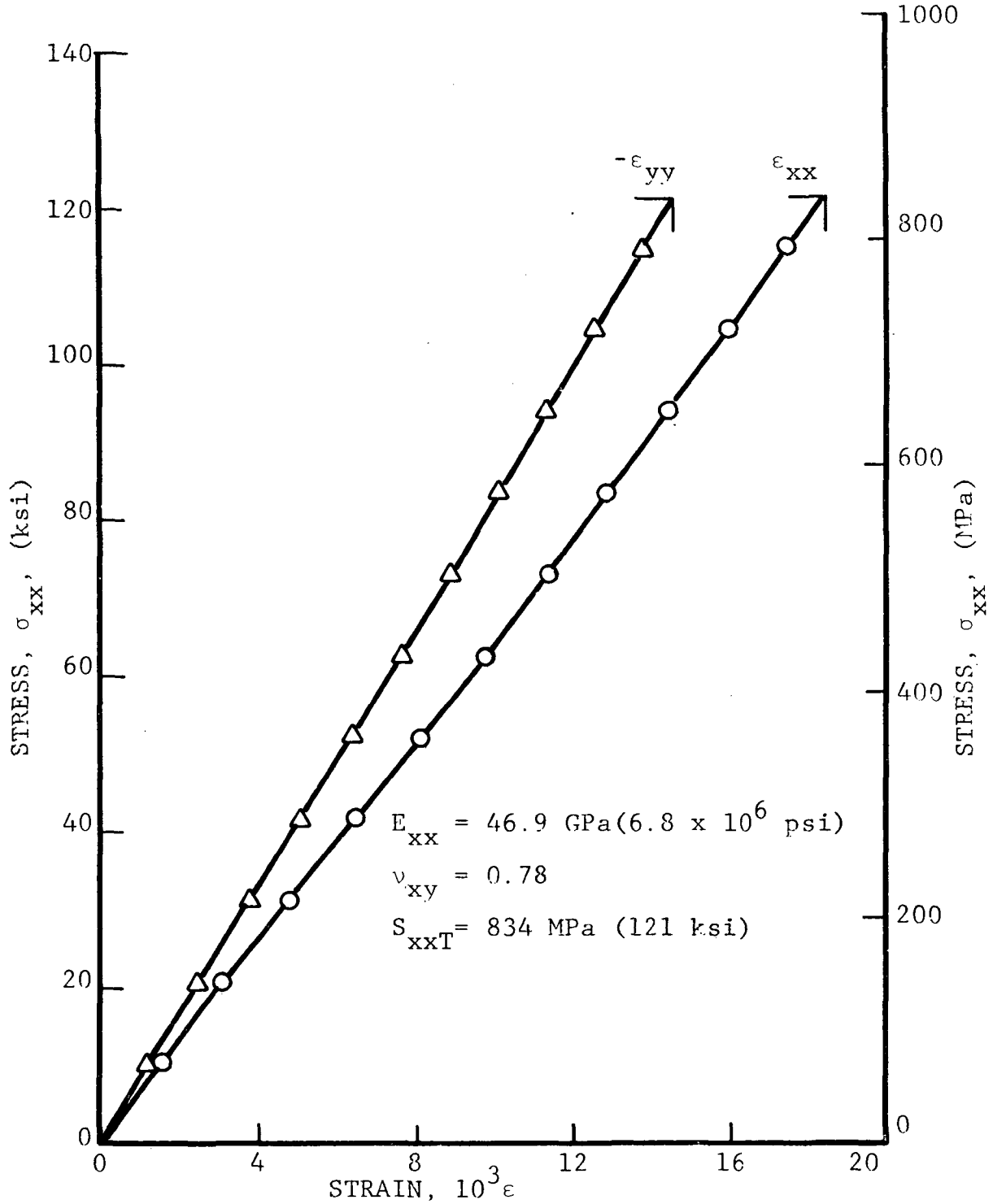

Figure 4.26 STRESS-STRAIN CURVES FOR $[+45/0_2]_s$ KEVLAR 49/ EPOXY FLATTENED TUBULAR SPECIMEN UNDER UNIAXIAL TENSILE LOADING

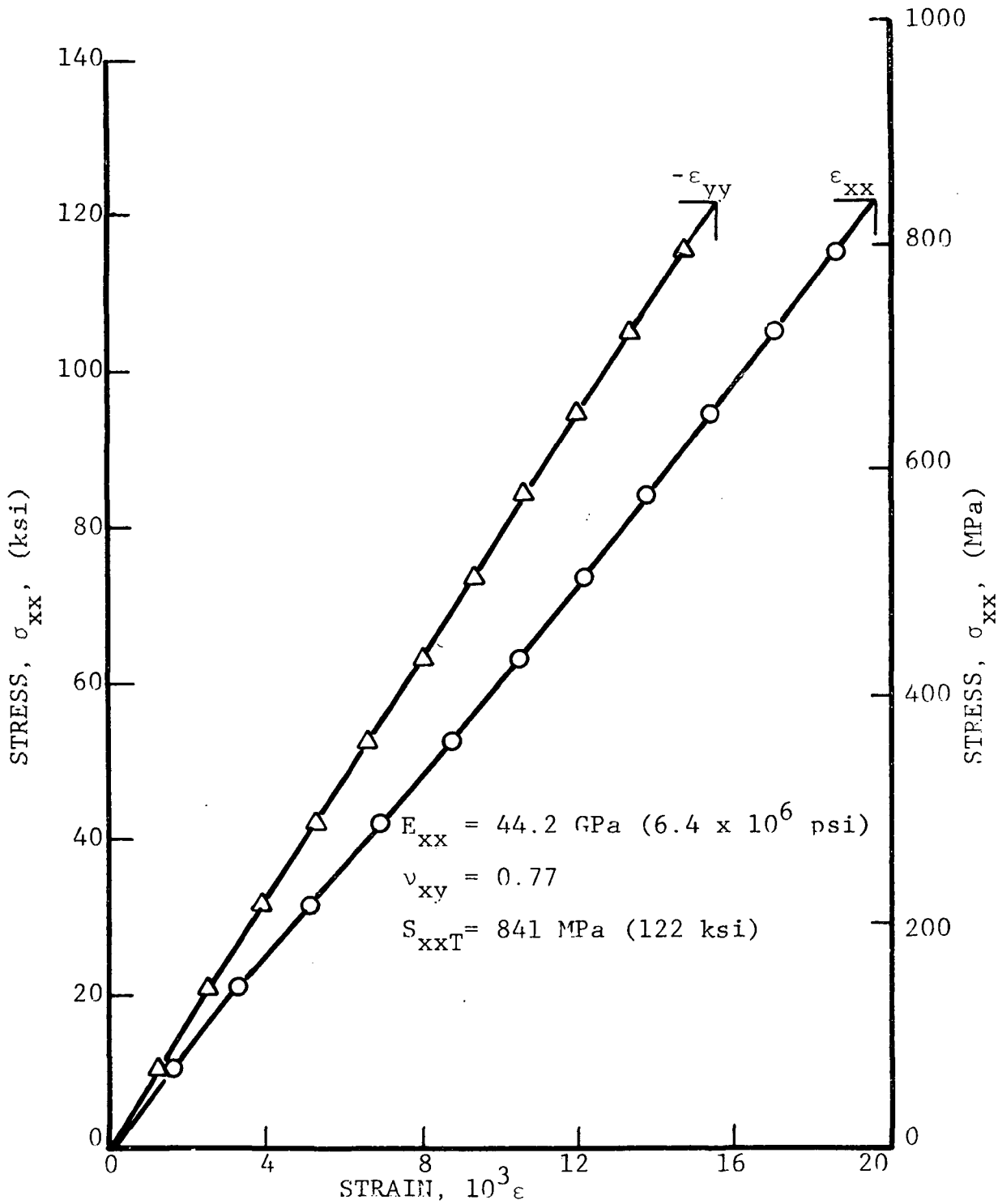

Figure 4.27 STRESS-STRAIN CURVES FOR $[+45/0_2]_s$ KEVLAR 49/ EPOXY FLATTENED TUBULAR SPECIMEN UNDER UNIAXIAL TENSILE LOADING

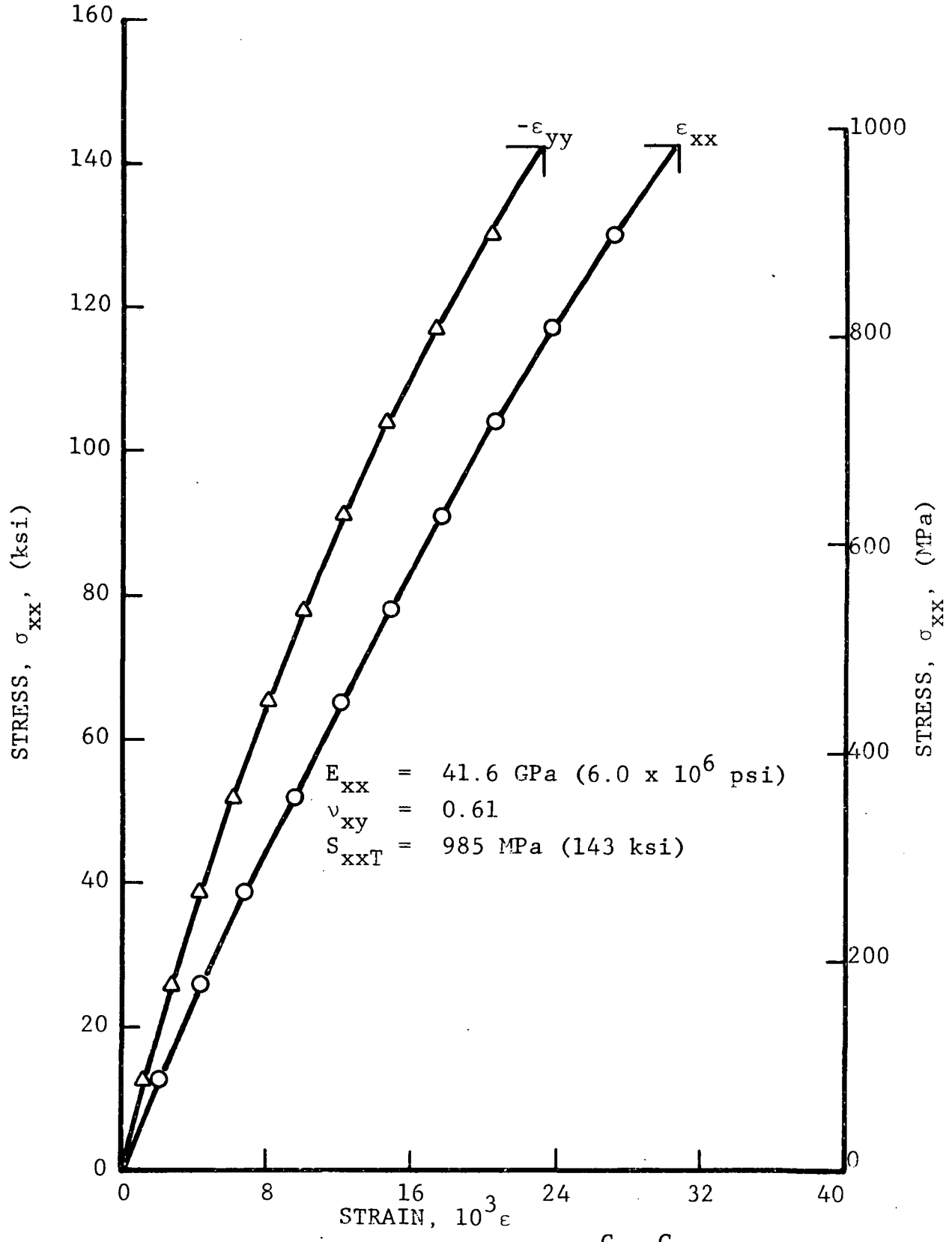

Figure 4.28 STRESS-STRAIN CURVES FOR $[+45^C/0_2^G]_s$ GRAPHITE/ S-GLASS/EPOXY FLAT COUPON UNDER UNIAXIAL TENSILE LOADING

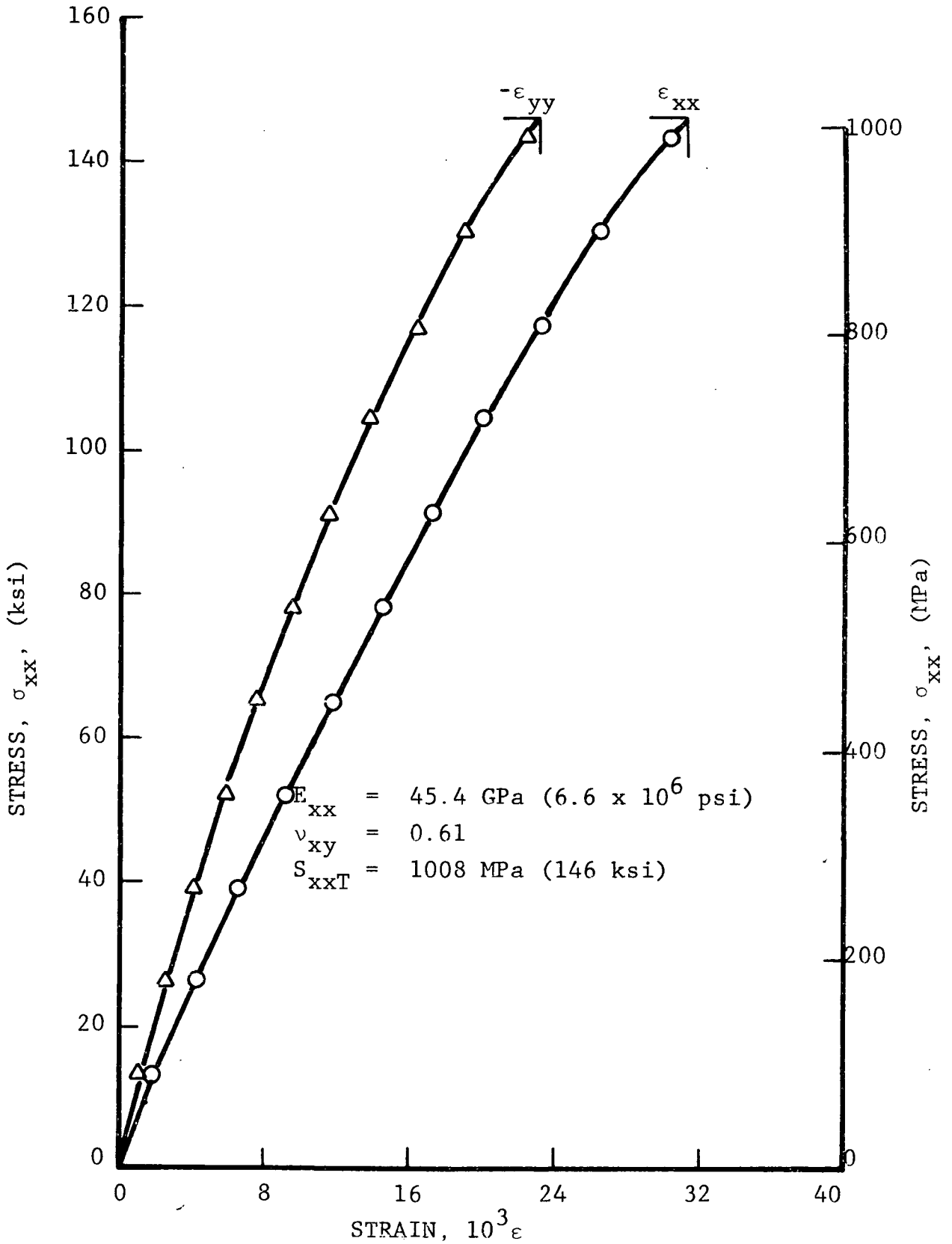

Figure 4.29 STRESS-STRAIN CURVES FOR $[\pm 45^C/0_2^G]_s$ GRAPHITE/ S-GLASS/EPOXY FLAT COUPON UNDER UNIAXIAL TENSILE LOADING

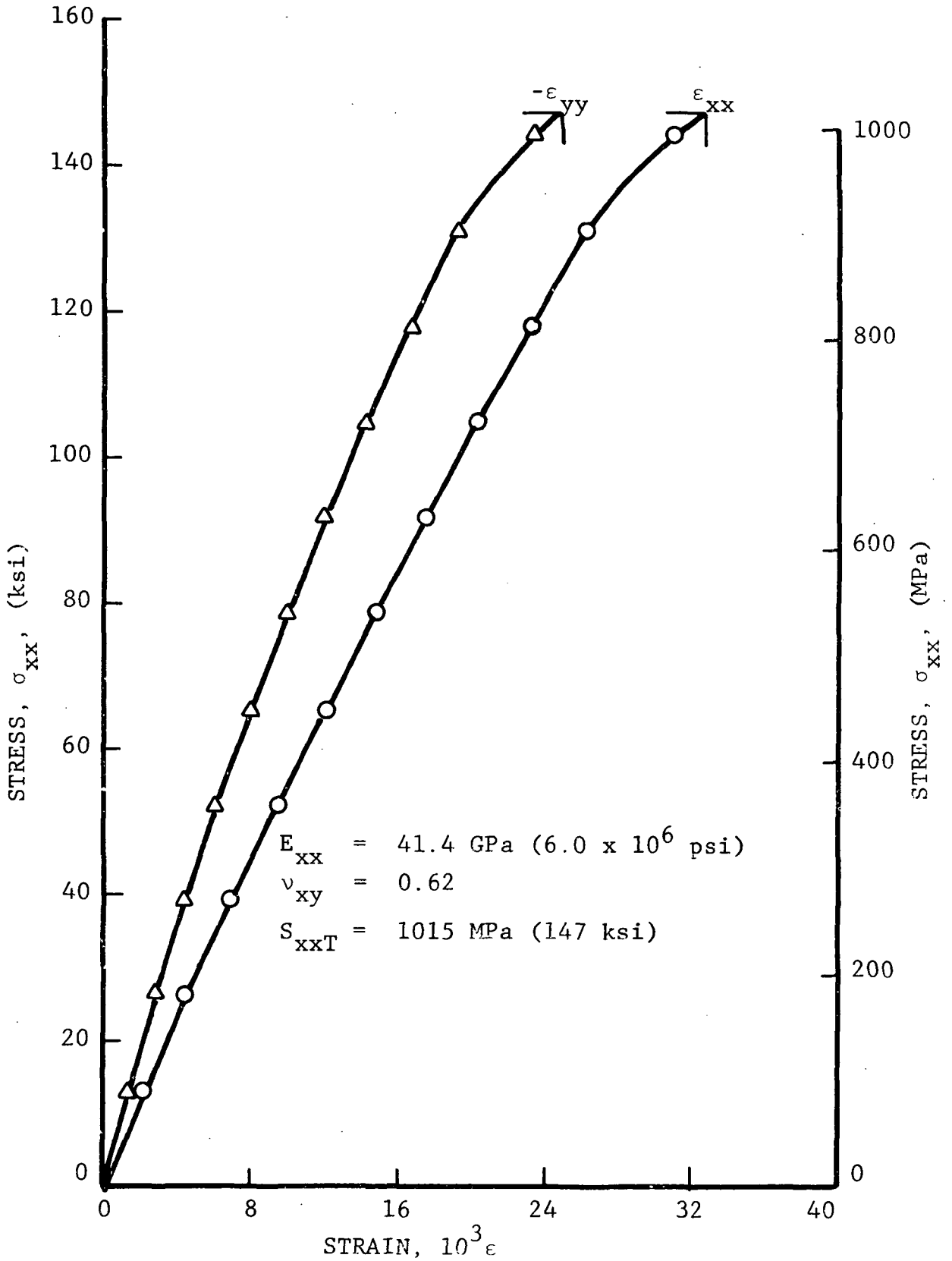

Figure 4.30 STRESS-STRAIN CURVES FOR $[\pm 45^C/0_2^G]_s$ GRAPHITE/ S-GLASS/EPOXY FLAT COUPON UNDER UNIAXIAL TENSILE LOADING

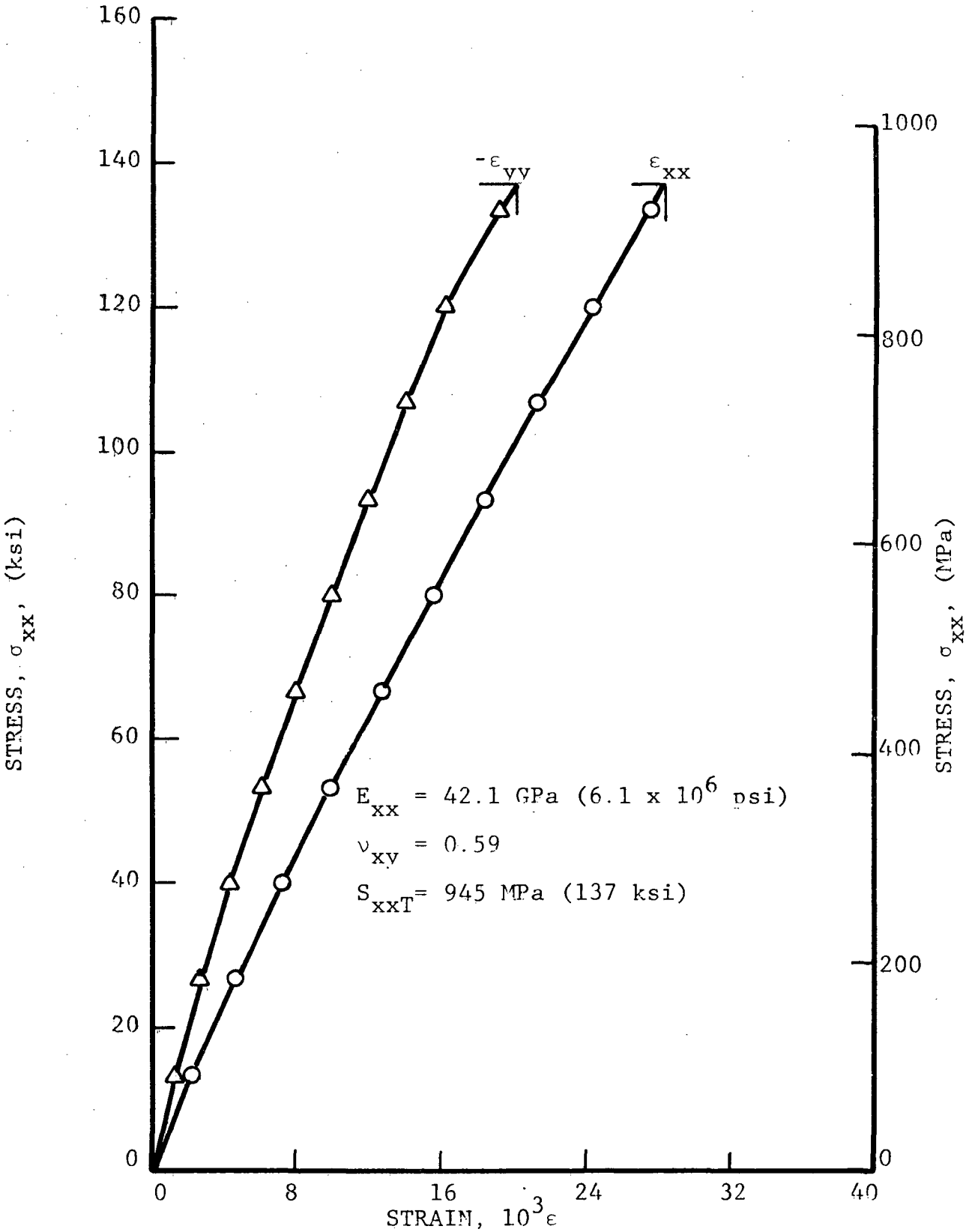

Figure 4.31 STRESS-STRAIN CURVES FOR $[\pm 45^C/0_2^G]_s$ GRAPHITE/S-GLASS/EPOXY FLATTENED TUBULAR SPECIMEN UNDER UNIAXIAL TENSILE LOADING

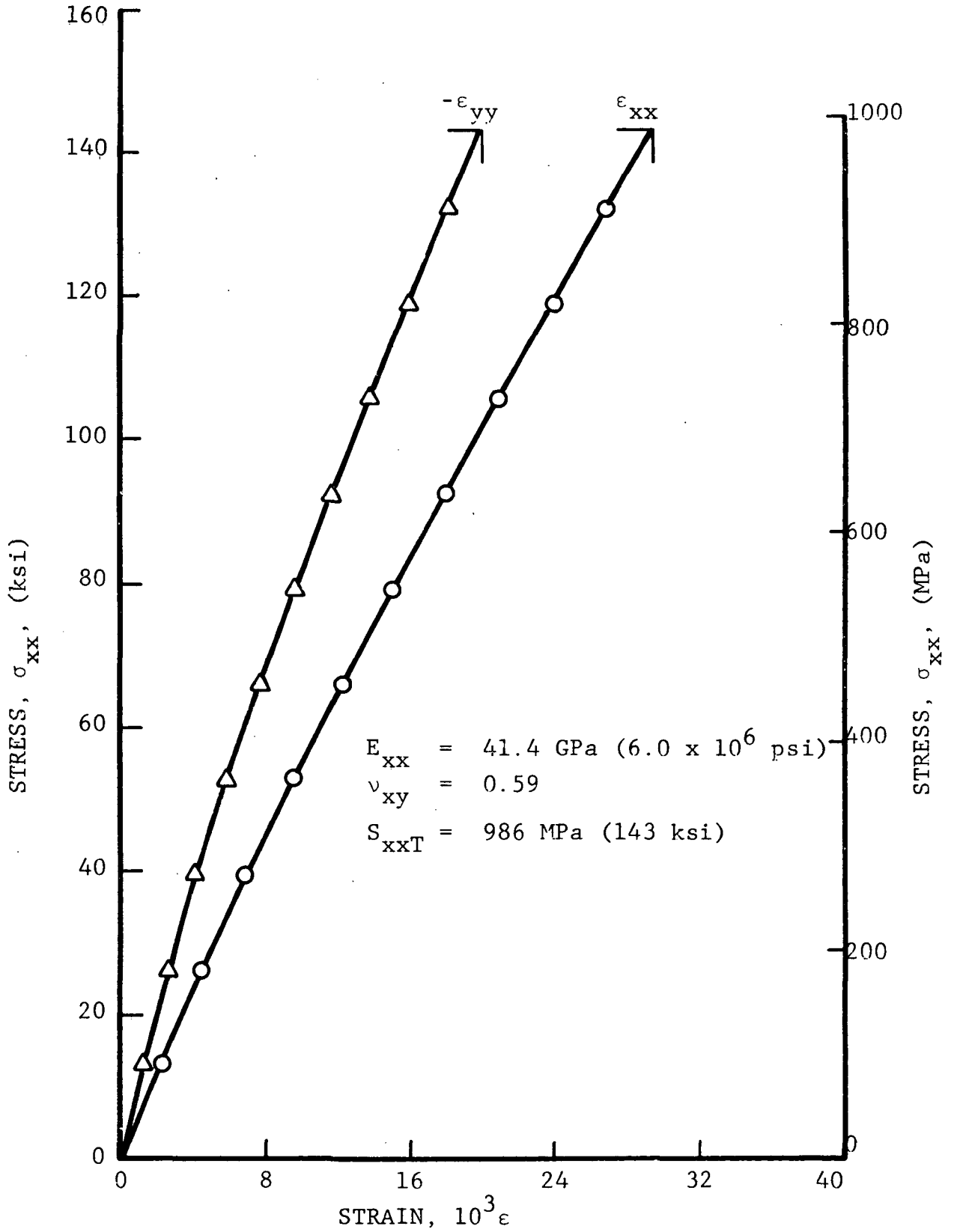

Figure 4.32 STRESS-STRAIN CURVES FOR $[+45^C/0_2^G]_s$ GRAPHITE/S-GLASS/EPOXY FLATTENED TUBULAR SPECIMEN UNDER UNIAXIAL TENSILE LOADING

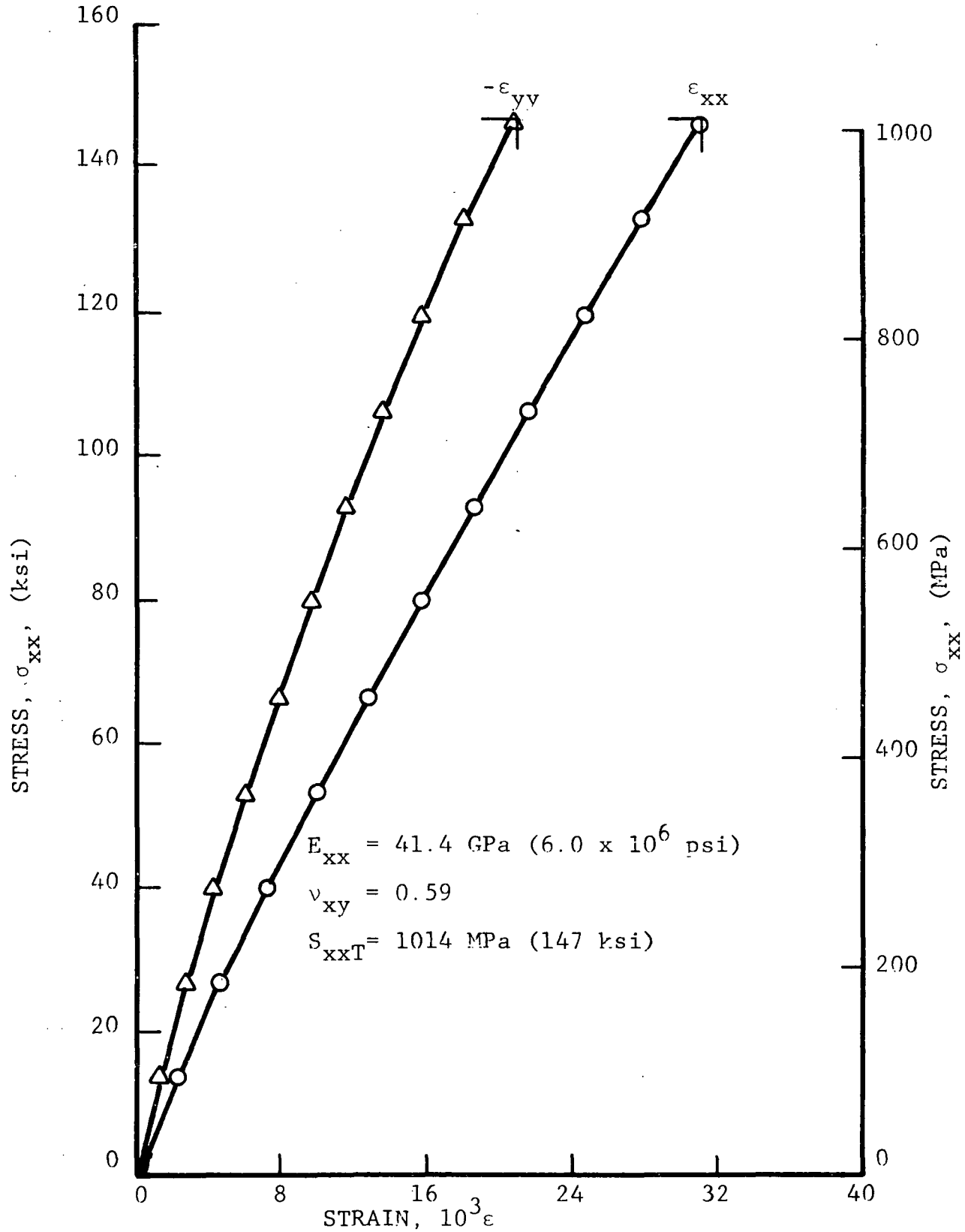

Figure 4.33 STRESS-STRAIN CURVES FOR $[\pm 45^C/0_2^G]_s$ GRAPHITE/ S-GLASS/EPOXY FLATTENED TUBULAR SPECIMEN UNDER UNIAXIAL TENSILE LOADING

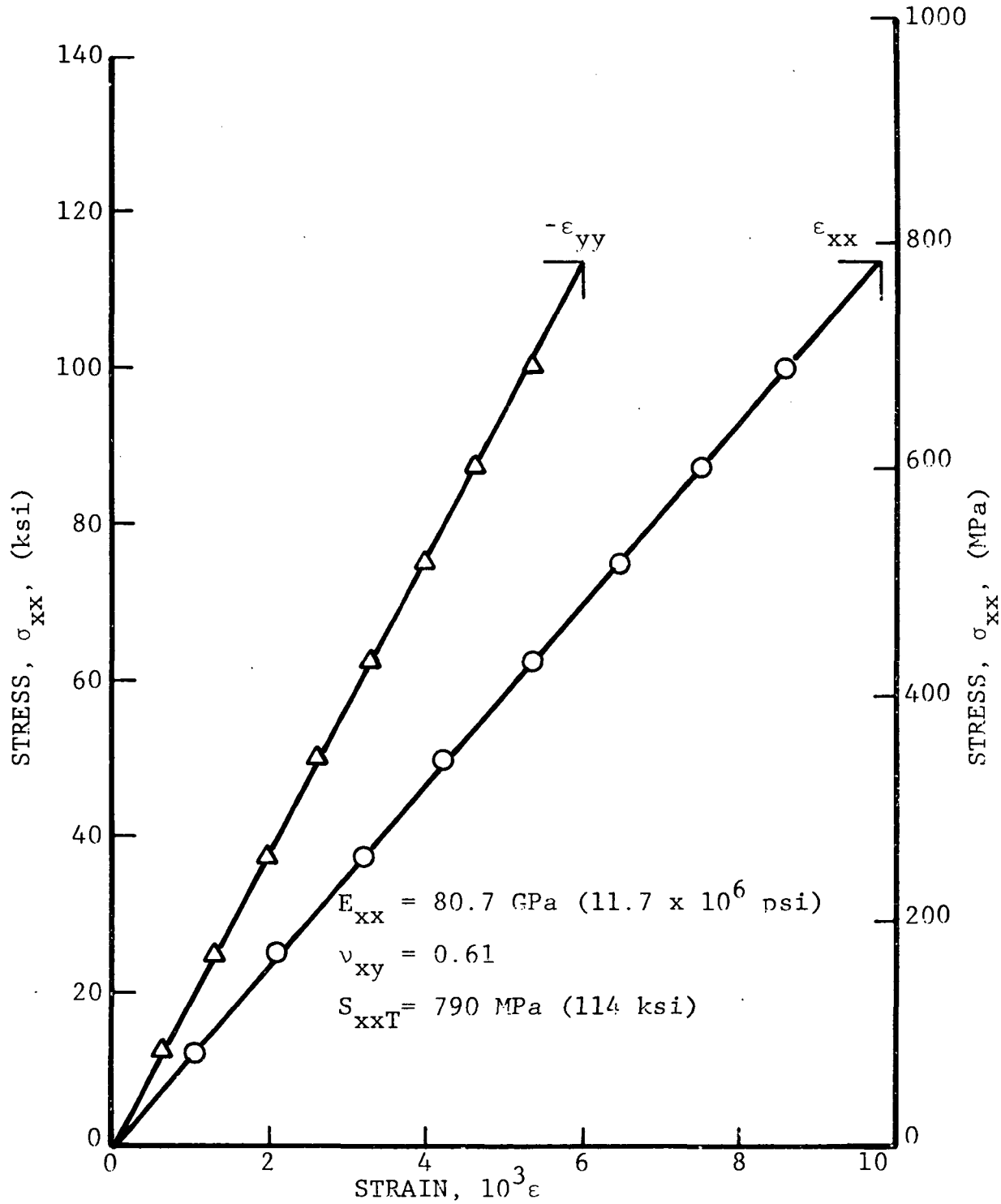

Figure 4.34 STRESS-STRAIN CURVES FOR $[0_2/\pm45]_s$ GRAPHITE/ EPOXY FLAT COUPON UNDER UNIAXIAL TENSILE LOADING

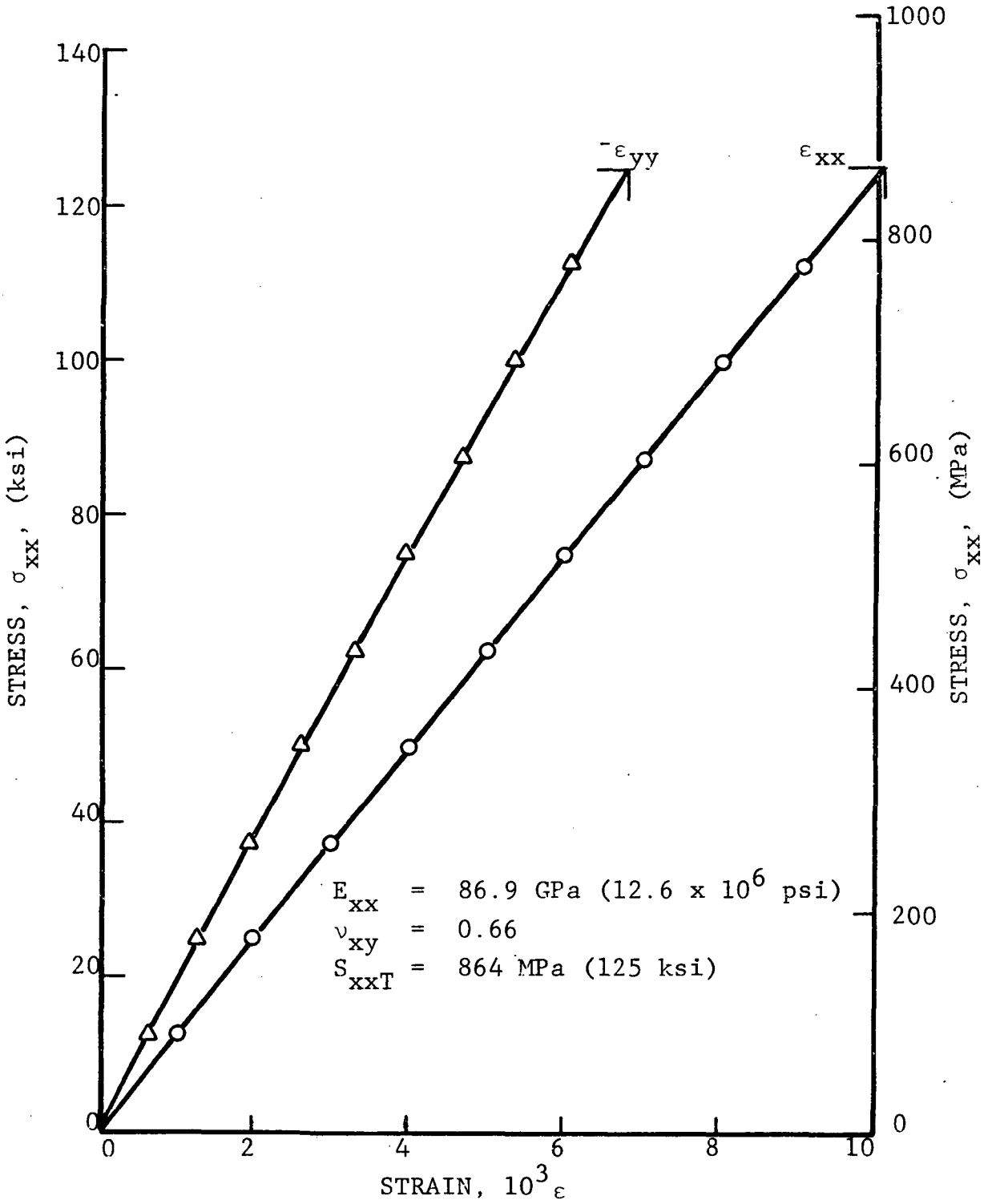

Figure 4.35 STRESS-STRAIN CURVES FOR $[0_2/\pm45]_s$ GRAPHITE/ EPOXY FLAT COUPON UNDER UNIAXIAL TENSILE LOADING

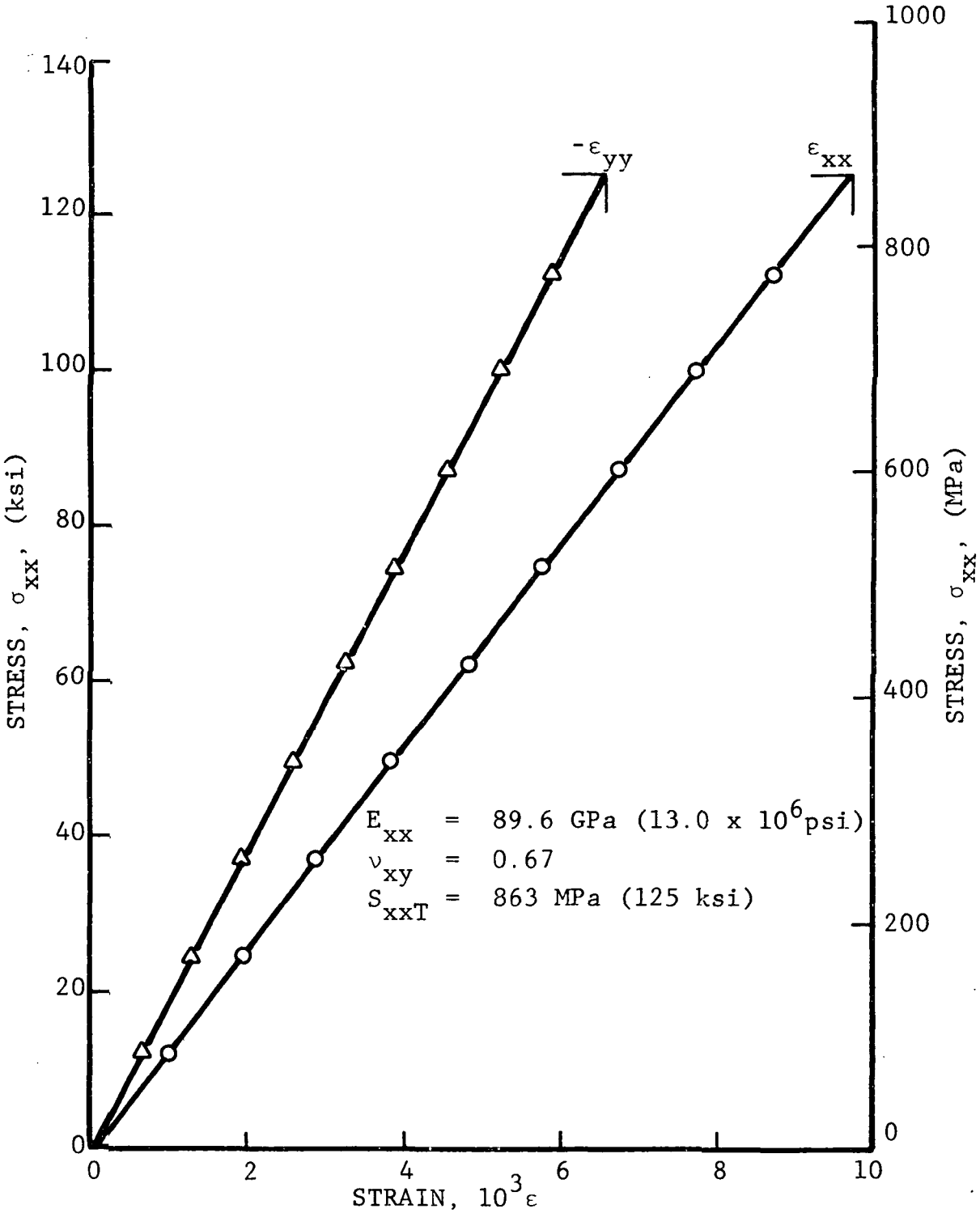

Figure 4.36 STRESS-STRAIN CURVES FOR $[0_2/\pm45]_s$ GRAPHITE/ EPOXY FLAT COUPON UNDER UNIAXIAL TENSILE LOADING

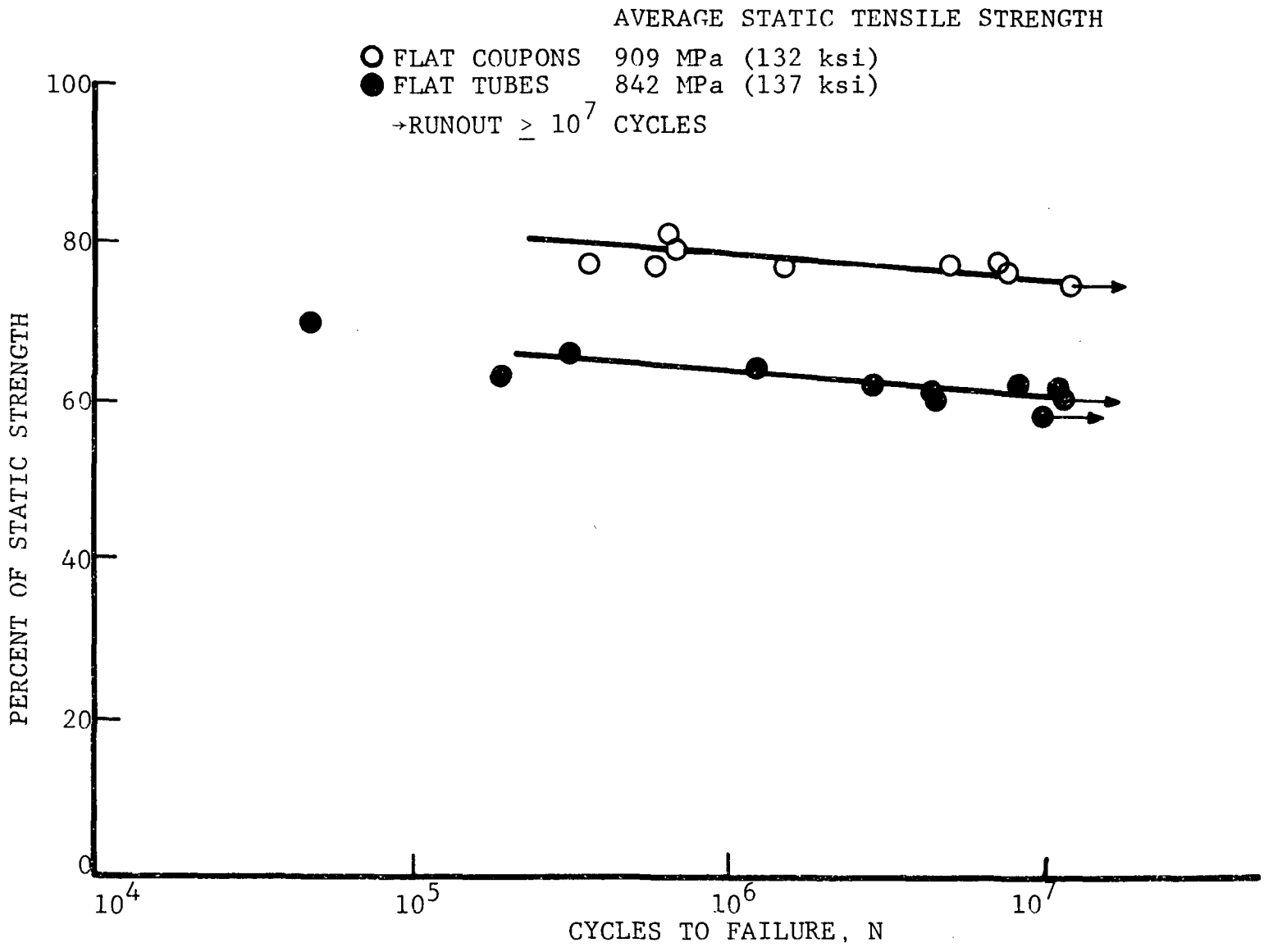

Figure 4-37 TENSILE CYCLING FATIGUE STRENGTH OF $[\pm 45/0_2]_s$ GRAPHITE/EPOXY SPECIMENS

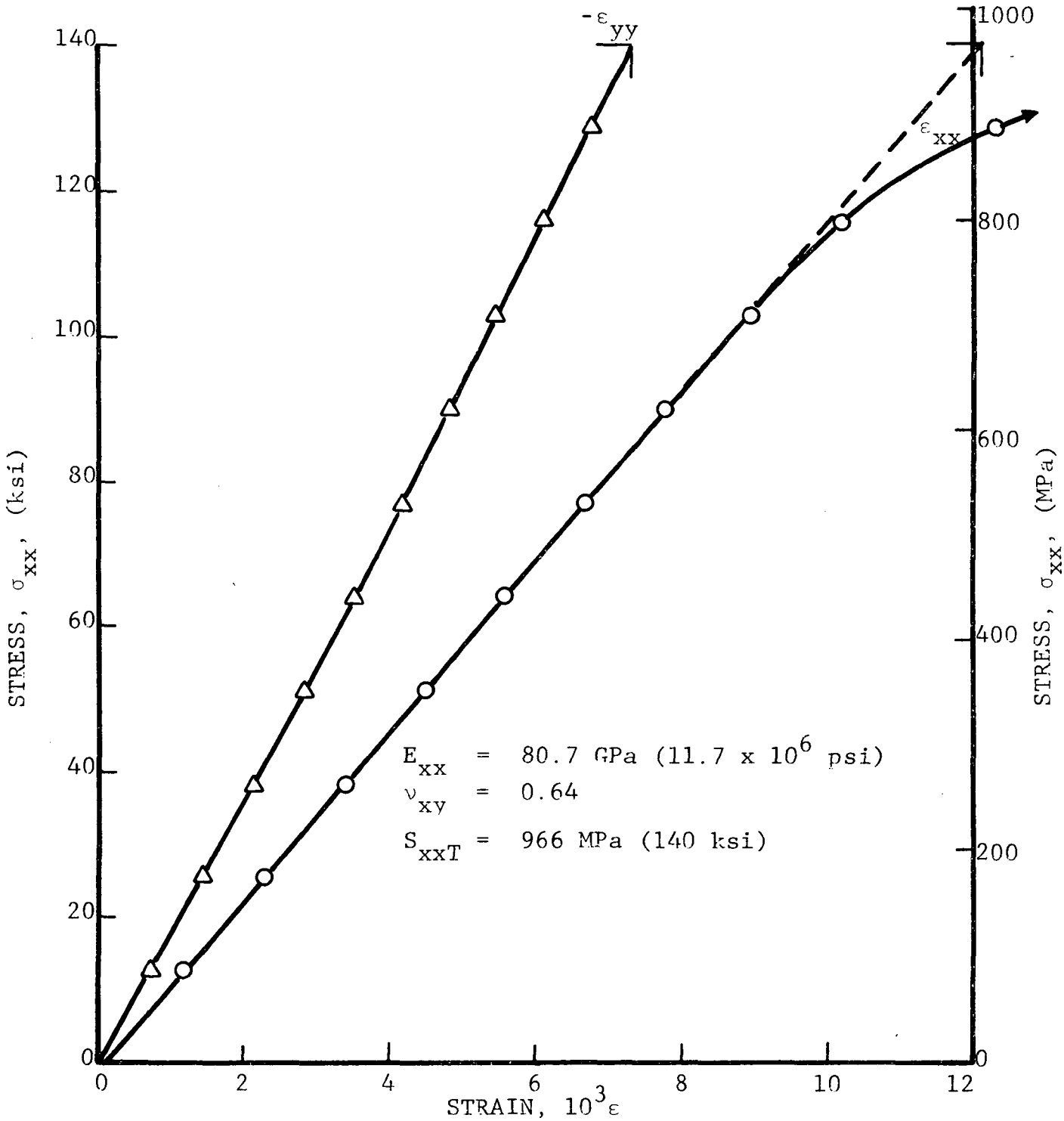

Figure 4.38 STRESS-STRAIN CURVES FOR $[+45/0_2]_s$ GRAPHITE/EPOXY FLATTENED TUBULAR SPECIMEN TESTED IN UNIAXIAL TENSION AFTER 10^7 CYCLES OF TENSILE FATIGUE TO 58 PERCENT OF STATIC STRENGTH

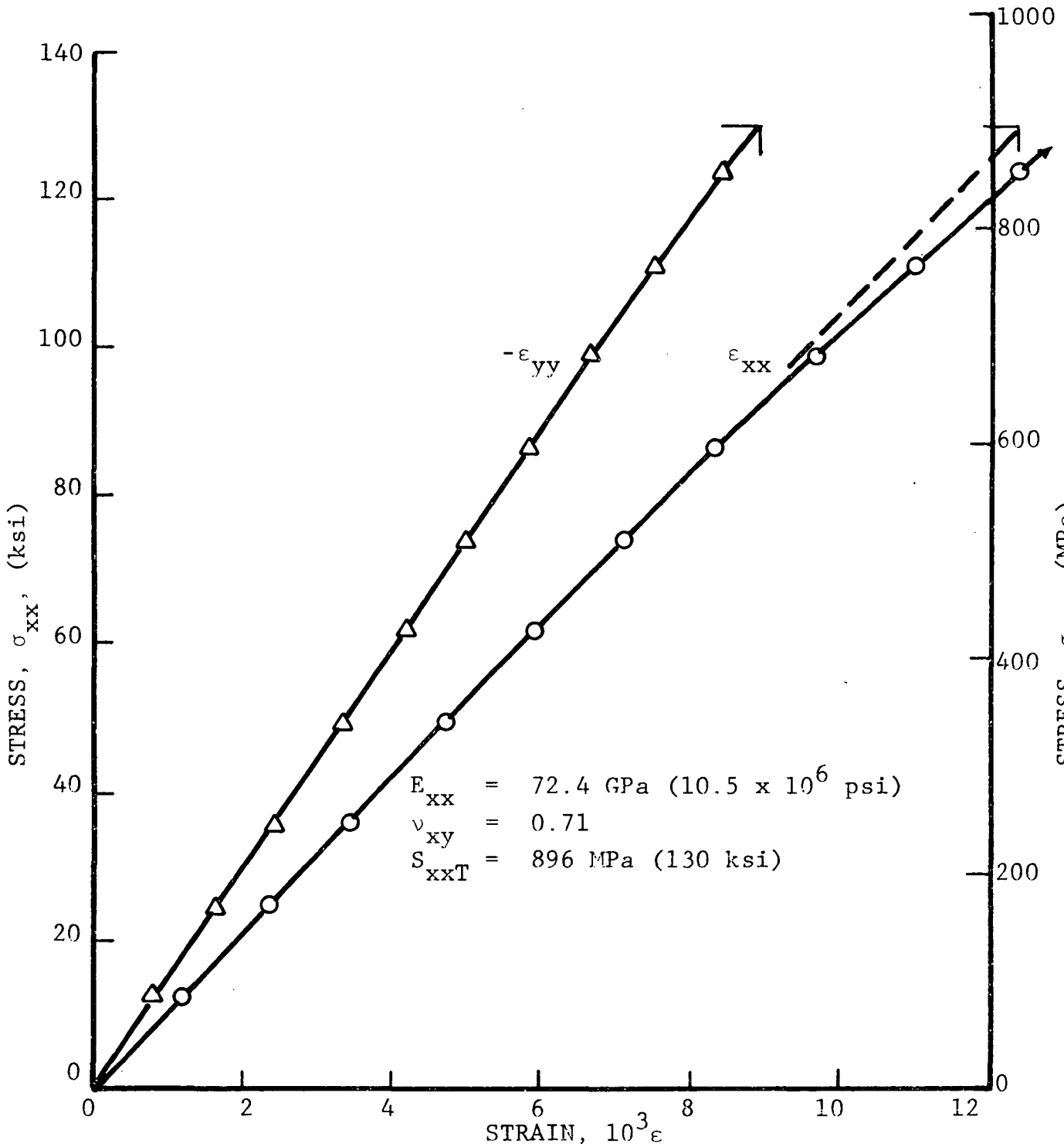

Figure 4.39 STRESS-STRAIN CURVES FOR $[+45/0_2]_s$ GRAPHITE/EPOXY FLATTENED TUBULAR SPECIMEN TESTED IN UNIAXIAL TENSION AFTER 1.23 x 10^7 CYCLES OF TENSILE FATIGUE TO 60.0 PERCENT OF STATIC STRENGTH

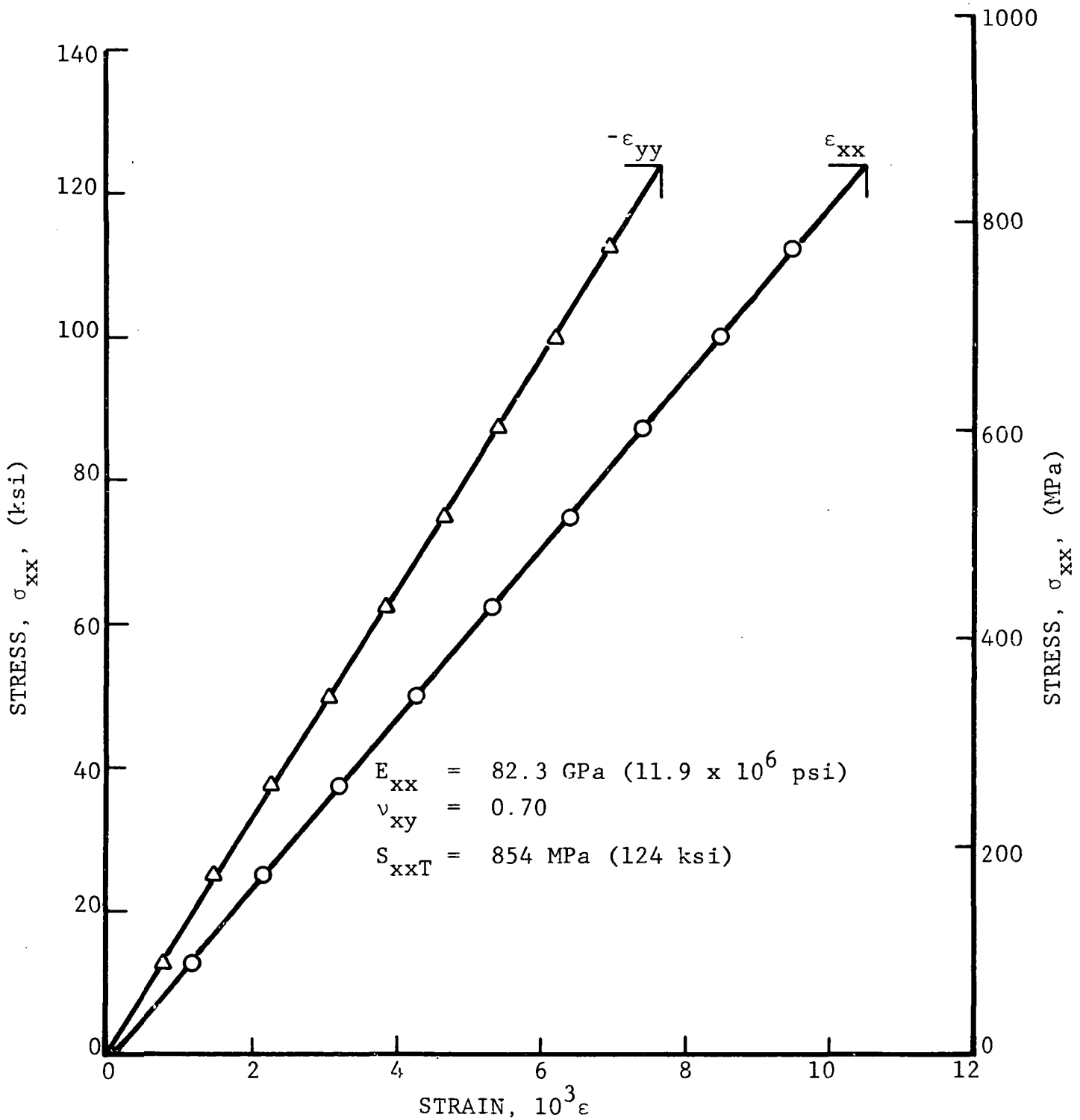

Figure 4.40 STRESS-STRAIN CURVES FOR $[\pm 45/0_2]_s$ GRAPHITE/EPOXY FLAT COUPON TESTED IN UNIAXIAL TENSION AFTER 1.24×10^7 CYCLES OF TENSILE FATIGUE TO 74.3 PERCENT OF STATIC STRENGTH

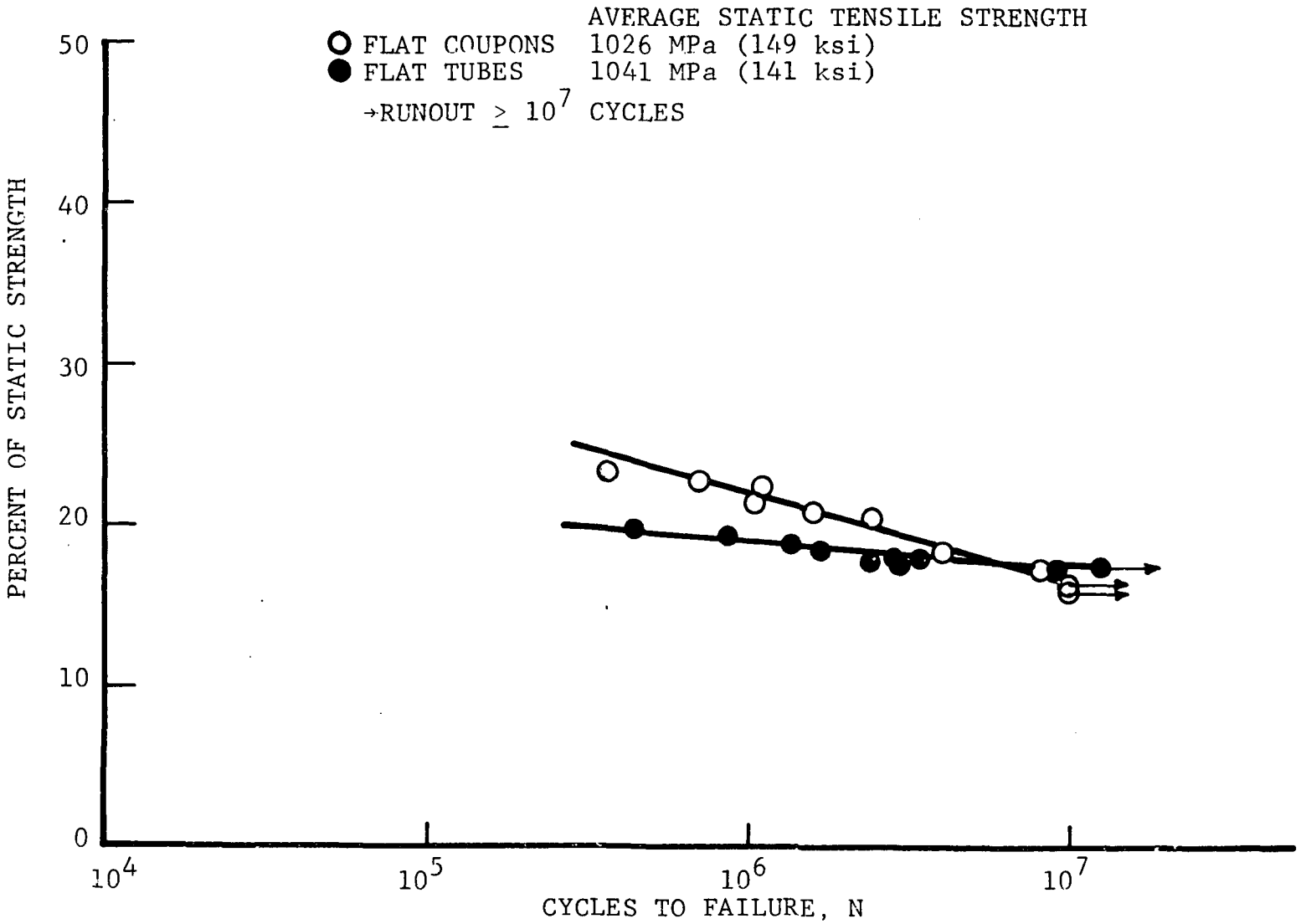

Figure 4-41 TENSILE CYCLING FATIGUE STRENGTH OF $[\pm 45/0_2]_s$ S-GLASS/EPOXY SPECIMENS

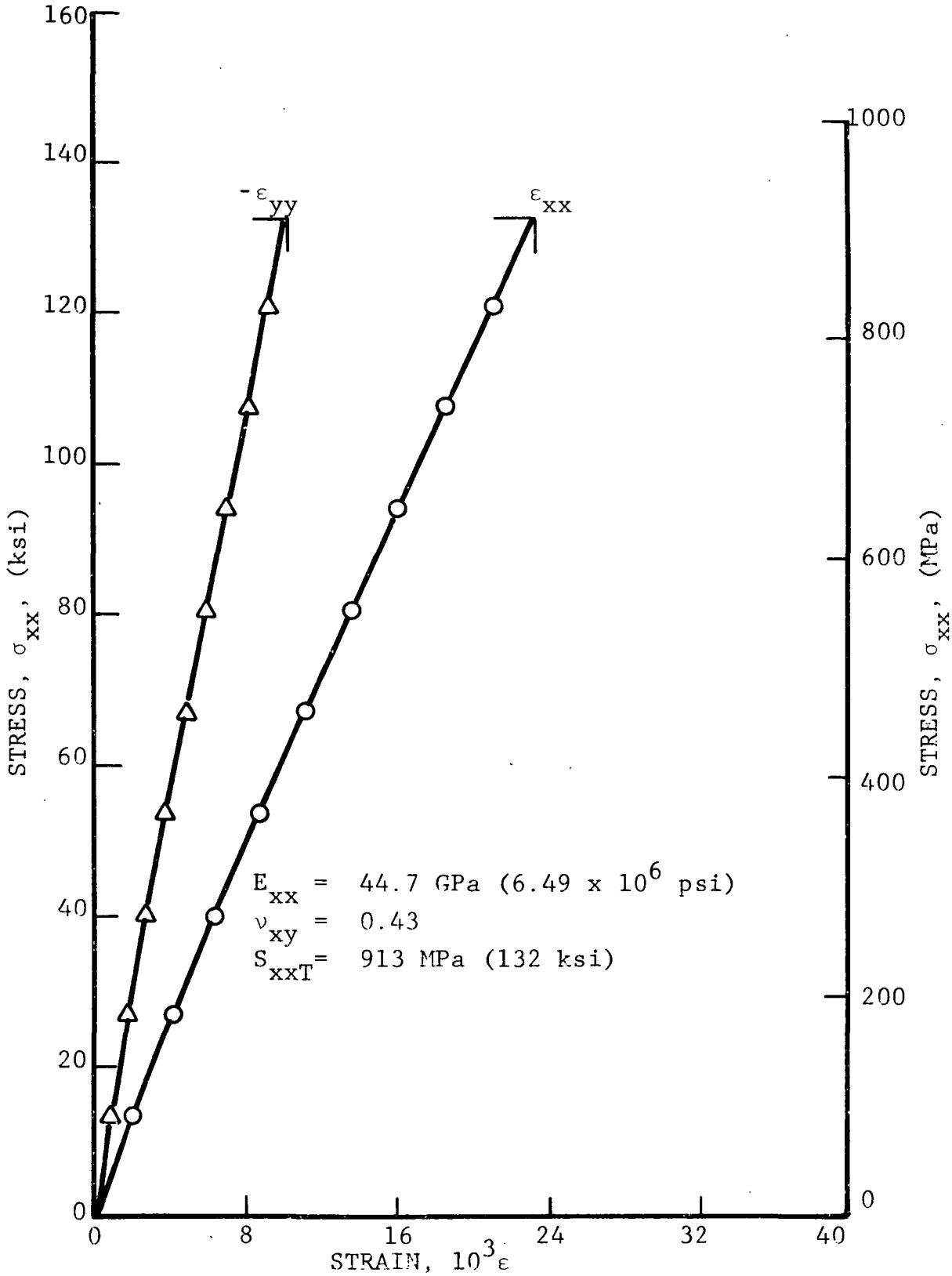

Figure 4.42 STRESS-STRAIN CURVES FOR $[\pm 45/0_2]_s$ S-GLASS/EPOXY FLATTENED TUBULAR SPECIMEN TESTED IN UNIAXIAL TENSION AFTER 1.239×10^7 CYCLES OF TENSILE FATIGUE TO 17.5 PERCENT OF STATIC STRENGTH

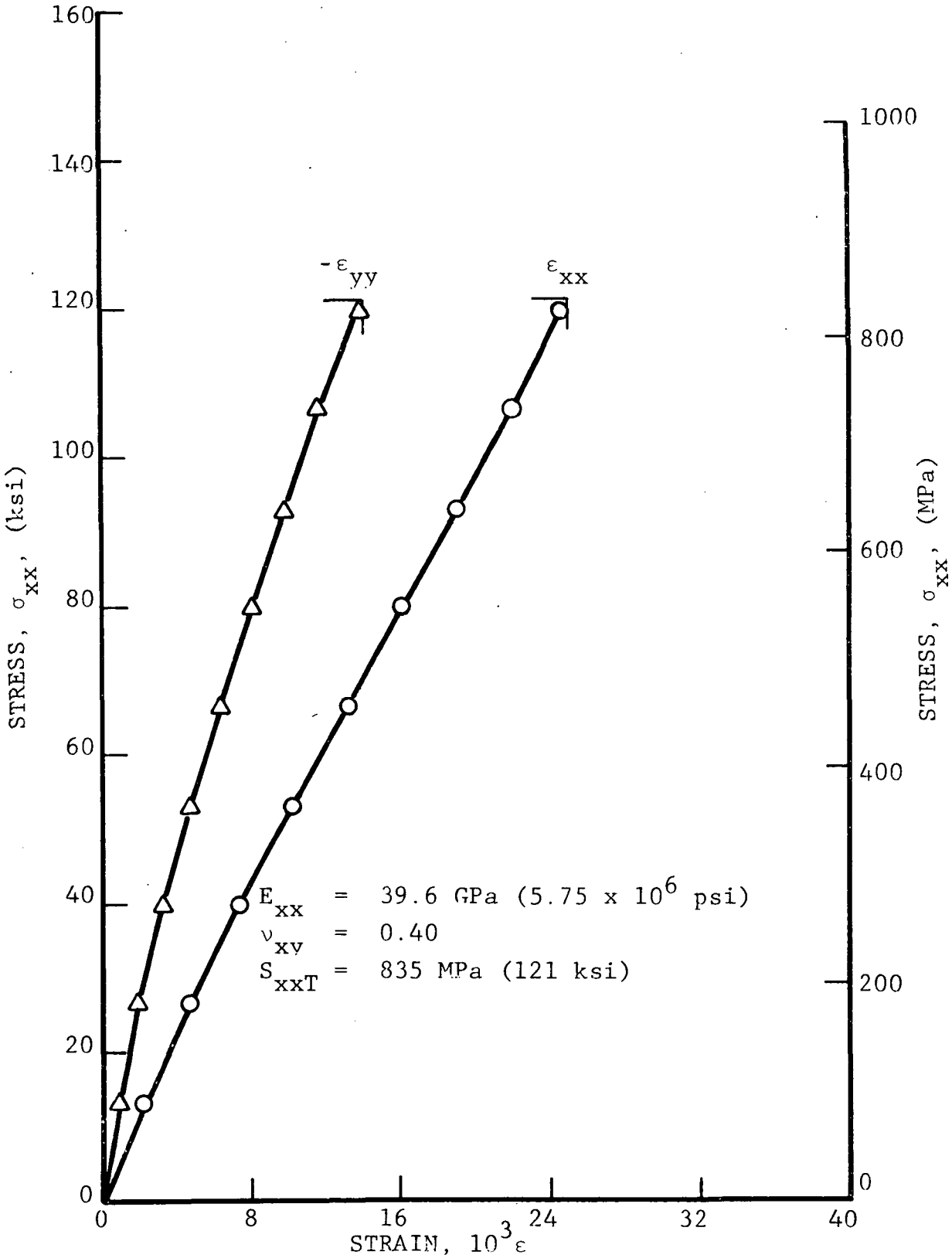

Figure 4.43 STRESS-STRAIN CURVES FOR $[\pm 45/0_2]_s$ S-GLASS/EPOXY FLAT COUPON TESTED IN UNIAXIAL TENSION AFTER 10^7 CYCLES OF TENSILE FATIGUE TO 16.0 PERCENT OF STATIC STRENGTH

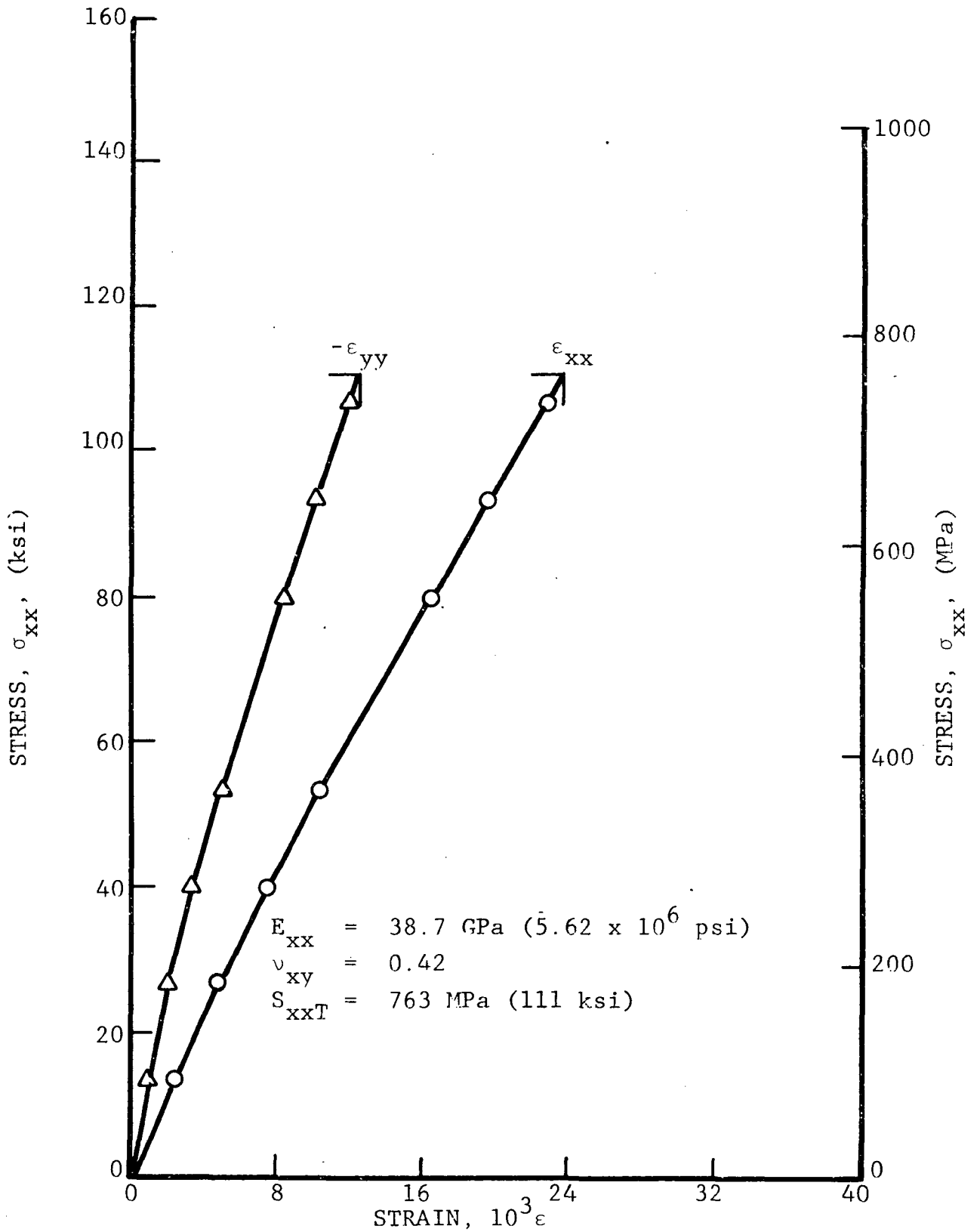

Figure 4.44 STRESS-STRAIN CURVES FOR $[+45/0_2]_s$ S-GLASS/EPOXY FLAT COUPON TESTED IN UNIAXIAL TENSION AFTER 10^7 CYCLES OF TENSILE FATIGUE TO 16.4 PERCENT OF STATIC STRENGTH

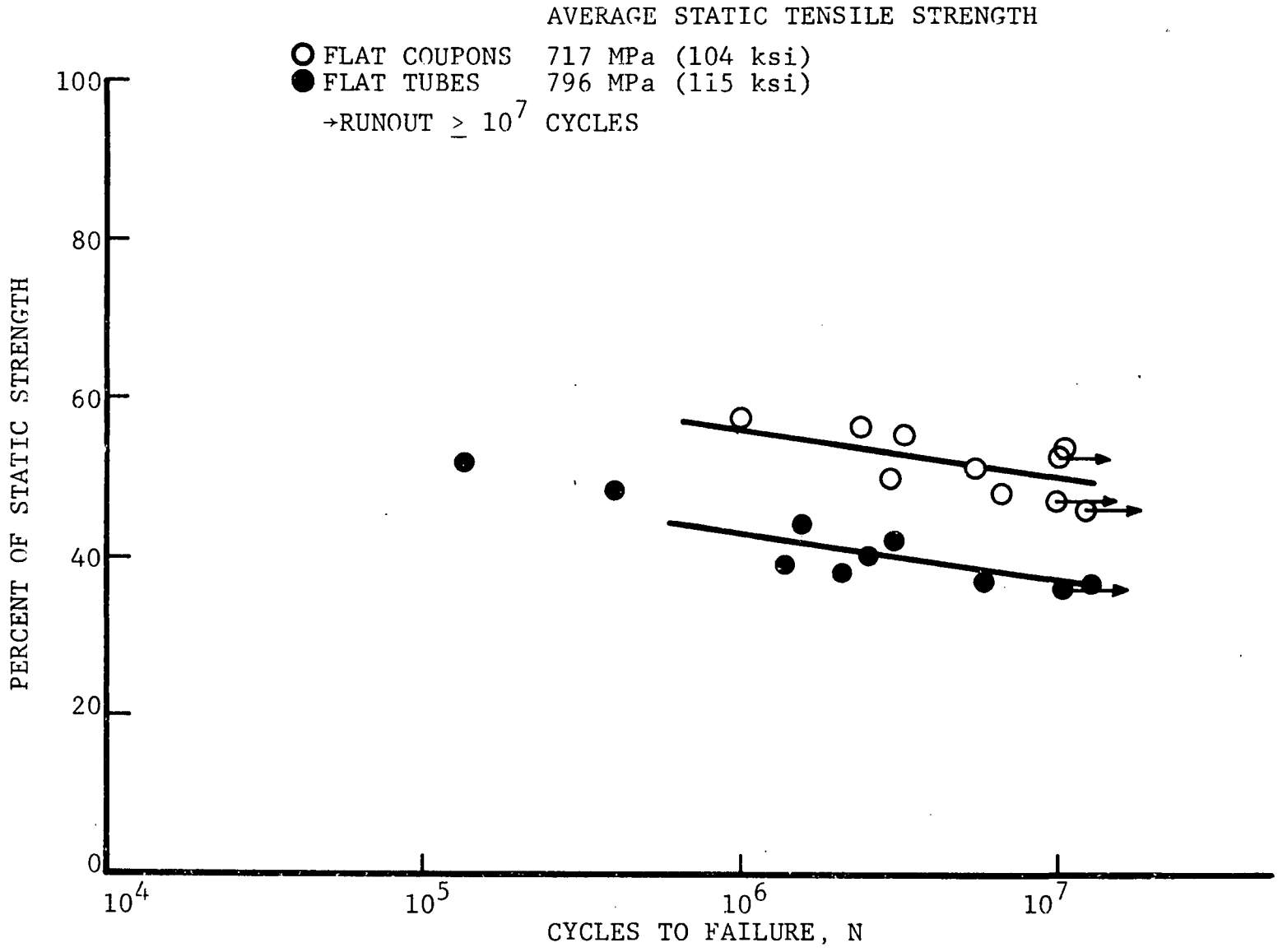

Figure 4-45 TENSILE CYCLING FATIGUE STRENGTH OF $[\pm 45/0_2]_s$ KEVLAR 49/EPOXY SPECIMENS

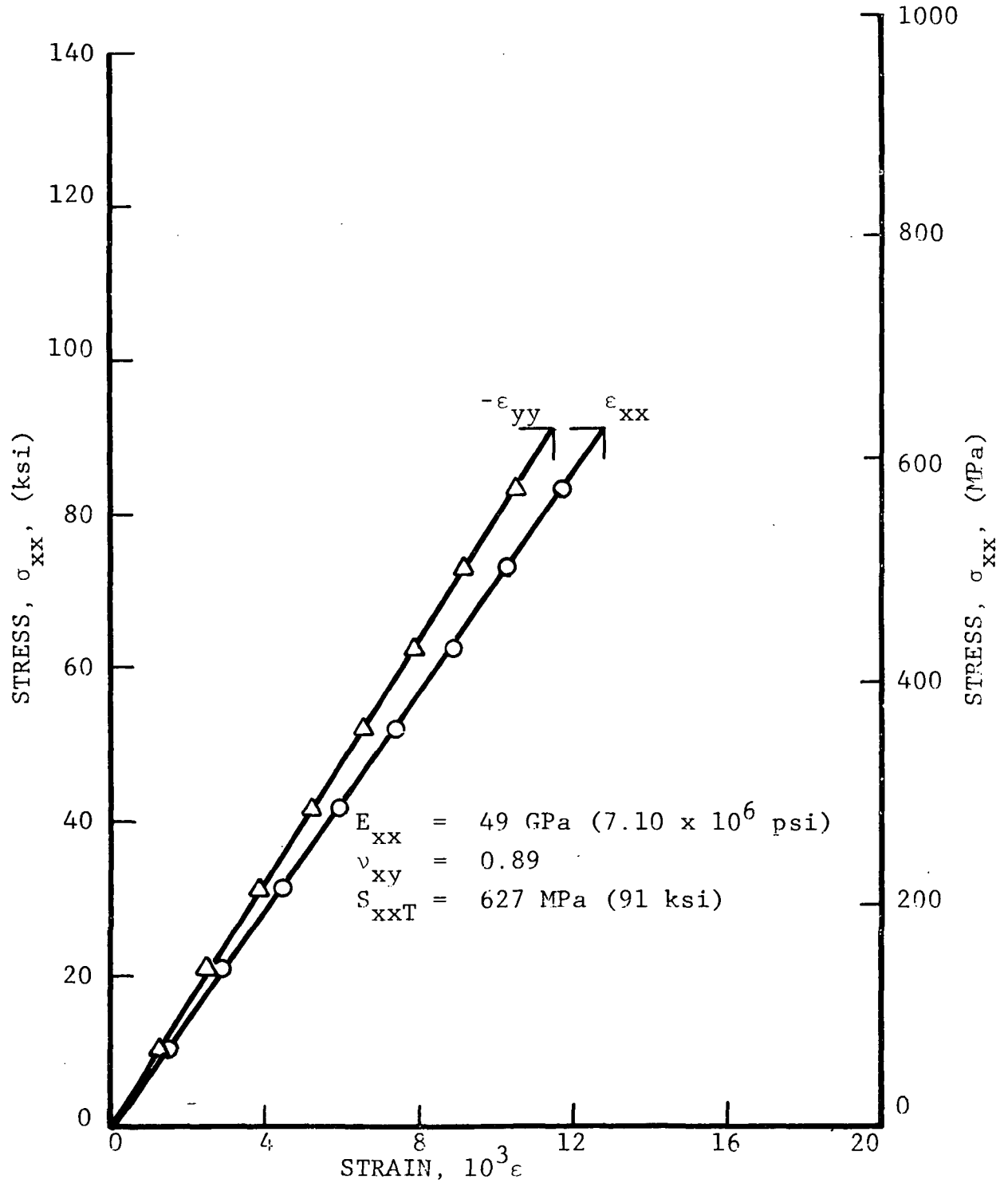

Figure 4.46 STRESS-STRAIN CURVES FOR $[\pm 45/0_2]_s$ KEVLAR 49/ FLATTENED TUBULAR SPECIMEN TESTED IN UNIAXIAL TENSION AFTER 1.025×10^7 CYCLES OF TENSILE FATIGUE TO 36.0 PERCENT OF STATIC STRENGTH

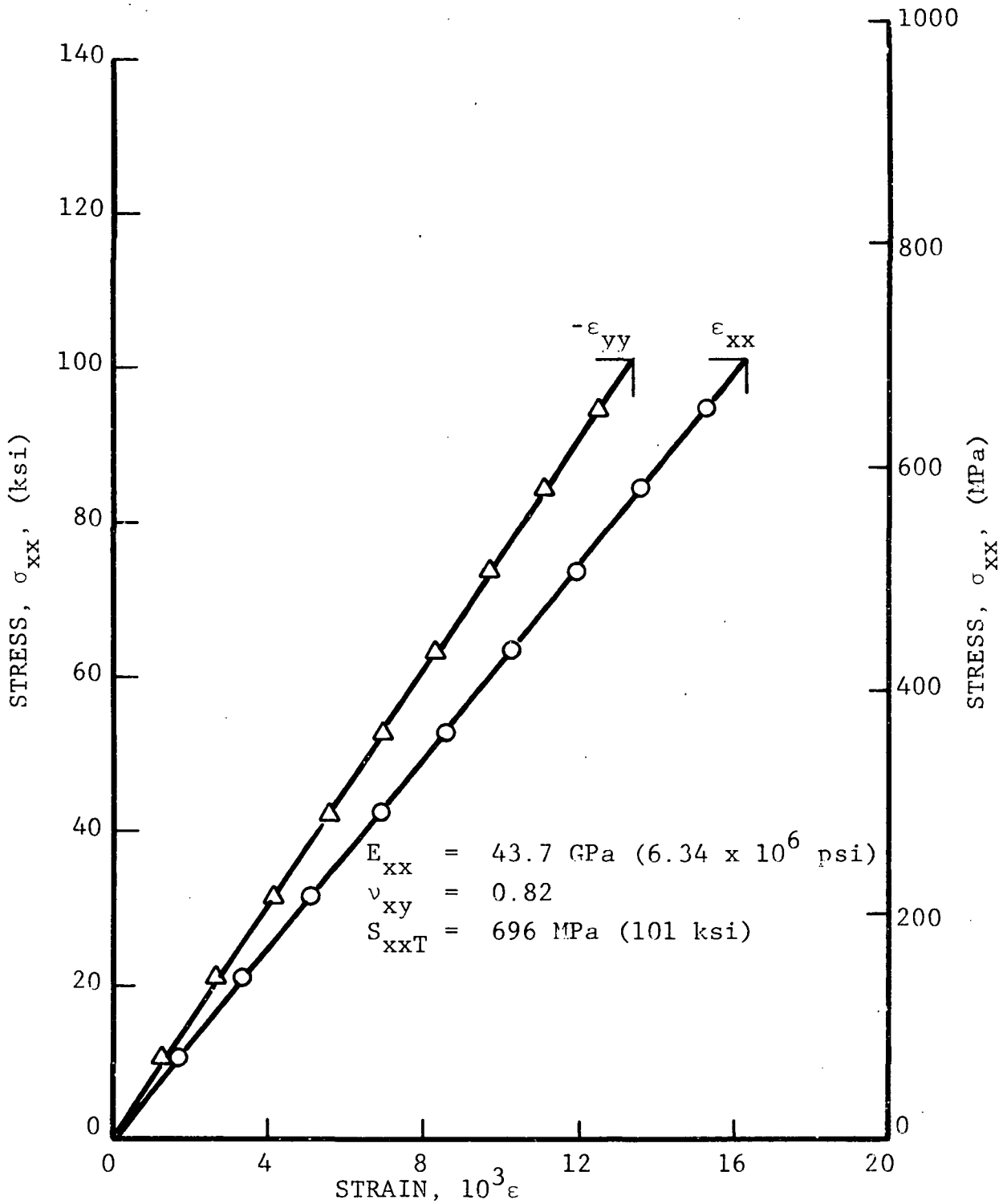

Figure 4.47 STRESS-STRAIN CURVES FOR $[\pm 45/0_2]_s$ KEVLAR 49/EPOXY FLAT COUPON TESTED IN UNIAXIAL TENSION AFTER 1.231×10^7 CYCLES OF TENSILE FATIGUE TO 46.0 PERCENT OF STATIC STRENGTH

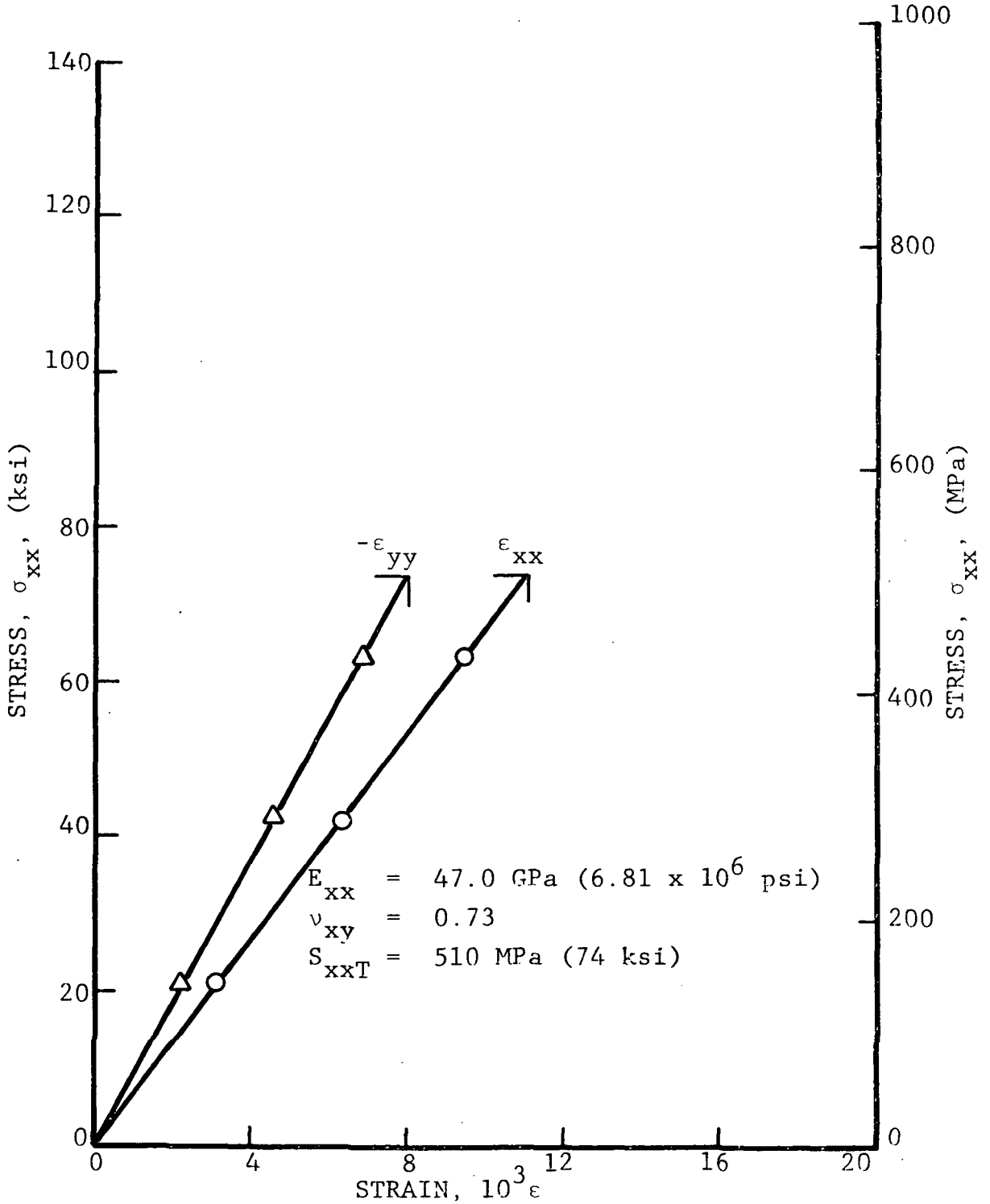

Figure 4.48 STRESS-STRAIN CURVES FOR $[\pm 45/0_2]_s$ KEVLAR 49/ EPOXY FLAT COUPON TESTED IN UNIAXIAL TENSION AFTER 1.0 x 10^7 CYCLES OF TENSILE FATIGUE TO 47.0 PERCENT OF STATIC STRENGTH

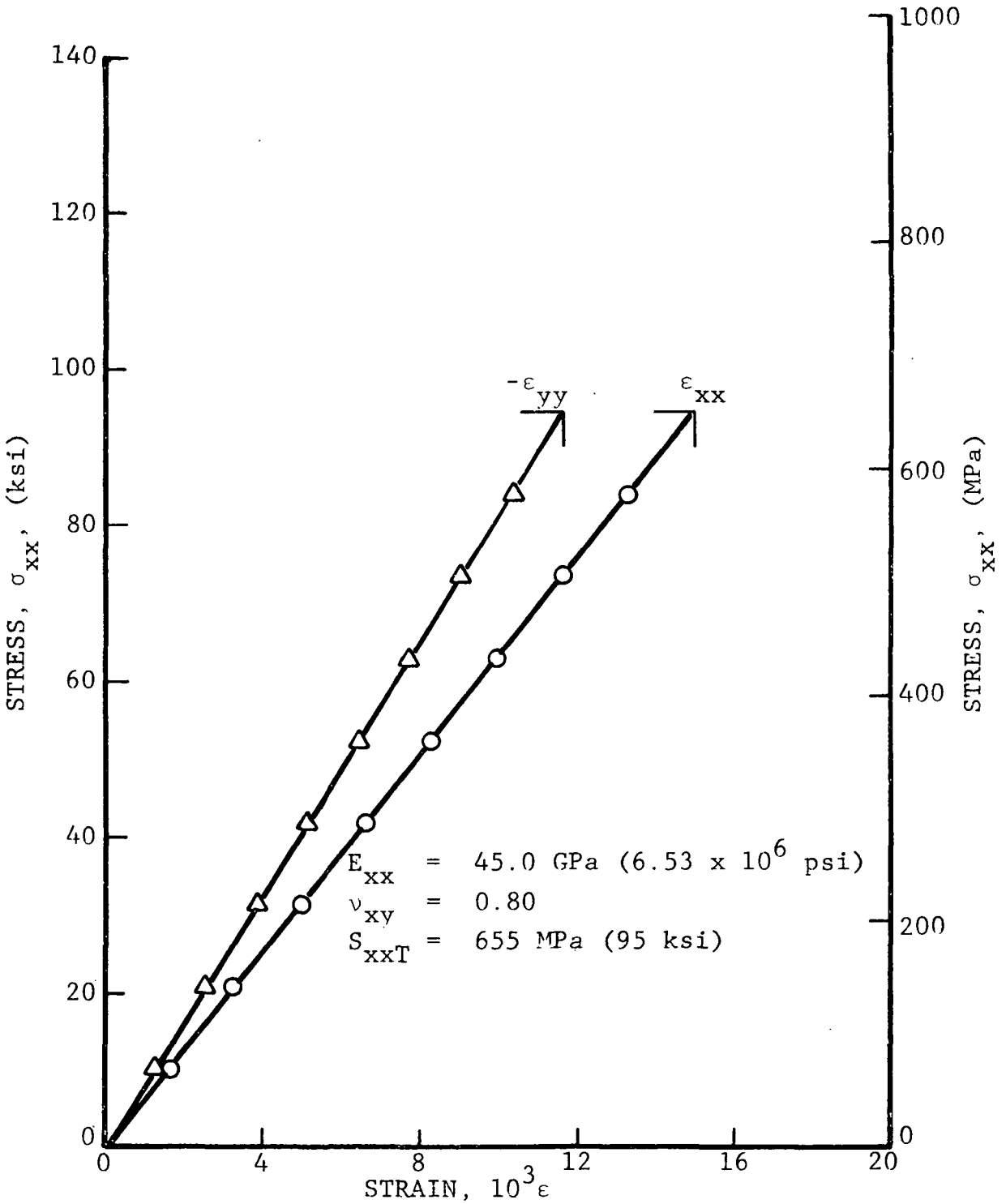

Figure 4.49 STRESS-STRAIN CURVES FOR $[\pm 45/0_2]_s$ KEVLAR 49/ EPOXY FLAT COUPON TESTED IN UNIAXIAL TENSION AFTER 1.02 x 10^7 CYCLES OF TENSILE FATIGUE TO 52.5 PERCENT OF STATIC STRENGTH

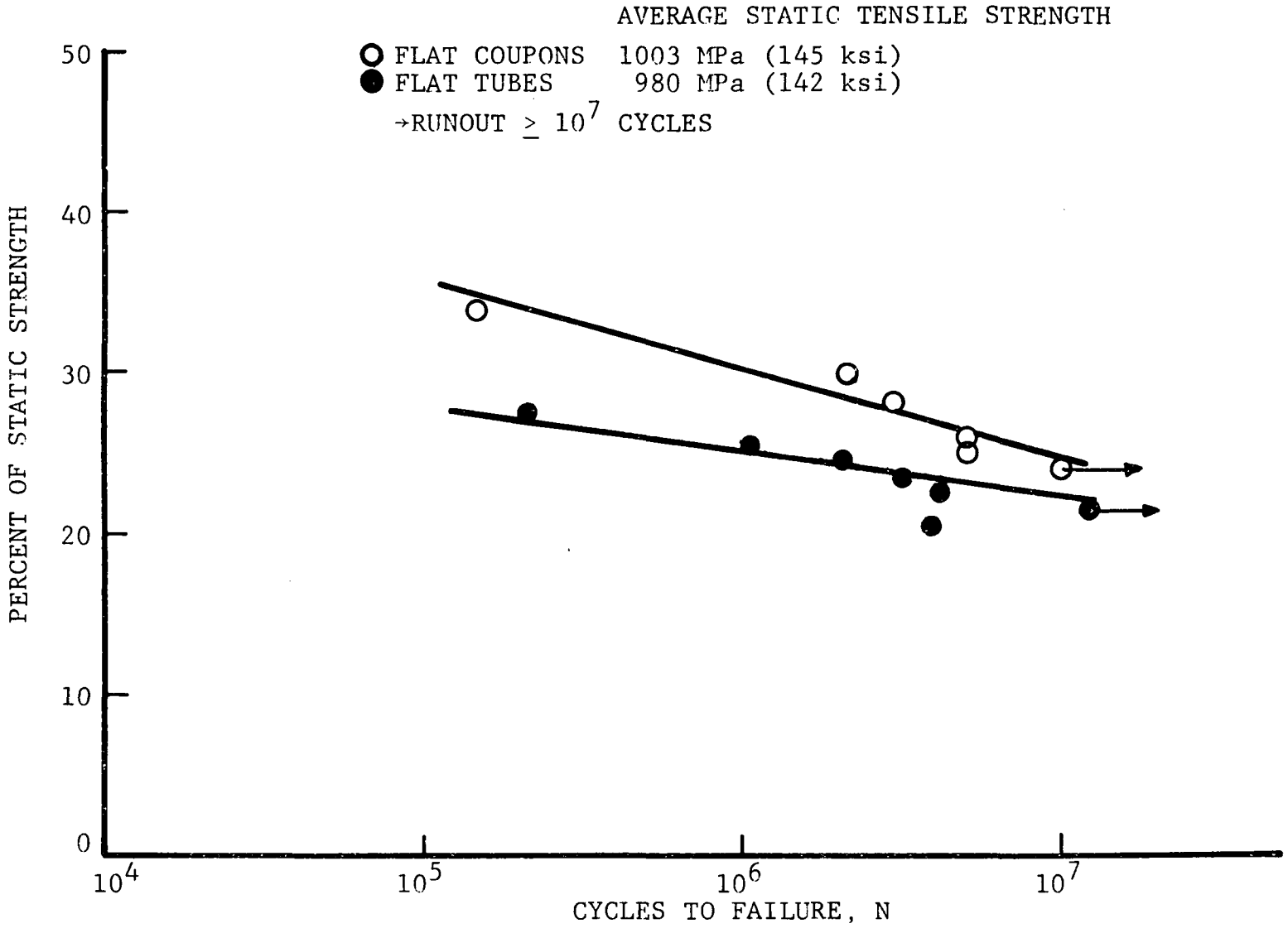

Figure 4-50 TENSILE CYCLING FATIGUE STRENGTH OF $[\pm 45^{C}/0_{2}^{G}]_{s}$ GRAPHITE/S-GLASS/EPOXY SPECIMENS

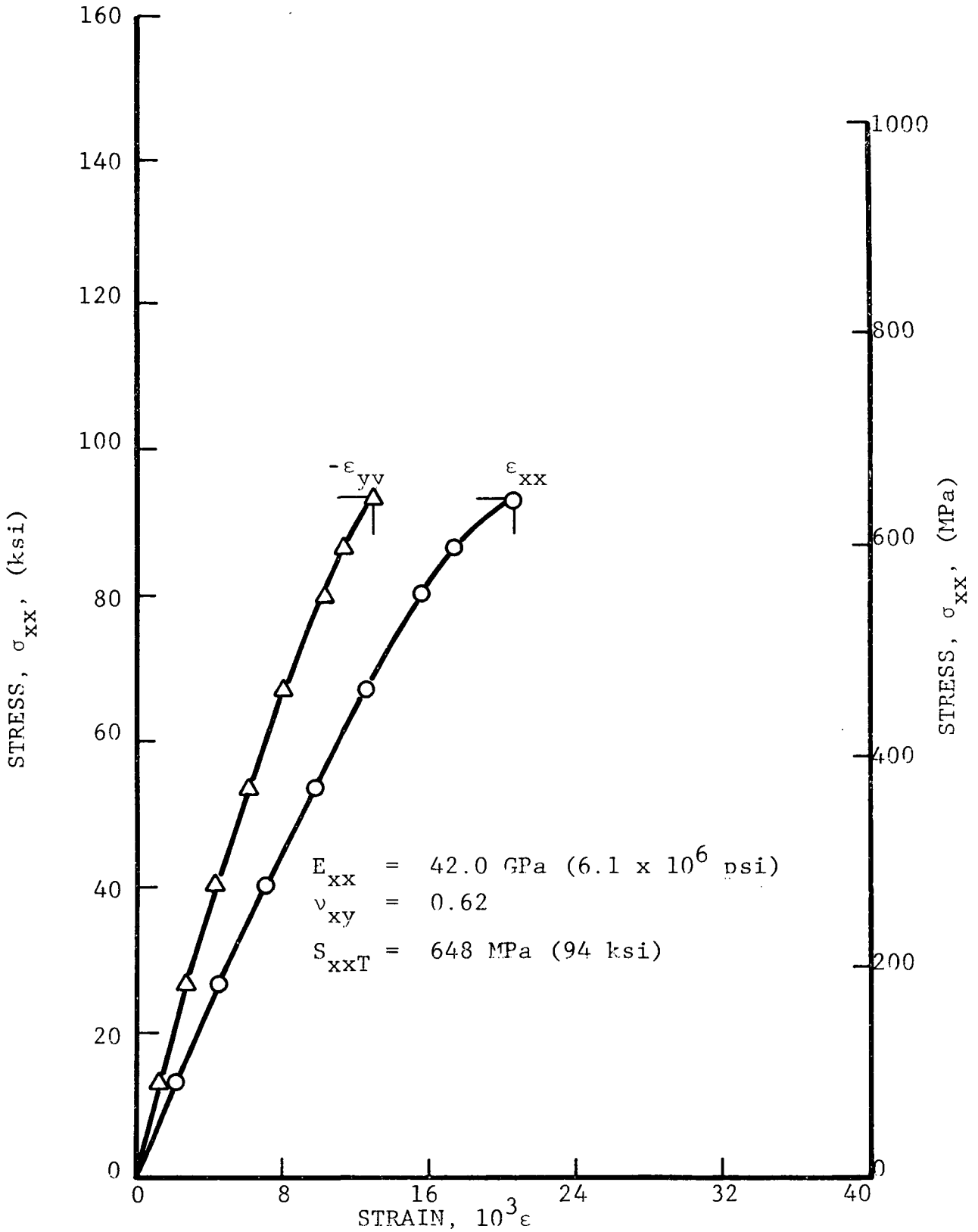

Figure 4.51 STRESS-STRAIN CURVES FOR $[\pm 45^C/0_2^G]_S$ GRAPHITE/ S-GLASS/EPOXY FLATTENED TUBULAR SPECIMEN TESTED IN UNIAXIAL TENSION AFTER 1.264×10^7 CYCLES OF TENSILE FATIGUE TO 20.5 PERCENT OF STATIC STRENGTH

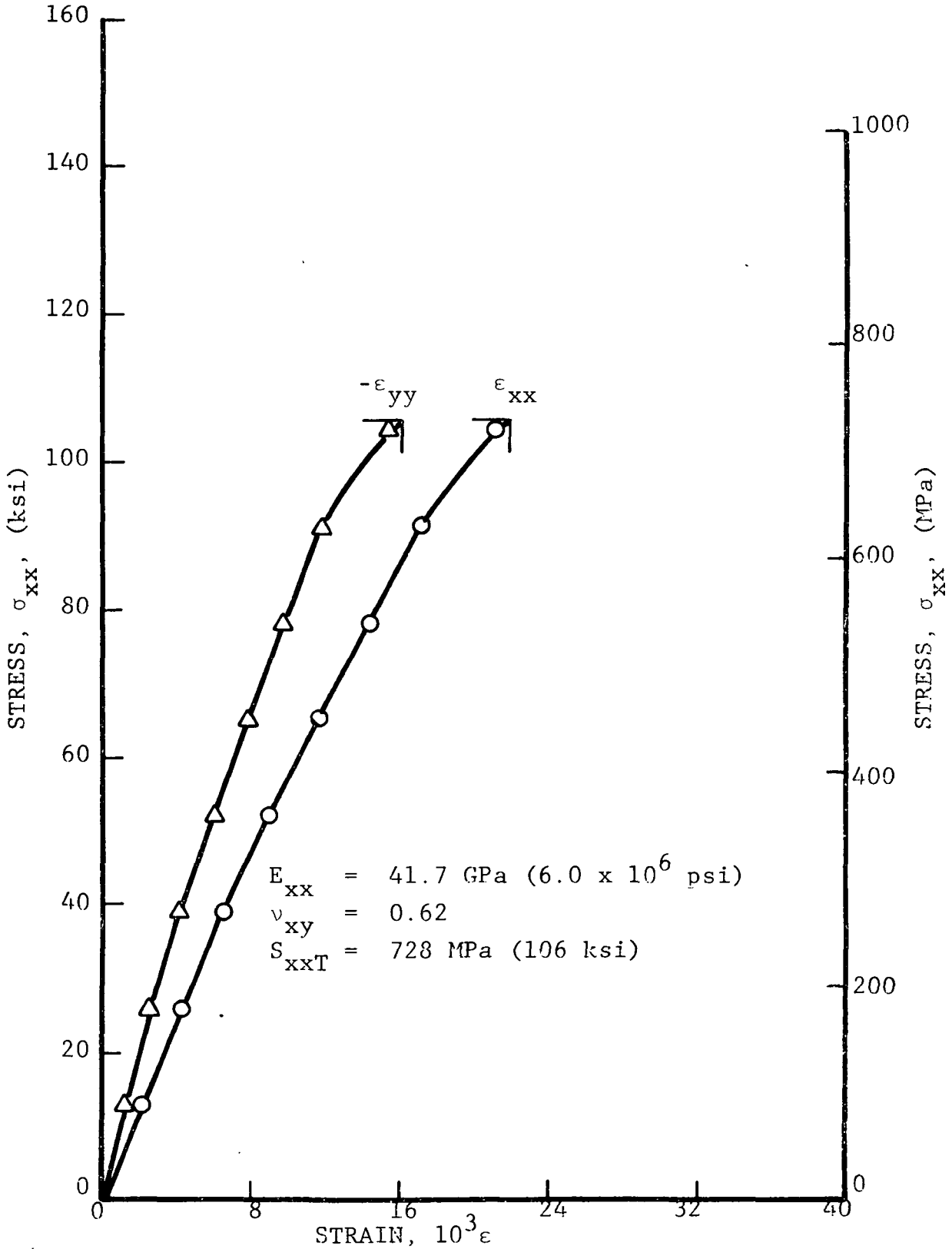

Figure 4.52 STRESS-STRAIN CURVES FOR $[+45^C/0_2^G]_s$ GRAPHITE/ S-GLASS/EPOXY FLAT COUPON TESTED IN UNIAXIAL TENSION AFTER 1.0 x 10^7 CYCLES OF TENSILE FATIGUE TO 24.0 PERCENT OF STATIC STRENGTH

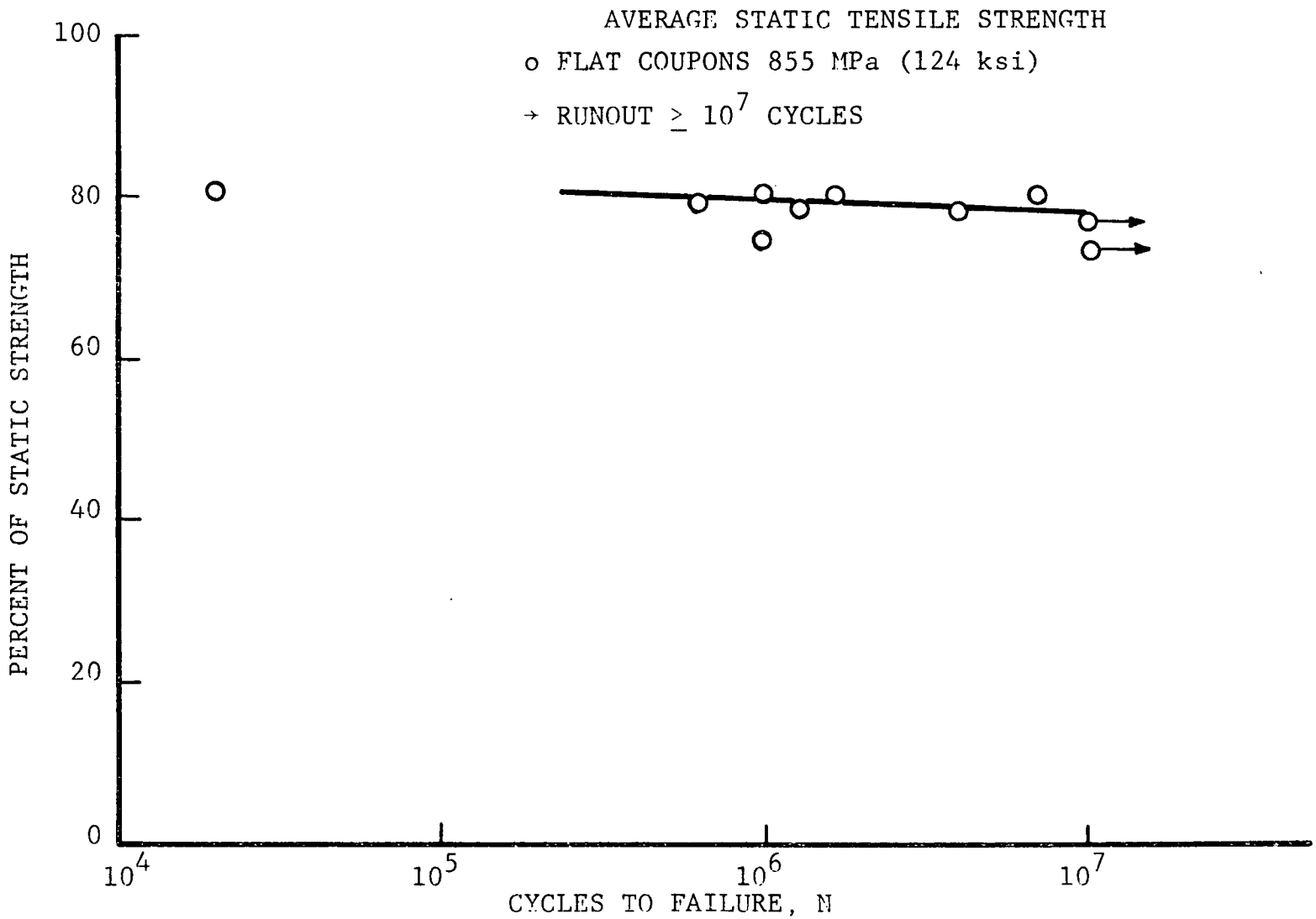

Figure 4.53 TENSILE CYCLING FATIGUE STRENGTH OF $[0_2/\pm45]_s$ GRAPHITE/EPOXY SPECIMENS

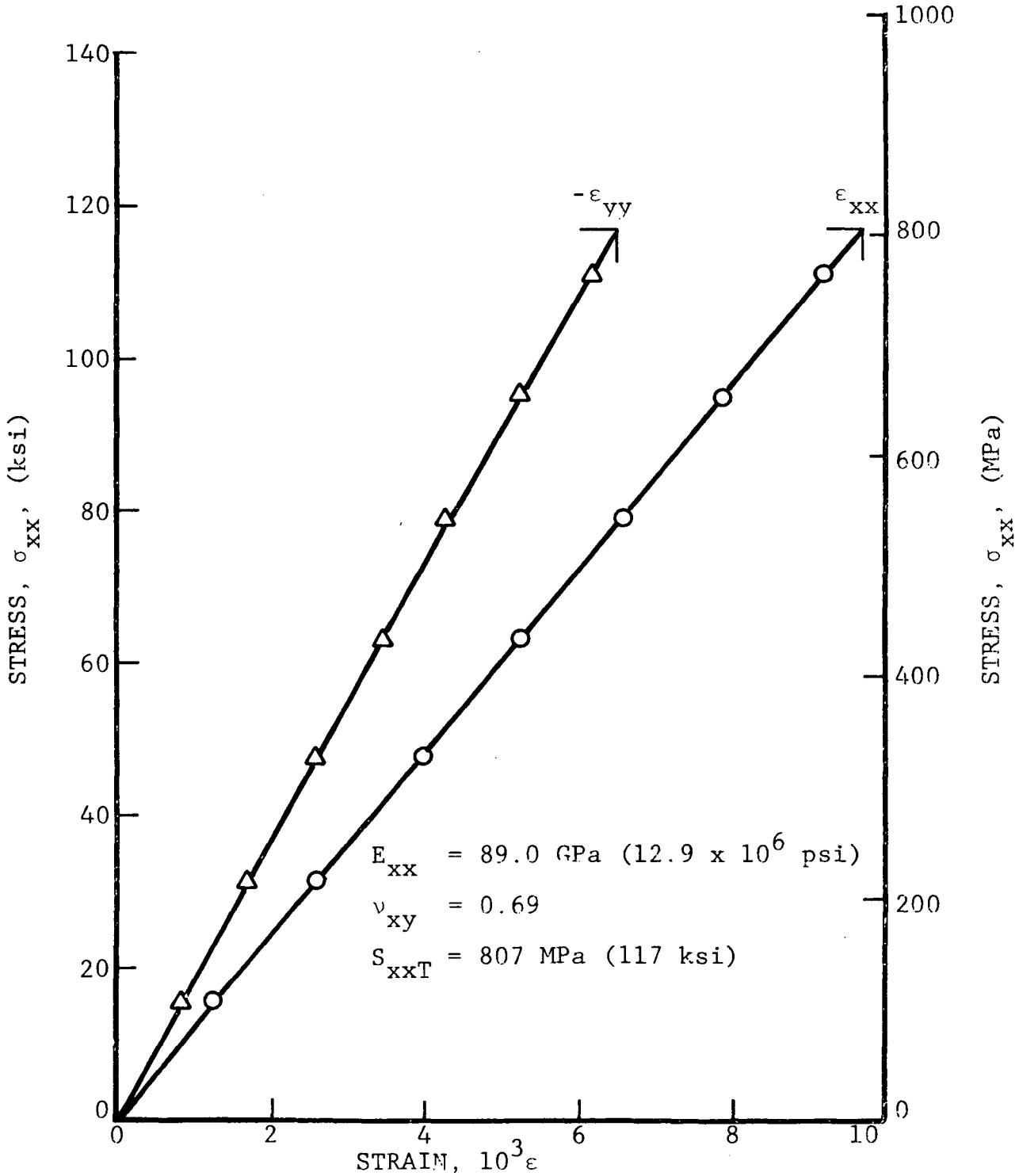

Figure 4.54 STRESS-STRAIN CURVES FOR $[0_2/+45]_s$ GRAPHITE/ EPOXY FLAT COUPON TESTED IN UNIAXIAL TENSION AFTER 1.04×10^7 CYCLES OF TENSILE FATIGUE TO 73.9 PERCENT OF STATIC STRENGTH

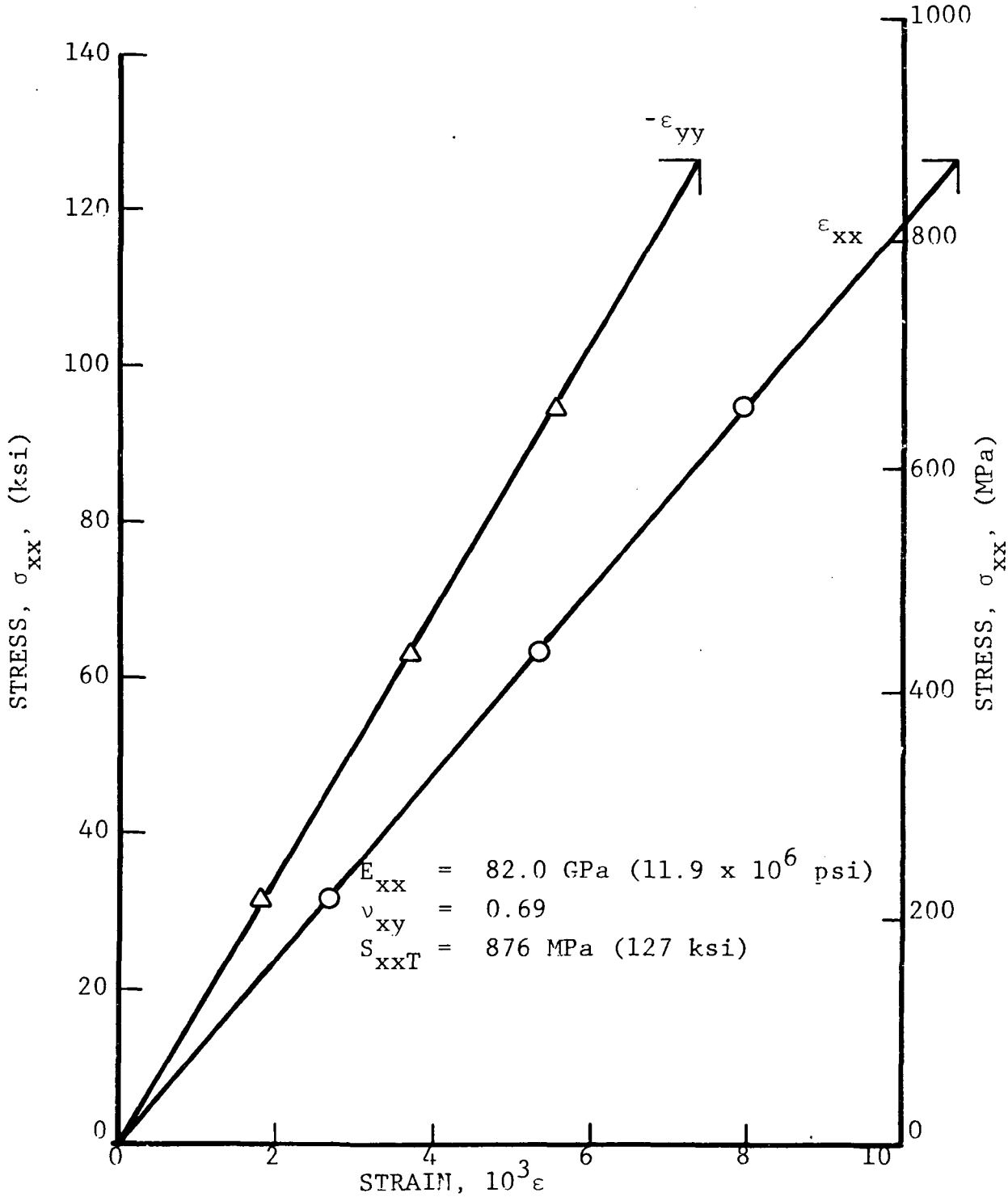

Figure 4.55 STRESS-STRAIN CURVES FOR $[0_2/\pm45]_s$ GRAPHITE/ EPOXY FLAT COUPON TESTED IN UNIAXIAL TENSION AFTER 1.0 x 10^7 CYCLES OF TENSILE FATIGUE TO 77.0 PERCENT OF STATIC STRENGTH

5.0 SUMMARY AND CONCLUSIONS

Significant interlaminar stress components exist near free edges in uniaxially loaded angle-ply flat coupon specimens used in determining laminate properties. It has been hypothesized in past research that damage due to loading of such specimens is initiated at the edges by these stresses and propagates toward the interior. The influence of the edge effects on the tensile properties of angle-ply laminate composites can be eliminated by utilizing an edgeless specimen such as a tube. A new type of edgeless cylindrical specimen was developed in a previous project[6] to circumvent difficulties encountered with round tubular specimens. It is a flattened tube consisting of two flat sides connected by curved sections and it can be handled much like the standard flat coupon.

The objective of this program was to systematically evaluate flattened tubular specimens of composite materials under static and cyclic uniaxial tensile loading and to compare them directly with flat coupon data of the same materials generated under corresponding loading conditions. The program required additional development for the refinement and fabrication of the flattened specimen configuration.

The specimens investigated were made of graphite/epoxy, S-glass/epoxy, Kevlar-49/epoxy and graphite/S-glass/epoxy hybrid materials. They were eight-ply laminates of $[\pm 45/0_2]_s$ construction except for the graphite/epoxy which also included specimens of $[0_2/\pm 45]_s$ construction.

Fabrication techniques and fixturing were developed for quantity production of the flattened tube specimens. These included the use of a split three-wedge flat mandrel for the tube layup, and RTV thermal-expansion pressure strips for compacting

the rounded sides of the specimen during the curing operation. A special end tab and insert design was devised to minimize gripping tab constraints. Both the external tabs and the plug inserts were made from $[\pm 45]_n$ glass/epoxy, minimizing the tab stiffness. To reinforce the transition between the tabs and specimen test section a slotted plug insert was devised, extending inside the tube beyond the external tab length.

Flattened tube specimens and flat coupons of corresponding materials and construction were fabricated and tested under tensile static and fatigue loads, and the results obtained for the two types of specimens were compared. Residual properties of fatigue specimens which survived 10 million cycles were also determined.

Comparison between the statically tested flattened tubes and flat coupons showed that for the $[\pm 45/0_2]_s$ graphite/epoxy, S-glass/epoxy and Kevlar 49/epoxy materials the flattened tubes exhibit somewhat higher average strengths than their corresponding flat coupons. This trend was generally also evident among the individual specimen strengths. The failure modes of the tubular specimens for these three materials were in general acceptable test section failures.

In the case of the graphite/S-glass/epoxy hybrid specimens failures for the flattened tubes occurred not only in the test section but also near the gripping tabs. Furthermore, even in the test section, failure occurred by splitting of the outer ± 45-degree graphite/epoxy plies along the transition between the rounded and flat sections of the specimen. As a consequence of such parasitic failures the average strength of the flattened tubes is somewhat lower than for the corresponding flat coupons.

Initial static testing of graphite/epoxy $[0_2/\pm 45]_s$ flattened tube specimens showed that all specimens were failing

with a parasitic mode at low strengths. This mode consisted of splitting along the fiber direction of the 0-degree plies along the crown of the rounded sides of the specimen. The fabrication and testing of these specimens was subsequently eliminated.

The comparison made between the fatigue-tested flattened tubes and flat coupons showed that the flattened tubes have a significantly lower fatigue strength. Most of that reduction can be attributed to parasitic failure modes. Essentially all flattened tube fatigue specimens failed with the parasitic failure mode of splitting the outer $\pm$45-degree plies along the transition between the rounded and flat sections of the specimen. It is believed that this failure mode can be eliminated by further refining the specimen fabrication technique.

Another possible cause of the lower fatigue strength of the flattened tubes is heating due to cycling. Temperatures during cycling were monitored on some of the specimens using clipped-on thermocouples. The flattened tubes become substantially hotter during cycling than flat coupons. This is due to the tubular shape. It encloses a trapped air volume. During cycling the specimen reaches a plateau temperature and shows a rapid rise above this plateau just before failure. For the graphite/epoxy specimens the longer the cycle life the greater was the temperature rise. This heating phenomenon may be either a contributing cause to specimen failure or a symptom of gradual specimen degradation. If it is a contributing cause it can be eliminated by air cooling of the specimen during cycling.

An examination of residual property data of the flattened tube and flat coupon specimens surviving 10^7 fatigue cycles shows that in most cases the residual strength is lower than the average static strength of the corresponding uncycled specimens. A similar trend, but in fewer cases is also evident for the

residual tensile modulus. Poisson's ratio generally shows no significant change.

It has been shown in this study that when the statically tested flattened tube specimens fail in an acceptable mode the specimens show a somewhat higher strength than the flat coupons. In the case of the fatigue tests no conclusive results could be obtained because of parasitic failure modes. These modes are believed to be induced by the present fabrication process which could be improved and refined further.

REFERENCES

1. R.B. Pipes and N.J. Pagano, "Interlaminar Stresses in Composite Laminates Under Uniform Axial Extension," J. Composite Materials, Vol. 4, 1970, p. 538.

2. A.H. Puppo and H.A. Evensen, "Interlaminar Shear in Laminated Composites Under Generalized Plane Stress," J. Composite Materials, Vol. 4, 1970, p. 204.

3. R.B. Pipes and I.M. Daniel, "Moire Analysis of the Interlaminar Shear Edge Effect in Laminated Composites," J. Composite Materials, Vol. 5, 1971, pp. 255-259.

4. I.M. Daniel, R.E. Rowlands and J.B. Whiteside, "Effects of Material and Stacking Sequence on Behavior of Composite Plates with Holes," Exp. Mechanics, Vol. 14, 1974, pp. 1-9.

5. I.M. Daniel and T. Liber, "Lamination Residual Stresses in Fiber Composites," IITRI Report D6073-I for NASA-Lewis Research Center; NASA CR-134826, March 1976.

6. T. Liber and I.M. Daniel, "Evaluation of Hybrid Composite Materials in Cylindrical Specimen Geometries," NASA CR-145006, IITRI D6089, NASA-Langley Research Center, April 1976.

7. I.M. Daniel and T. Liber, "Lamination Residual Stresses in Hybrid Composites," IITRI Report D6073-II for NASA-Lewis Research Center, NASA CR-135085, June 1976.

NASA CONTRACTOR REPORT 145353
NASA CONTRACT NAS1-14663

DISTRIBUTION LIST

	No. Copies
NASA Langley Research Center Hampton, VA 23665	
Attn: Report & Manuscript Control Office, Mail Stop 180A	1
Structures Laboratory, USARTL (AVRADCOM), Mail Stop 266	2
George L. Roderick, Mail Stop 188E	25
NASA Ames Research Center Moffett Field, CA 94035	
Attn: Library, Mail Stop 202-3	1
US Army Research & Technology Laboratories (AVRADCOM), Mail Stop 207-1	2
Aeromechanics Laboratory, USARTL (AVRADCOM), Mail Stop 215-1	2
NASA Dryden Flight Research Center P.O. Box 273 Edwards, CA 93523	
Attn: Library	1
NASA Goddard Space Flight Center Greenbelt, MD 20771	
Attn: Library	1
NASA Lyndon B. Johnson Space Center 2101 Webster Seabrook Road Houston, TX 77058	
Attn: JM6/Library	1
NASA Marshall Space Flight Center Marshall Space Flight Center, AL 35812	
Attn: Library, AS61L	1
Jet Propulsion Laboratory 4800 Oak Grove Drive Pasadena, CA 91103	
Attn: Library, Mail 111-113	1
National Aeronautics & Space Administration Washington, D.C. 20546	
Attn: RW	1
RWS/Dr. Michael Salkind	1
NASA John F. Kennedy Space Center Kennedy Space Center, FL 32899	
Attn: Library, NWSI-D	1

DISTRIBUTION LIST (Continued)

	No. Copies
NASA Lewis Research Center 21000 Brookpark Road Cleveland, OH 44135	
Attn: Library, Mail Stop 60-3	1
Robert H. Johns, Mail Stop 49-3	1
Gordon T. Smith, Mail Stop 49-3	1
Propulsion Laboratory, USARTL (AVRADCOM), Mail Stop 500-317	2
University of Wisconsin Department of Engineering Mechanics Madison, WI 53706	
Attn: Professor R.E. Rowlands	1
United Aircraft Corporation Pratt & Whitney Aircraft East Hartford, CT 06118	
Attn: Dr. T.A. Cruse, Scientific Analysis Group	1
University of Wyoming Department of Mechanical Engineering Laramie, WY 82070	
Attn: Professor Donald F. Adams	1
University of Minnesota 107 Aeronautical Engineering Building Minneapolis, MN 55455	
Attn: Professor Phil Hodge	1
Northrop Corporation Aircraft Division 3901 W. Broadway Hawthorne, CA 90250	
Attn: Glen C. Grimes, Engineering Specialist Structures R&T, Dept. 3780/62	1
McDonnell Douglas Corporation P.O. Box 516 St. Louis, MO 63166	
Attn: Dr. Michael P. Renieri, Bldg. 34, Post 350	1
Dr. Gary D. Renieri, Bldg. 106, Level 4, Post C-5	1
Department of the Navy Office of Naval Research Arlington, VA 22217	
Attn: Dr. Nicholas Perrone, Director, Structural Mechanics Program	1

DISTRIBUTION LIST (Continued)

	No. Copies
National Science Foundation Washington, D.C. 20550 Attn: Dr. Clifford J. Astill, Solid Mechanics Program	1
Wright-Patterson Air Force Base, OH 45433 Attn: MBM/Dr. Nicholas J. Pagano	1
Air Force Flight Dynamics Laboratory Wright-Patterson Air Force Base, OH 45433 Attn: Dr. George P. Sendeckyj, Structures Division Dr. J.C. Halpin	1 1
Air Force Materials Laboratory Wright-Patterson Air Force Base, OH 45433 Attn: Dr. J.M. Whitney, Nonmetallic Materials Division Dr. H.T. Hahn, Nonmetallic Materials Division	1 1
University of Delaware Department of Mechanical & Aerospace Engineering 107 Evans Hall Newark, DE 19711 Attn: Dr. R. Byron Pipes	1
Battelle Columbus Laboratories 505 King Avenue Columbus, OH 43201 Attn: Dr. Edmund F. Rybicki	1
E.I. duPont de Nemours & Co., Inc. Experimental Station/B262 Wilmington, DE 19898 Attn: Dr. Carl H. Zweben, Textile Fibers	1
IIT Research Institute 10 W. 35th Street Chicago, IL 60616 Attn: Dr. I.M. Daniel, Science Advisor	1
General Dynamics Corporation Fort Worth, TX 76101 Attn: M.E. Waddoups	1

DISTRIBUTION LIST (Concluded)

	No. Copies
McDonnell Douglas Corporation Douglas Aircraft Company 3855 Lakewood Boulevard Long Beach, CA 90846 Attn: Dr. Longin B. Greszczuk	1
Lockheed Aircraft Corporation Lockheed-California Company P.O. Box 551 Burbank, CA 91520 Attn: Larry R. Markham, Dept. 7572, Bldg. 63, Plant A1	1
Applied Technology Laboratory US Army Research & Technology Laboratories (AVRADCOM) Fort Eustis, VA 23604 Attn: J. Robinson/SAVDL-EU-SS	2
Department of the Army US Army Materials & Mechanics Research Center Watertown, MA 02172 Attn: Dr. E. Lenoe Dr. J. Perkins	1 1
Picatinny Arsenal Materials Engineering Laboratory, Bldg. 183 Dover, NJ 07801 Attn: Charles Wright	1
NASA Scientific & Technical Information Facility 6571 Elkridge Landing Road Linthicum Heights, MD 21090	27 plus original